

# **Concept and Mission Design of a Small Space Tug for Debris Remediation in Low Earth Orbit**

---



by

**Muhammad Zubair      190585**

**Hassan Yousaf        190605**

**Hasan Anwar Hussain   190621**

An undergraduate thesis submitted in partial fulfillment of the  
requirements for the degree of  
Bachelor of Engineering (B.E.) in Mechanical Engineering

DEPARTMENT OF MECHANICAL AND AEROSPACE ENGINEERING

**AIR UNIVERSITY**

**2023**

# Concept and Mission Design of a Small Space Tug for Debris Remediation in Low Earth Orbit

---



by

**Muhammad Zubair**      **190585**

**Hassan Yousaf**        **190605**

**Hasan Anwar Hussain**   **190621**

An undergraduate thesis submitted in partial fulfillment of the  
requirements for the degree of

Bachelor of Engineering (B.E.) in Mechanical Engineering

SUPERVISOR

Prof. Dr. Ali Sarosh

**AIR UNIVERSITY**

ISLAMABAD

2023

# CERTIFICATE/APPROVAL SHEET

## Department of Mechanical Engineering

It is hereby certified that Muhammad Zubair (190585), Hassan Yousaf (190605), and Hasan Anwar Hussain (190621) have successfully completed their thesis.

---

**Prof Dr. Ali Sarosh**

Associate Professor

*Air University*

Supervisor

---

**Prof Dr. Syed Irtiza Ali Shah**

Professor

*Air University*

Co-Supervisor

---

**Prof. Dr. Sohail Iqbal**

*Air University*

Head of Department, Department of Mechanical and Aerospace Engineering

DMAE (AU) Report for PEC FYDP 2022-23

## DECLARATION

We declare that all material in this thesis is our work, and that which is not our own work has been mentioned as such, and that no material from this work has previously been submitted or approved for the award of a degree by this or any other university.

-----

Muhammad Zubair

(190585@students.au.edu.pk)

-----

Hassan Yousaf

(190605@students.au.edu.pk)

-----

Hasan Anwar Hussain

(190621@students.au.edu.pk)

Dated: \_\_\_\_\_

DMAE (AU) Report for PEC FYDP 2022-23

## Acknowledgments

All thanks be to ALLAH the Almighty, the nourisher and cherisher of the entire world, who has bestowed knowledge and wisdom on all men. Numerous salutes to Hazrat Muhammad, صَلَّى اللهُ عَلَيْهِ وَآلِهِ وَسَلَّمَ. We are thankful to worthy Head of Department, Dr. Sohail Iqbal for their help in resolving the administrative issues. We are grateful to Dr. Sohail Iqbal, the worthy Head of Department, for his assistance in resolving the administrative obstacles. We owe Prof. Dr. Ali Sarosh our heartfelt appreciation and have the wonderful pleasure and honor of paying our deep respects to him. We were able to accomplish this research because of his collaboration and friendly interest, motivating direction, helpful recommendations, and discussions. His tireless efforts to instill the value of persistent hard work will act as a beacon for the rest of our life. We would also like to take this occasion to offer our heartfelt appreciation to our co-supervisor, Prof Dr. Syed Irtiza Ali Shah. We have no words to express our gratitude for our loving parents and siblings' sacrifices, numerous prayers, unending support, encouragement, and unwavering determination. Their presence and moral support constantly boosted our spirits. We are appreciative to all of our teachers for their generous assistance. We are also extremely obliged and thankful to our respected seniors Engr. Mushabbar Husnain Noor and Engr. Muhammad Osama for their guidance and valuable advice throughout the tenure of the project. We are thankful to our colleagues for always supporting us.

# Concept and Mission Design of a Small Space Tug for Debris Remediation in Low Earth Orbit

## Abstract

The space sector is constantly threatened by orbital debris, including rocket bodies and defunct satellites. As of March 2023, the Space Surveillance Network (SSN) traced about 33680 pieces of space debris. An estimation says that there are about 1 million pieces between 1 and 10 cm and 130 million fragments smaller than 1 cm. Therefore, it is very vital to perform Active Debris Removal Missions. Various options as listed below are evaluated and the most viable method shall be chosen based on a well-defined criterion. Solar Sails, Drag Augmentation Devices, Space Balloons, Laser Orbital Debris Removal –both ground-based and space-based and Space Tugs are some of the techniques that can be used for Active Debris Removal (ADR). Out of these technologies, the Space Tug system will be designed, and a robotic prototype will be developed that can be used to eradicate space debris from Low Earth Orbit. This research focuses on the development of alternative mission strategies for minimal energy missions for ADR. Following the concurrent engineering approach so far, two mission strategies are worked upon i.e., Home capture and Nodal capture. These missions are supported by a dedicated spacecraft bus. The parking orbit chosen was the Sun-synchronous orbit as the satellite's secondary objective is to function as an Earth observation satellite during its waiting orbit. System design of other vital subsystems is also presented. A LIDAR-based robotic arm will also be integrated on the mechanical bus for capturing the debris. A 3D model of the mechanical bus was designed which was then followed by static, thermal, and modal analysis of the bus to satisfy the launch conditions and ensure its survivability in space.

*Keywords: Space debris Remediation (SDR), Active Debris Removal (ADR), Robotic Arm, Home Capture, Nodal Capture, System Design, Concurrent Engineering, Sun-synchronous Orbit*

## Table of Contents

Chapter 1: Introduction .....	1
1.1 Problem Statement .....	3
1.2 Motivation.....	3
1.3 Objectives .....	3
1.4 Scope of the thesis .....	4
1.5 Thesis Layout.....	4
Chapter 2: Literature Survey.....	5
2.1 Foundations.....	5
2.1.1 Books .....	5
2.1.2 Papers.....	5
2.2 Prior Work .....	11
Chapter 3: Methodology .....	12
3.1 Program Level.....	12
3.2 Project Level .....	12
3.3 Debris Selection Methodology .....	13
Chapter 4: System Concept Design .....	15
4.1 System Tradeoff Study .....	15
4.2 H2Z Conceptual Design.....	16
4.2.1 H2Z System Specifications.....	16
4.2.2 H2Z System Preliminary Configuration .....	17
4.3 CAD Model.....	17
4.4 Payload Subsystem .....	23
4.4.1 Robotic Arm.....	23
4.4.2 Imaging Payload .....	26
4.5 Structure Subsystem.....	28
4.5.1 Material Selection and Evaluation .....	28

4.5.2 Launch Vehicle Interface .....	31
4.5.3 Mass Budget.....	32
4.6 Propulsion Subsystem.....	32
4.7 Attitude Determination and Control Subsystem .....	35
4.8 Guidance Navigation and Control Subsystem .....	38
4.9 Electrical Power Subsystem.....	40
4.9.1 Power Budget.....	41
4.10 Telemetry, Tracking and Command Subsystem.....	43
4.10.1 TT&C Link Budget.....	45
4.11 Command and Data Handling Subsystem .....	48
4.12 Thermal Control Subsystem .....	49
4.12.1 Dissipation Budget.....	52
Chapter 5: Mathematical Formulation .....	53
5.1 Debris Selection Math Model .....	53
5.2 Mission Math Model.....	54
5.2.1 Home Capture .....	54
5.2.2 Node Capture .....	58
5.3 System Math Model.....	60
5.3.1 Payload Subsystem .....	61
1. Imaging Payload: .....	61
2. Robotic Arm: .....	63
5.3.2 Structure Subsystem.....	64
5.3.3 Propulsion Subsystem.....	65
5.3.4 Attitude Determination and Control Subsystem.....	68
5.3.5 Telemetry, Tracking, and Command Subsystem.....	69
5.3.6 Electric Power Subsystem.....	71
5.3.7 Thermal Control System .....	77



Chapter 6: Results and Discussion.....	78
6.1 Debris Selection .....	78
6.2 Mission Design Results.....	79
6.2.1 Mission Objectives.....	79
6.2.2 Mission Requirements .....	79
6.2.3 Mission Operation Phases and Modes .....	79
6.2.4 Satellite Parking Orbit.....	81
6.2.5 Orbit Environment .....	81
6.2.6 Illumination Condition Analysis.....	82
6.2.7 Ground Station .....	83
6.2.8 Analysis of Orbit Ground Coverage .....	83
6.2.9 Mission Life .....	84
6.2.10 End-of-Life Analysis .....	84
6.2.11 Mission Strategies .....	85
6.2.12 Home Capture .....	86
6.2.13 Node Capture .....	87
6.3 System Design .....	88
6.3.1 Payload.....	89
6.3.2 Structure Subsystem.....	90
6.3.3 Propulsion Subsystem.....	91
6.3.4 Attitude Determination and Control Subsystem.....	93
6.3.5 Electric Power Subsystem.....	93
6.3.6 Telemetry, Tracking, and Command Subsystems .....	95
6.3.7 Thermal Control System .....	96
6.4 Analysis.....	96
6.4.1 H2Z Linear Static Analysis:.....	99
6.4.2 H2Z Modal Analysis.....	100

6.4.3 H2Z Thermal Analysis.....	102
Chapter 7: Conclusions and Recommendations .....	103
7.1 Mission Conclusions.....	103
7.2 System Conclusions .....	103
7.3 Recommendations for Further Work .....	104
References.....	105
Appendix-A Mission Design Codes .....	107
Appendix-B System Design Codes.....	111

DMAE (AU) Report for PEC FYDP 2022-23

## List of Figures

Figure 1.1 Evolution of debris with time .....	2
Figure 3.1 Program Level Methodology .....	12
Figure 3.2 Project Level Methodology .....	13
Figure 3.3 Debris Selection Methodology .....	14
Figure 4.1 1.5U H2Z Mechanical Bus .....	17
Figure 4.2 H2Z with Launch Vehicle Adapter .....	18
Figure 4.3 Closed View of Mechanical Bus .....	18
Figure 4.4 Actual Robotic Arm .....	19
Figure 4.5 Concept demonstrator for the Actual Robotic Arm .....	19
Figure 4.6 Concept demonstrator for the Actual Robotic Arm along with LiDAR ....	20
Figure 4.7 LV adapter .....	20
Figure 4.8 Module 1 .....	21
Figure 4.9 Module 2 .....	21
Figure 4.10 Module 3 .....	22
Figure 4.11 Propulsion Module .....	22
Figure 4.12 Rocket engine nozzle .....	23
Figure 4.13 Design properties for some commonly used Metals SMAD .....	31
Figure 4.14 Major components of a general ACS system .....	36
Figure 4.15 Alternative navigation systems .....	39
Figure 4.16 System context of TTC .....	44
Figure 4.17 Link Budget .....	45
Figure 4.18 Interfaces and capabilities of CDH subsystem .....	49
Figure 4.19 Thermal environment of a spacecraft .....	50
Figure 5.1 Hohmann Transfer .....	55
Figure 5.2 General Plane Change Maneuver .....	56
Figure 5.3 Apses Line Rotation Maneuver .....	57
Figure 5.4 Phasing Maneuver .....	58
Figure 5.5 Angular difference between both objects .....	59
Figure 5.6 Orbits after Hohmann Transfer .....	59
Figure 5.7 GSD 5 cm .....	61
Figure 5.8 GSD 30 cm .....	61
Figure 5.9 Ground Sampling Distance .....	62

Figure 5.10 Swath width Representation .....	62
Figure 5.11 Nozzle Contour .....	68
Figure 5.12 Altitude versus Damage Fluence Graph.....	75
Figure 5.13 Power density versus Electron Fluence Graph.....	76
Figure 5.14 Multiplication factor versus Altitude Graph.....	76
Figure 6.1 Sensitivity Plots .....	78
Figure 6.2 Parking Orbit of H2Z.....	81
Figure 6.3 Impact Flux of Debris and Meteoroid .....	81
Figure 6.4 Radiation Environment within altitude (150 km - 1000km) .....	82
Figure 6.5 Beta Angle Graph for 1 year .....	82
Figure 6.6 Illumination duration for 1 year .....	82
Figure 6.7 Percent Time coverage of 1 day vs. Latitude .....	83
Figure 6.8 Coverage time contour .....	83
Figure 6.9 Summary of Access to Ground Station .....	84
Figure 6.10 Ground Track Plot for Rawat .....	84
Figure 6.11 Height of apogee, perigee, and inclination graph for EOL .....	85
Figure 6.12 Home Capture Simulations.....	87
Figure 6.13 Node Capture Simulations.....	88
Figure 6.14 Geometry .....	97
Figure 6.15 Mesh .....	98
Figure 6.16 Launch Static Simulation .....	100
Figure 6.17 Component level Simulation .....	100
Figure 6.18 Maximum normal mode frequency .....	101
Figure 6.19 First normal mode frequency.....	102
Figure 6.20 Thermal Analysis of H2Z (maximum and minimum temperatures) .....	102

## List of Tables

Table 1.1 Significant Research Methodologies .....	11
Table 4.1 Relevant space tugs for benchmarking .....	15
Table 4. 2 System Tradeoff study .....	16
Table 4.3 Motor Specifications for Joint 1, 2 and 3.....	24
Table 4.4 Motor Specifications for Joint 4 and End effector.....	24
Table 4.5 Motor Specifications for LIDAR-Scan.....	24
Table 4.6 ARDUINO Mega 2560 Specifications .....	25
Table 4.7 ARDUINO UNO Specifications.....	25
Table 4.8 RF Module Specifications .....	26
Table 4.9 Joystick Specifications.....	26
Table 4.10 Specifications of Imaging payload .....	27
Table 4.11 Specifications of structure subsystem.....	28
Table 4.12 Properties for material selection .....	29
Table 4.13 Comparison of frequently used metal alloys .....	30
Table 4.14 Mass Budget .....	32
Table 4.15 Comparison between chemical engines.....	33
Table 4.16 Propellant Specifications .....	34
Table 4.17 Comparison between different types of nozzle.....	35
Table 4.18 Specifications in ADCS .....	37
Table 4.19 Selected market ADCS components.....	37
Table 4.20 Specifications of GPS .....	39
Table 4.21 Specifications of EPS.....	40
Table 4.22 Specifications of typical Li-ion battery .....	41
Table 4.23 Power Budget.....	42
Table 4.24 Input parameters to component efficiency method.....	43
Table 4.25 Input parameters to damage fluence method .....	43
Table 4.26 Specifications of TTCS.....	44
Table 4.27 Selected Components of TT&C.....	45
Table 4.28 TM Downlink Link Budget .....	46
Table 4.29 TC Uplink Link Budget .....	47
Table 4.30 Specifications of CDH.....	48
Table 4.31 H2Z Unit Temperature Ranges.....	50

Table 4.32 Specification of TCS.....	51
Table 5.1 Sensitivity Analysis Data.....	53
Table 5.2 GSD Representation .....	61
Table 6.1 NORAD ID of Selected Debris for Mission.....	78
Table 6.2 Mission event sequence .....	80
Table 6.3 Parking Orbit Elements of H2Z.....	81
Table 6.4 Key parameters for EOL.....	84
Table 6.5 Description of Maneuvers.....	85
Table 6.6 Strategies List .....	86
Table 6.7 Home Capture Delta-V Budget.....	86
Table 6.8 Node Capture Delta-V Budget.....	87
Table 6.9 Key Parameters of Imaging Payload .....	90
Table 6.10 Sizing Parameters of H2Z Bus.....	90
Table 6.11 Main Engine design for H2Z .....	92
Table 6.12 Disturbance torques .....	93
Table 6.13 Sizing of reaction wheels and momentum wheels.....	93
Table 6.14 EPS Result .....	94
Table 6.15 EPS parameters from damage Fluence Method.....	94
Table 6.16 TM Uplink results.....	95
Table 6.17 TM Downlink .....	95
Table 6.18 Aluminum 6061 Mechanical and Thermal properties .....	97
Table 6.19 Mesh Properties .....	98
Table 6.20 Loads/BC's .....	98
Table 6.21 Results of Linear Static Analysis.....	99
Table 6.22 Modal Frequencies for modes 1-10 .....	101

## Symbols and Abbreviations

### *English upper case*

$\Delta V_p$	Change in velocity at perigee
$\Delta V_a$	Change in velocity at apogee
$\Delta V_T$	Total change in velocity
$V_{Pt}$	Velocity at the perigee of the transfer orbit
$V_{at}$	Velocity at the apogee of the transfer orbit
$V_{Pi}$	Velocity at the perigee of the initial orbit
$V_{fa}$	Velocity at the apogee of the transfer orbit
$T_f$	Time of flight for Hohmann Transfer
T	Time of phasing orbit
$V_{ti}$	The tangential component of velocity
$V_{ri}$	The radial component of velocity
$p_1$	Chamber Pressure
$p_2$	Exit Pressure
$A_t$	Throat area of the nozzle
$A_2$	Exit area of the nozzle
$\frac{A_2}{A_t}$	Nozzle Area Expansion Ratio
$I_{sp}$	Specific Impulse
$F$	Thrust
$C_F$	Coefficient of thrust
$m_p$	Propellant mass
$m_f$	Final mass of the spacecraft
$m_{fuel}$	Fuel mass
$m_{ox}$	Oxidizer mass
$v_2$	Exhaust Velocity
$D_t$	Throat Diameter
$D_e$	Exit Diameter
$T_t$	Throat Temperature
$c^*$	Characteristic velocity
$L^*$	Characteristic Length

$\frac{A_c}{A_t}$	Chamber Contraction Ratio
$A_c$	Area of chamber
$V_c$	Volume of chamber
$\lambda$	Nozzle efficiency
$L_{con}$	Length from the converging cone entrance to the nozzle throat
$\theta_{cn}$	Nozzle cone half angle
$L_n$	Nozzle length
$t_b$	Burn Time
$V$	Volume of spacecraft
$A_b$	The cross-section area of the spacecraft
$I$	Moment of Inertia of spacecraft
$P_{sun}$	Average Power Required for Sunlight Phases
$P_e$	Average Power Required for Eclipse phases
$P_{charge}$	The power Required from the solar array to meet the eclipse load
$P_{array}$	Power Required to be available from array
$P_o$	Power output with the sun normal to the surface of the cells
$P_{BOL}$	Beginning-of-life (BOL) power production capability
$P_{EOL}$	End-of-life (EOL) power production capability
$E_B$	Battery-stored Energy
$M_B$	Estimated Battery mass
$D$	Diameter of aperture
$S_D$	Swath width in kilometers
$S_D$	Area of solar array required to produce the required power
$\eta_{cell}$	Solar cell efficiency for Tripple Junction GaAs cells
$\eta_{packing}$	Cell packing efficiency
$D$	Array degradation factor
$\delta\theta$	Array pointing error
$\eta_{misc}$	Miscellaneous degradation of the solar cell.
$T_{avg}$	The average temperature that is to be maintained in the satellite
GSD	Ground Sampling Distance
SW	Swath width in degrees



$C/N_o$	Carrier to noise density ratio
$EIRP$	Equivalent Isotropic Radiated Power
$L_S$	Space loss
$E_b/N_o$	Energy per bit to noise density ratio
RIP	Received Isotropic Power
$D_r$	Receive Antenna Diameter
$D_T$	Transmit Antenna Diameter
N	Noise Power
$T_g$	Maximum Gravity Torque
$T_{sp}$	Torque due to Solar Radiation
$T_m$	Magnetic Torque
$T_a$	Torque due to Aerodynamics
RPO	Rendezvous and Proximity Operations

***English lower case***

$r_i$	The radial distance at the $i^{\text{th}}$ position
$a$	Semi major axis
$e$	eccentricity
$s$	Linear dimension of spacecraft

***Greek upper case***

$\theta_{FOV}$	Angular Field of View
$\theta_i$	True anomaly at the $i^{\text{th}}$ position
$\Omega$	Right Ascension of Ascending Node
$\emptyset$	Half Power beamwidth

***Greek lower case***

$\mu$	Earth's gravitational constant
$\gamma_i$	Flight path angle
$\alpha$	Variation in inclination

## **Chapter 1: Introduction**

Debris in low Earth orbit (LEO) is created when spacecraft are left there after their missions have concluded. The debris includes spent rocket stages, shards of metal and plastic from explosions and crashes, as well as bits of paint and dust. According to the Inter-Agency Space Debris Coordination Committee (IADC), "any man-made objects, including pieces and parts therein, in Earth orbit or re-entering the atmosphere that is non-functional" fall into this category. Spacecraft in orbit around these objects pose a significant danger. Orbital debris is a persistent problem in this industry. Even the tiniest particles in orbit carry tremendous quantities of energy due to the high velocities. These items may easily pierce the aluminum and silicon that make up functioning satellites. Furthermore, additional debris is created with each impact, increasing the risk. This might set off a domino effect known as the Kessler Syndrome[1]. About 36,500 bits of space debris bigger than 10 centimeters were tracked by the Space Surveillance Network (SSN) in March of 2022. According to estimates, there are around 1,000,000 particles smaller than 10 centimeters and 130,000,000 fragments larger than 1 centimeter. Over the last decade, the likelihood of a collision has grown seven-fold owing to the proliferation of space junk. The growth of the commercial space sector and the increase in collisions are the primary causes of this increase in population. In 2007, China fired an anti-satellite missile at its own Fengyun satellite, shattering it into 3,000 pieces. A collision between the defunct Cosmos 2251 and the operational Iridium 33 satellites occurred in 2009. This collision resulted in the creation of around 5,000 pieces of debris. The International Space Station (ISS) had to take evasive action in November 2021 because of a debris cloud created by a Russian anti-satellite test. The Russian satellite BLITS altered its orbit and spin in January 2013. An impact with debris from the Fengyun-1C was suspected. Due to these causes, the frequency with which conjunctions occur increased, which in turn increased the likelihood of collisions[2].

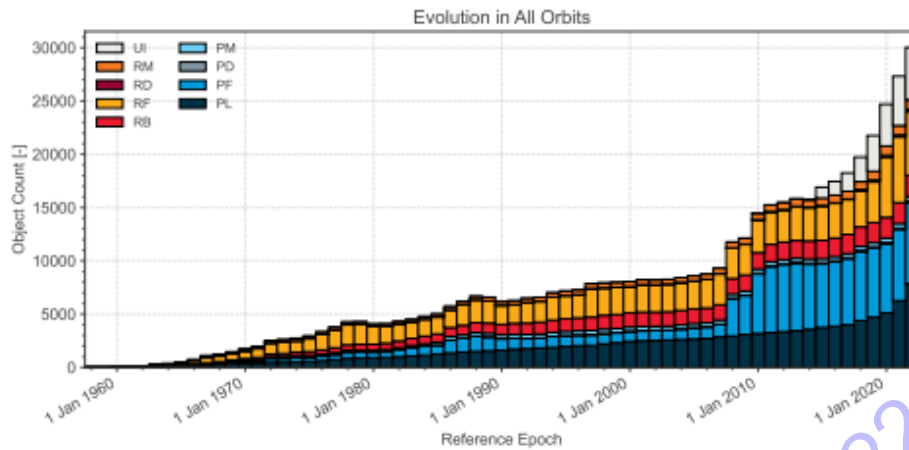


Figure 1.1 Evolution of debris with time

Many operational satellites are concentrated in what is called Low Earth Orbit, an altitude range of around 200 to 2,000 kilometers above the planet's surface. Some of this is due to the reduced launch costs (shorter distance to go) associated with this orbit. Miniature "CubeSat" satellites have been widely available recently, making it affordable for the public without a scientific or governmental background to launch their equipment into orbit. Increasing the number of people using the service increases the population in low Earth orbit. Transferring satellites to higher operating orbits with the use of space tugs would enable the platform mass to be decreased (due to less performing propulsion subsystem). The concept of a space tug as a supplementary vehicle for a geostationary orbiting space station emerged in the decades after World War II. It was also the name of a 1953 book by science fiction writer Murray Leinster. Space tugs are versatile vehicles that can move satellites into desired orbital locations, refuel and resupply spacecraft already in orbit, and clean up orbital trash.

A generic, on-orbit system that can be tailored to a mission's unique needs would be an efficient way to address refueling and maintenance concerns as space continues to fill up. The removal of space junk may also be accomplished with its help. As an adjunct to this, tug mechanisms are also used in space exploration missions. Large spacecraft assembly is another area where these techniques may be put to use. In this context, the creation of a novel element like a Space Tug is desirable[3].

The goal of this research is to find effective ways to use space tug technology for Active Debris Removal (ADR) in densely inhabited orbits. Active debris removal (ADR) is the process of bringing previously hidden objects into view by placing them on a disposal orbit (either one in which atmospheric drag will limit their lifespan or a

"graveyard orbit" where they won't interfere with other objects)[4]. When used for ADR, space tugs may be quite efficient. Space tugs are multipurpose spacecraft that may be used to acquire a broad range of targets for rehabilitation and then relocate them to more favorable orbits for other satellites. Space tugs also have relevance in the military arena as they may be made to undertake counter-space operations.

A space tug system, that utilizes some type of towing, functions at the safer system and hence there is very little likelihood of subsequent debris creation by minimizing the danger of collision. This sounds like an intriguing and effective strategy to be evaluated and researched. While there are several ways in which space tug technology improves ADR missions, there are also certain drawbacks to consider, most notably the safety and dependability of the space tug itself.

### **1.1 Problem Statement**

Orbital debris, which includes rocket boosters and abandoned satellites, poses a persistent threat to the space industry. The increasing amount of space debris poses a serious threat to space sustainability. Therefore, it is very vital to perform Active Debris Removal Missions.

This research focuses on the use of active methods for debris removal and hence involves designing a mechanical spacecraft bus and minimal energy missions that will perform debris remediation in low earth orbit.

### **1.2 Motivation**

In January 2022 a Chinese satellite (SJ-21) performed a rendezvous mission with its defunct satellite (COMPASS G2) in the GEO orbit and then towing to a graveyard orbit (300 km higher than GEO). The motivation for this project came from this recent novel idea where we can perform rendezvous missions in LEO orbits and instead of towing them to the graveyard orbit, the debris can be burnt in the Earth's atmosphere by dropping it to the re-entry altitude.

### **1.3 Objectives**

The project will have three major objectives:

- i. Development of minimal energy mission design strategies for debris remediation in low earth orbit.
- ii. Design of an innovative Space Debris Remediation spacecraft system (mission specific).

- iii. Integration of previously developed technologies on the mechanical bus to perform SDR operations.

#### **1.4 Scope of the thesis**

The scope of the thesis is:

- i. Debris Analysis and Selection
- ii. Debris Remediation and Mission Design
- iii. Spacecraft System Design
- iv. Integration of previously developed technologies on mechanical bus
- v. Spacecraft Bus Design and Analysis

#### **1.5 Thesis Layout**

In this way, the thesis is structured. Chapter 1 presents an introduction. The literature survey is presented in Chapter 2, followed by the methodology in Chapter 3. Subsequently, the system concept design is discussed in Chapter 4 which is followed by the mathematical formulation in Chapter 5. Consequently, Results (in Chapter 6) followed by Conclusions and Recommendations for further work are presented in Chapter 7. Appendix contains codes for mission and system design.

DMAE (AU) Report for DECDYDP 2022-23

## **Chapter 2: Literature Survey**

Various research papers along with books were studied as a part of the literature review which are described in the subsequent sections.

### **2.1 Foundations**

The most important book that is a bible for satellite designers is Space Mission Analysis and Design. This book was studied in detail to develop a deep understanding of the processes involved in designing a mission and a spacecraft.

#### **2.1.1 Books**

**Space Mission Analysis and Design (SMAD):** Wiley J. Larson et al in [5] provides fundamentals of Mission and System Design. Detailed mathematical models for component sizing of the subsystems are also provided.

**Spacecraft Systems Engineering:** Swinert et al in [6] provides in-depth information on each subsystem with detailed math models and considers the modern design conditions which should all be accounted for.

**Elements of Rocket Propulsion:** Sutton et al [7] provide complete information on the required equations to calculate the necessary parameters to design the Rocket engine for the Propulsion subsystem

**Fundamentals of Astrodynamics:** Karel F. Wakker in [8] provides complete mathematical formulations for different orbital maneuvers. In addition, it also provides a basic understanding of orbits, types, and the fundamentals of orbital mechanics.

#### **2.1.2 Papers**

To eliminate five pieces of space debris annually over ten years, this article compares the usefulness vs the life-cycle cost of seven Active Debris Removal (ADR) design possibilities. Some of the Design Options include a robotic arm, a throw net and harpoon, the COBRA IRIDES, three-coordinated electromagnetic spacecraft, eddy currents, and the Electro-Dynamic Debris Eliminator. The Utility Analysis considered many different criteria, including performance, risk, and political viability. The harpoon is the most cost-effective tool. Perhaps the net's price could be cut in half, making it more competitive with the throw net. One of the ways the efficiency was measured was by calculating the delta-v cost. It was most probable that the throw net would come in handy. However, when looking at utility per dollar spent, it becomes clear that the harpoon is the best option. Furthermore, political viability is crucial to the success of

any design choice if the highest weighted criteria are considered. While several designs are feasible and competitive, it soon becomes clear that the best choice is the one that is welcomed by people all around the world [9].

This paper provides suggestions for figuring out and handling a space debris evacuation program in the present geopolitical climate after examining the political problems of designing and executing workable frameworks. To demonstrate the need of developing and disseminating dynamic evacuation frameworks in the next years, this essay first provides a background on the expanding space garbage issue. Since just a few nations hold the vast bulk of the space debris masses, yet all governments will profit from their cleaning, distributing the predicted high expenses presents its own set of challenges [10].

To clean up space in geostationary orbit, this research suggests and constructs a Space Tether-Net system. The DISCOS database is used to locate the debris in this orbit, and then a tether net mission is planned. Data Management Compute, Attitude & Orbital Control, and Target Tracking are among the critical subsystems that contribute to the mission design that makes use of this system [11].

Several satellites, each with the capability of retrieving a single piece of rubbish, may be sent into orbit as an alternative for cleaning up the mess. The benefit of this approach is that the satellite may be built using conventional satellite mechanics, and target trash can be removed without requiring a change in orbit. However, if more than one satellite has to be deployed, then several launches will be necessary. One additional possibility is to use one satellite to remove multiple pieces of space junk. This strategy can efficiently clear off space and reduce launch costs. However, every time junk is removed, this satellite's orbit must be changed, calling for an optimized orbit transition procedure. In this study, the authors developed a satellite route optimization technique for efficient debris clean-up in orbit. Because of the similarities between the TSP and the challenge of clearing the skies of various debris, we adapted an EA designed to solve the TSP and applied it to the latter. To boost the efficiency of recurrent debris removal, we optimized the satellite's thrust so that the overall radar cross-section (RCS), which indicates the quantity of space debris, was maximized while total thrust was minimized. We were able to extend the TSP solution technique to numerous targets by integrating it with the satellite trajectory simulation. One hundred pieces of space junk were selected at random from a database to put the new technology through its pace. The results indicated a trade-off between total RCS and total thrust [12].

SHERPA1 and 2 is a strong propellant satellite that was developed as part of the Shuttle Expendable Rocket for Payload Augmentation. Currently, the SHERPA is working on a PDR-level design. The SHERPA may carry out a range of missions, which includes orbit transfers, minor satellite movements, space situational awareness missions, and experiments. The SHERPA is offered in three distinct versions: a propulsion unit, a freestanding propulsive satellite, and a self-contained long-duration propulsive satellite. Each version can use either an electric or a chemical propulsion module. The SHERPA integrates numerous technologies created by the Air Force Research Laboratory of the USA into a single package. As a low-cost satellite bus, SHERPA may also suit some additional mission needs. Several tasks that are either now impossible or too costly to do may be accomplished with the help of SHERPA, a space asset. Independent of the host launch vehicle or satellite, SHERPA presents a way for delivering small package missions to the orbits of interest. It is the goal of SHERPA to make it possible for secondary payloads to be launched on the Shuttle, ELV, and EELV for the first time. The SHERPA's capabilities are boosted by the inclusion of SBIR technology into three variations. SHERPA might be employed in a range of military applications, including enhancing the speed and responsiveness of space accessibility for micro missions[13]. Focusing on-orbit control for multiple debris removal, this research delves into the subfield of operational research termed "active debris removal." The chaser's long-range trajectory, which serves as a dress rehearsal for the later rendezvous control, is a crucial element of the mission. An innovative mode, the fly-by trajectory, is initially created for long-range trajectory control matching to debris collection by compact with Whipple material. In contrast to the more commonplace rendezvous and capture mode, relative velocity is not required when switching to fly-by mode. Long-range trajectories fall into one of two categories, depending on the necessary speed now of collision. A novel ADR approach is presented in mission design for tiny debris, and it involves retrieving the debris in a limited volume by using a fly-by trajectory. Using impact force, this method embeds debris of medium or small size in the Whipple substance. This method reduces the need for pinpoint accuracy in controls during close-range relative motion. The primary concern of trajectory programming is long-range orbit control, as this is what establishes the capture and transfer order as well as the time and energy required for each step. A hybrid optimization approach is used to address the issue of multiple debris removal simultaneously. Three situations, including



rendezvous and fly-by, are simulated to show the usefulness of the proposed algorithm[14].

This study builds a 7-degrees-of-freedom (DOF) redundant space manipulator that can operate in microgravity to trace the path of big space debris in geostationary orbit. There are two main areas in which researchers are devoting their time and energy. To begin, we employ the popular Virtual Manipulator (VM) kinematics mode to build a Jacobi kinematics mode of a 7-DOF redundant manipulator in the free flight mode. Second, to improve the inverse kinematics trajectory of the space manipulator, an inverse kinematics optimization method based on weighted least-norm (WLN) is devised. In the condition of centroid in carrier moving position, a larger tracking precision of the end effector may be performed via modeling of segment route planning from the original location to the position of target debris in the free-flying mode[15].

Technology for actively removing debris from space, such as a harpoon, net, or drag sail, has previously received a lot of attention. Removed with restrictions is the primary concern. Spacecraft designed to clear away trash have lately been put to use servicing and seizing freighters. Airbus designed and constructed the debris-grabbing net experiment on board the spacecraft. The spacecraft is the heaviest cargo ever sent into orbit from the ISS. Because of the magnitude of the issue, however, active space debris removal technologies like harpoons and nets may not be enough, necessitating the creation of more sophisticated space debris removal systems. The lack of reliable predictions has prevented the widespread adoption of techniques that include redirecting debris or the spacecraft itself to avoid danger. As a consequence of this study, we suggest a hybrid autonomous debris removal system. Several widely-used, linked systems with varying modes of operation make up the whole. Flexible structural design and cutting-edge autonomous technologies make the system operable in a wide range of environments. The process may be thought of as having three distinct phases: detection, prevention, and suppression. The designed system may be operated manually or automatically. To avoid any losses, the correct technique is implemented according to debris identification. The layout takes advantage of current technologies while doing away with their drawbacks. It is thought that this technique will increase the likelihood of a successful cleaning of space debris[16]

Based on the results of this study, researchers propose a novel autonomous system that can be controlled wirelessly from a base on the ground. It's tubular, with a hinged opening on one end that can be closed on demand. The device may be sent into space

like a satellite and will follow a predefined orbit around the planet, picking up trash as it goes. The inside is partitioned between a regular storage area and a magnetic storage area for storing all magnetic metals. The tube will automatically seal at both ends and return its contents to Earth once it is full. The system is adaptable, allowing for customization based on factors such as debris type, quantity, and location. The system has a self-defense system, an anti-collision system (ACS), and a maneuvering system for use in space. If processed in this way, not only would the orbits be cleared of junk, but valuable materials now drifting through space may be put to good use. Space debris clean-up is challenging, time-consuming, and expensive because current technology shows promise but has limits in that it can only capture one or two pieces of debris or just a specific sort of debris with only a particular material type. The results suggest that a hybrid autonomous debris removal system could be a viable solution to the growing problem of space debris with the caveat that its use should be regulated

This paper presents the idea of operations and early design for a constellation mission to actively remove big pieces of trash from low Earth orbit. The project entails deploying six nano-satellites from a mother ship mini-satellite. To determine the attitude state of the debris and acceptable docking sites for the nano-satellites, the mother ship must first achieve a relative orbit of a few kilometers around the target space junk. Methodically, the nano-satellites will deploy and dock with the wreckage. Nano-satellites collaborate to conduct a structural investigation of the debris once they have established contact to determine the most secure detumble and deorbit maneuvering patterns. The mother ship docks with the debris and then uses maneuvers to take it out of orbit. Engineering expenses for the mission's mass and propellant systems have been calculated, as has a rough estimate of the total price tag. They are shown alongside each spacecraft's operational architecture and the mission design outcomes obtained from the Systems Tool Kit. Active Debris Removal with a constellation mission consisting of a mother ship and six 12U Cubesat nano-satellites was demonstrated through a preliminary mission design. Positive results show adequate propellant margins in the current design. All the major problems with the original blueprint are laid out, and solutions to fix them are proposed. For the design version shown above, the mother ship was anticipated to carry all six 12U CubeSats, together with a full 300 kg propellant load. The goal of this second design iteration is to see whether we can successfully deorbit one of the three CubeSats by letting it fall alone

off the launch pad. The three remaining satellites and the mother ship's remaining fuel will be utilized to detonate a second rocket stage[16].

A deorbiting platform is capable of approaching target debris, transferring it to an altitude orbit, and, in the case of a multiple-target operation, departing from the first target and approaching the second. Since these missions often have a large total impulse, electric propulsion (EP) is essential for reducing the propellant mass consumption required for every maneuver and, therefore, increasing the mass available to deorbit a sizable quantity of debris on every mission. To demonstrate the value of such a system, this paper examines the Alta HT-100 Hall effect thruster, a low-power, low-cost EP device. In this article, we provide the preliminary results of mission analysis and spacecraft design for an ADR mission employing a small platform equipped with an EP system. The chaser satellite was designed with a launch mass in the region of 200 kg after suitable mission and operating conditions were defined to meet the specifications of most existing secondary payload launch systems. To save mission time and expense, the spacecraft was developed using commercial off-the-shelf (COTS) components in mind for its primary subsystems. Several potential debris collection payloads have been suggested, with the D-Cone from the Politecnico di Milano, the Kraken robotic arm from Tethers Unlimited, and the harpoon capture device from Astrium being the most promising for the ADR mission. When considering the above list of physical and orbital characteristics, it has been shown that a high-specific-impulse EP system, such as the Alta HT-100 Hall effect thruster, may be used to target and deorbit up to five different types of trash on a single trip. Typically, a mission may deorbit 1.8 T of trash, spread among three distinct categories; in extreme situations, a single mission can deorbit more than 3 T of junk from the LEO zone. It has also been shown that a platform with the same initial mass and a chemical green propulsion system can deorbit merely 1 T of garbage every mission. However, there are advantages to executing an ADR mission with a chaser equipped with a chemical propulsion system in terms of total mission time, the complexity of the deorbiting phase, and the overall likelihood of collision with many other objects during the deorbiting phase. In addition, the total cost of the operation would climb dramatically if a separate mission were sent for every piece of orbital debris[17].

Table 1.1 Significant Research Methodologies

Author Name	Research Methodology
<b>Raguraman et al</b>	Review of various ADR techniques and challenges associated
<b>Guang et al</b>	Design of Space Tether Net System for ADR
<b>W. Barbee et al</b>	Design of spacecraft missions to remove multiple orbital debris objects
<b>Aleina et al</b>	Concept of a Reusable Space Tug
<b>Ali Aborehab et al</b>	Designed an efficient small satellite structure
<b>Fram et al</b>	A Review of SHERPA Space Tug
<b>Chamot</b>	Mission and System Architecture Design for active removal of rocket bodies in Low Earth Orbit
<b>Rimani et al</b>	Proposed Multidisciplinary Mission and System Design Tool for a Reusable Electric Propulsion Space Tug
<b>Udrea et al</b>	Designed a Multi-Satellite Mission for controlled ADR from LEO
<b>Y.Patel et al</b>	Designed mechanical, power, and propulsion systems for a CubeSat
<b>Noble et al</b>	Performed Design and Evaluation for an Orbital Debris Remediation System

## 2.2 Prior Work

In August 2021 ELSA-d completed its first demonstration of complex rendezvous and proximity operations in low earth orbit. This satellite is the world's first satellite whose mission is to perform testing of various capturing technologies in low earth orbit regimes for on-orbit operations and debris remediation. Currently, many other space-faring nations are involved in designing a space debris remediation satellite

## Chapter 3: Methodology

Both program and project-level methodologies are discussed below.

### 3.1 Program Level

This methodology describes the work that has been previously done, what is being done now, and what will be the future goal. The robotic arm which was developed at SSRL NUST along with the PNSS-1 of SUPARCO are the inputs to the current project. The parking orbit of PNSS-1 is used as the waiting/parking orbit of H2Z. By following the concurrent engineering approach mission design, system design, CAD modeling, and simulations were done simultaneously. These tasks were completed by the student team at the Department of Mechanical and Aerospace Engineering. While on the other hand, the student team from the Department of Electrical and Computer Engineering designed the Attitude Determination and Control System and the Telemetry Tracking Command System for H2Z.

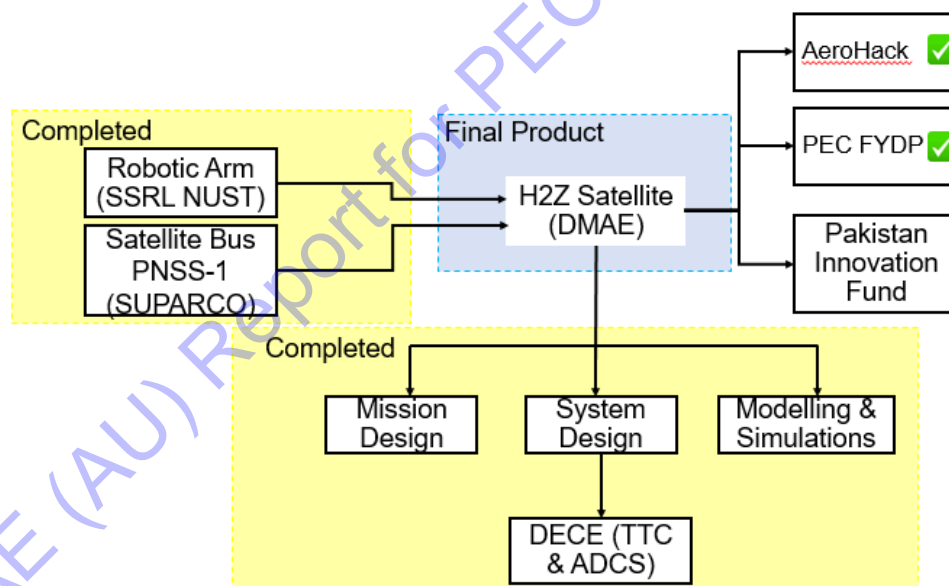


Figure 3.1 Program Level Methodology

### 3.2 Project Level

This project follows a concurrent engineering approach. As discussed earlier all three processes are being carried out simultaneously. The mission designer must first identify the debris which is followed by selection refinement and consequently, 5 debris are selected which are to be removed from their orbits. The next step is to design the parking orbit (for now the PNSS-1 parking orbit has been selected). The next and most

important step in mission design is to design the mission sequence and evaluate alternative mission strategies for the minimal energy mission design. This is an iterative process that leads to the design of different mission strategies for debris remediation. Simultaneously the system design begins by selecting a baseline design followed by the mass and power budget of the spacecraft. Consequently, the sub-systems are designed which include TCS, Propulsion, Payload (robotic arm and the camera), GNC, CDH, and EPS. This again is an iterative process that requires the component selection according to the spacecraft's needs.

The alternative design study of the mechanical bus is initially done by the CAD modeler which was then followed by the CAD modeling of the mechanical bus on SOLIDWORKS 2021. Subsequently, modal and static analyses, were performed for the bus using MSC NASTRAN/PATRAN Student Version 2022 and thermal analysis was performed on COMSOL Multiphysics 6.1.

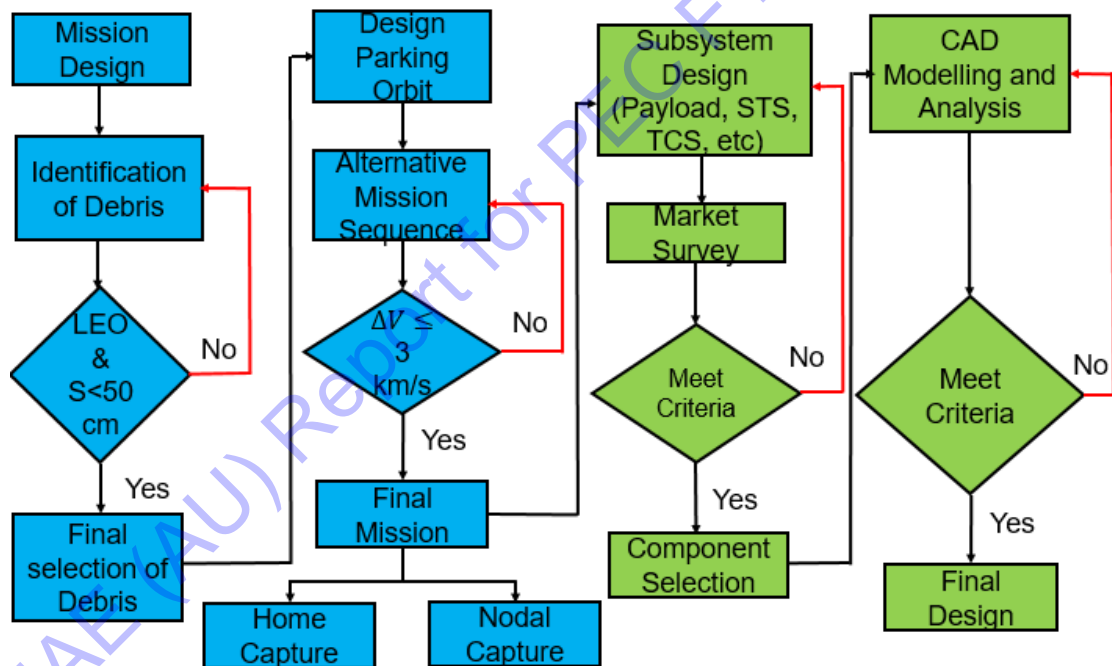


Figure 3.2 Project Level Methodology

### 3.3 Debris Selection Methodology

By using European Space Agency (ESA) database for debris (DISCOS) a total of 40 debris were selected that were in the sun-synchronous orbits. The debris whose size was less than 50 cm was selected. These debris pieces are fragments of the CZ-2C rocket body and weigh 1 kg each. All the initial orbital elements of the debris were noted from the DISCOS database.

The next step was to down-select the 5 debris that would cost less fuel for the mission. For this purpose, a primary mission sequence was designed i.e., Home Capture, the details of which are mentioned in the previous section of the report. The cost of each mission, which is represented by a variable delta V was calculated for each debris.

Next, a pseudo debris was made that had same orbital elements as of the H2Z and then each orbital element was varied one at a time while keeping others constant, and the delta V value was determined for the pseudo debris. The mathematical model is described in section 5.1

To determine which orbital elements, have a great effect on the delta-V of the mission, the design of experiment was made which comprised 64 different cases (6 orbital elements). It comprises 2 cases for each orbital element:

- Both debris and H2Z have identical values for a specific orbital element.
- Both debris and H2Z have different values for a specific orbital element.

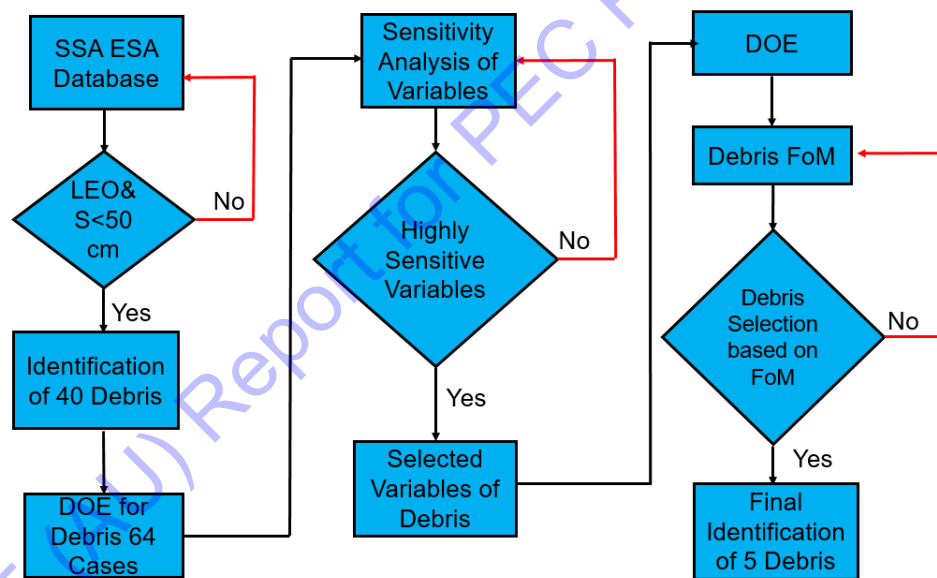


Figure 3.3 Debris Selection Methodology

## Chapter 4: System Concept Design

This chapter aims to present a comprehensive system concept design of H2Z. In order to accomplish this, an extensive trade-off study has been conducted, followed by requirements engineering and design exercises. Subsequently, the conceptual design of H2Z is developed. After highlighting all the essential system specifications, each subsystem is explained in detail, including its specific requirements and the product selected from the market.

### 4.1 System Tradeoff Study

The Secure World Foundation publishes a comprehensive annual report on global counter space operations that includes details of all missions involving rendezvous and proximity operations. This report proved to be an invaluable resource for our team, as we sought to identify suitable space tugs for our missions and benchmark values to size our spacecraft. By carefully analyzing the details of all the docking and RPO missions that have been conducted between 2003 and 2022, we were able to draft a list of potential candidate spacecraft. Further evaluation of these candidates helped us to identify the most suitable spacecraft for our mission requirements.

Following table shows all the candidate spacecraft which were seen to be the most relevant space tugs that can be benchmarked for our case.

Table 4.1 Relevant space tugs for benchmarking

Orbit	Chaser	Target	Mass in kg (chaser, target)
LEO	ASTRO	NEXTSat	700, 224
GEO	SJ-17	Chinasat 5A	4000, 2984
GEO	Mycroft	S5	100, 60
LEO	SJ-15	SY 7	2700, 204

Through an analysis of Table 4.1 and observing the general trend in [Sw 2022], it has been found that a chaser satellite can successfully tug a target with a mass ranging from 25 to 30 percent of the chaser's mass. To start the design process, it was necessary to carry out a system trade off study to understand the design philosophy of existing space tug. Table below constitutes of a system level comparison of the space tugs discussed in Table 4. 2 having mass in between 900 and 100 kg.



Table 4. 2 System Tradeoff study

Parameters	ASTRO	NEXTSat	Mycroft	SY7
Bus Dry Mass (kg)	250 kg	300	100	900
Size (m)	2.5x2.5x2.5	1.5x1.5x2.5	N/A	N/A
Power (W)	250	300	N/A	N/A
Pointing Accuracy (degrees)	N/A	0.01	N/A	N/A
Orbit	SSO	LEO	GSO	N/A
Compatible with Launch Vehicle	LauncherOne	Electron	Arian 6	Falcon Heavy
Design Life (years)	3	2	7	5

Due to the high amount of drag present in LEO and the necessary fuel requirements, a value of 900 kg was selected as the upper limit for H2Z's mass. This decision was made to ensure that the spacecraft's mass does not exceed the determined limit, allowing for successful execution of the mission.

## 4.2 H2Z Conceptual Design

Special consideration was given to the following design principles to ensure the long-term use of the design for future H2Z missions:

- Simplicity
- Compactness
- Modularity
- Accessibility for AIT (assembly, integration, and testing) and re-work
- Cost-effectiveness
- Manufacturability

### 4.2.1 H2Z System Specifications

Key specifications of the H2Z space tug are as follows:

- Mass  $\approx 900\text{kg}$
- Average Power  $\geq 600\text{W}$
- Payload
  - 4-DoF LiDAR based Robotic Arm
  - Colored Imaging Camera (Wide Swath)
- Data Transmission System UHF band, 256kbps

- Dimensions Cuboid (1 x 1 x 1.5 m)
- Solar Cell Body Mounted
- Pointing Accuracy  $<0.5^\circ$
- Communication Radio amateur VHF/UHF band
- TM Rate 1.2 kbps
- TC Rate 1.2 kbbs
- Thermal Control Passive with heaters

#### 4.2.2 H2Z System Preliminary Configuration

To be done as a part of later project.

#### 4.3 CAD Model

After going through multiple design iterations, the following CAD model was evolved which represented a tri-modular bus configuration with a volume of 1500U. The motivation of using the tri-modular bus configuration came from the tried and tested fully functional design of the PNSS-1 [SCR report]

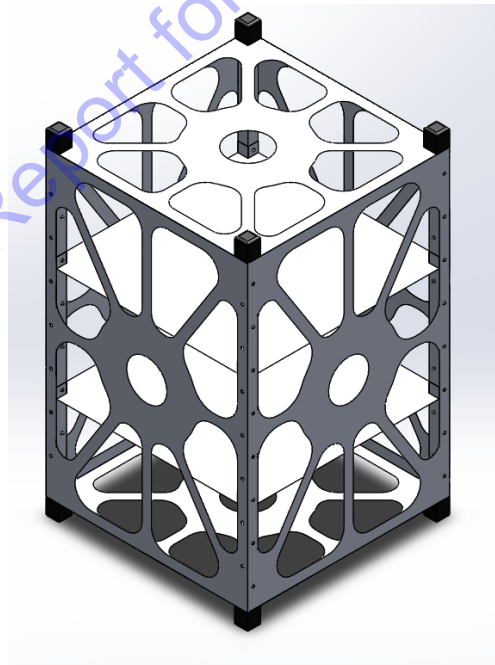


Figure 4.1 1.5U H2Z Mechanical Bus



Figure 4.2 H2Z with Launch Vehicle Adapter



Figure 4.3 Closed View of Mechanical Bus

Figure 4.4 shows the actual robotic arm developed at SERP Lab NUST, the components of which are listed in section 4.4.1 and section 6.3.1 while Figure 4.5 shows the concept demonstrator for the actual robotic arm.

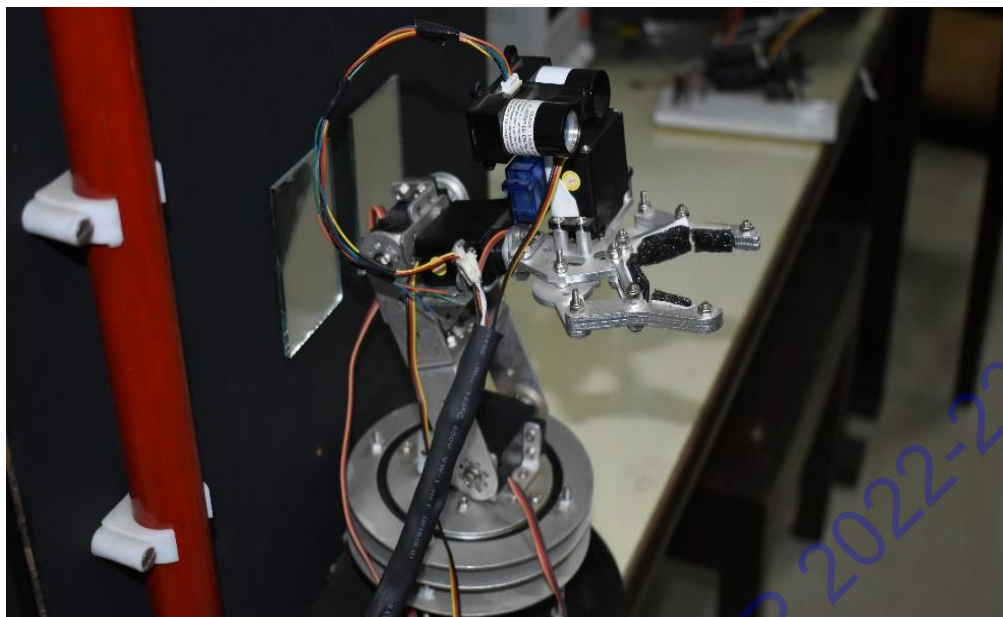


Figure 4.4 Actual Robotic Arm



Figure 4.5 Concept demonstrator for the Actual Robotic Arm



Figure 4.6 Concept demonstrator for the Actual Robotic Arm along with LiDAR

Following image shows the CAD model of the launch vehicle adapter, the details of which are mentioned in section 4.5.2.

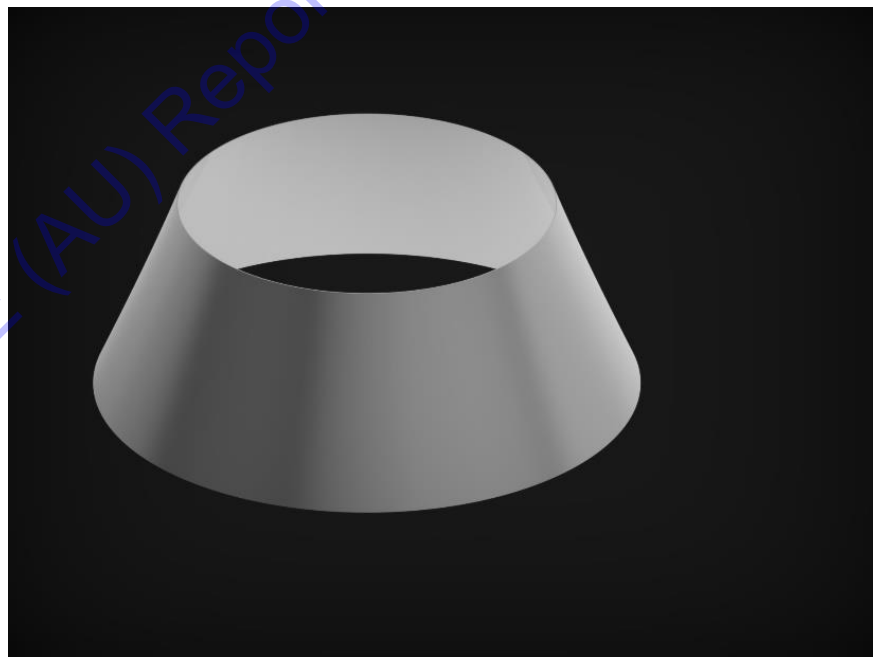


Figure 4.7 LV adapter

Following three modules were integrated in the H2Z mechanical bus making it a tri modular configuration

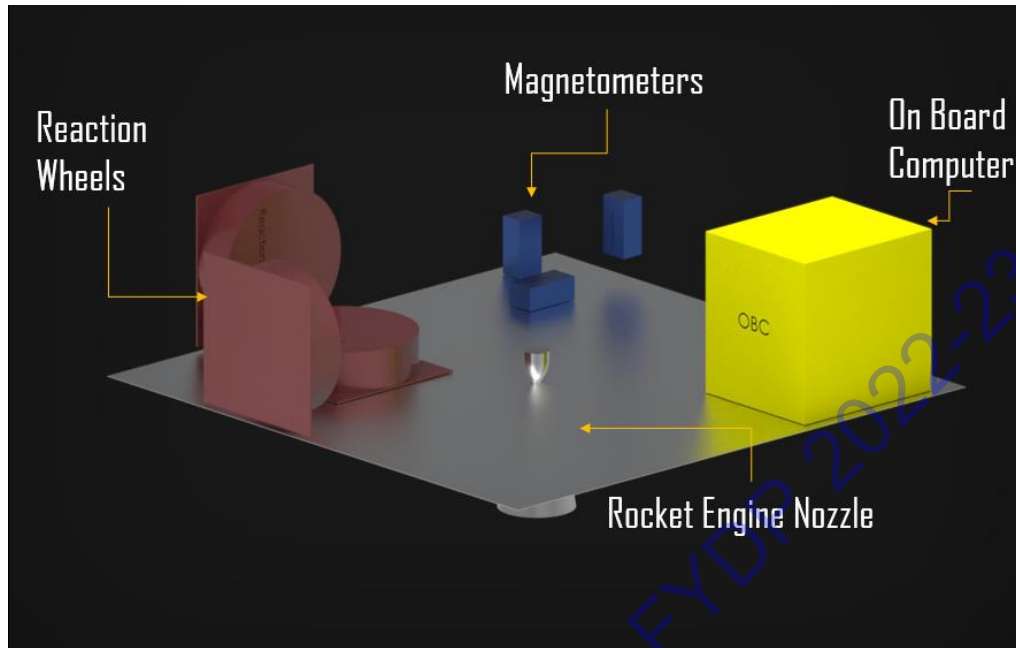


Figure 4.8 Module 1

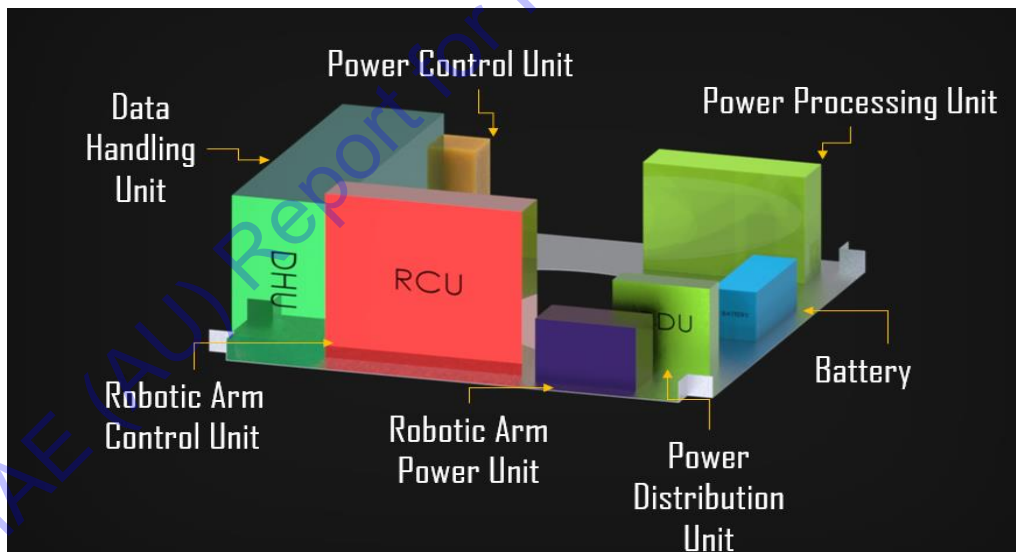


Figure 4.9 Module 2

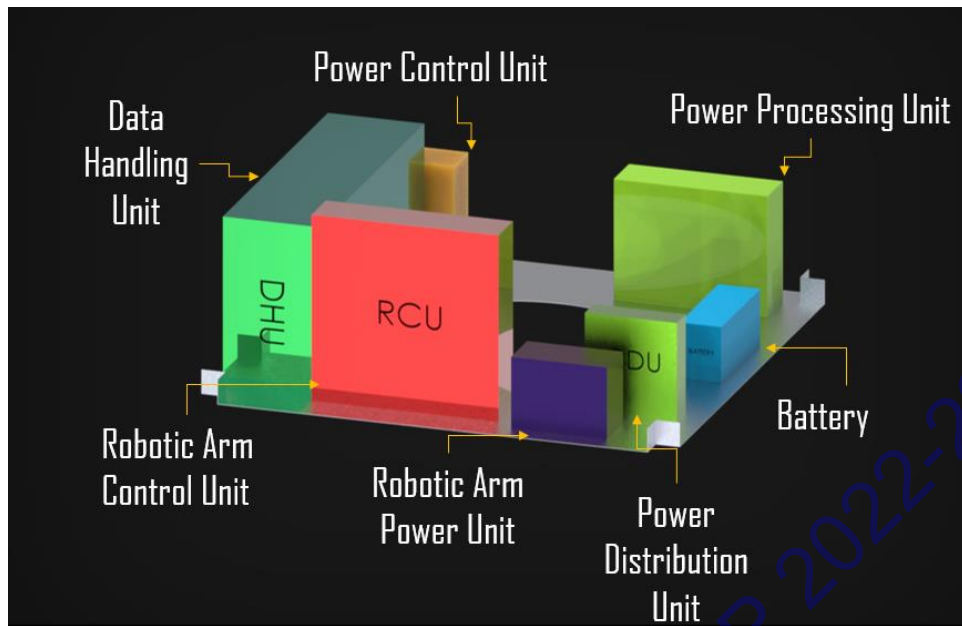


Figure 4.10 Module 3

Following is the propulsion module that was integrated in the H2Z mechanical bus.

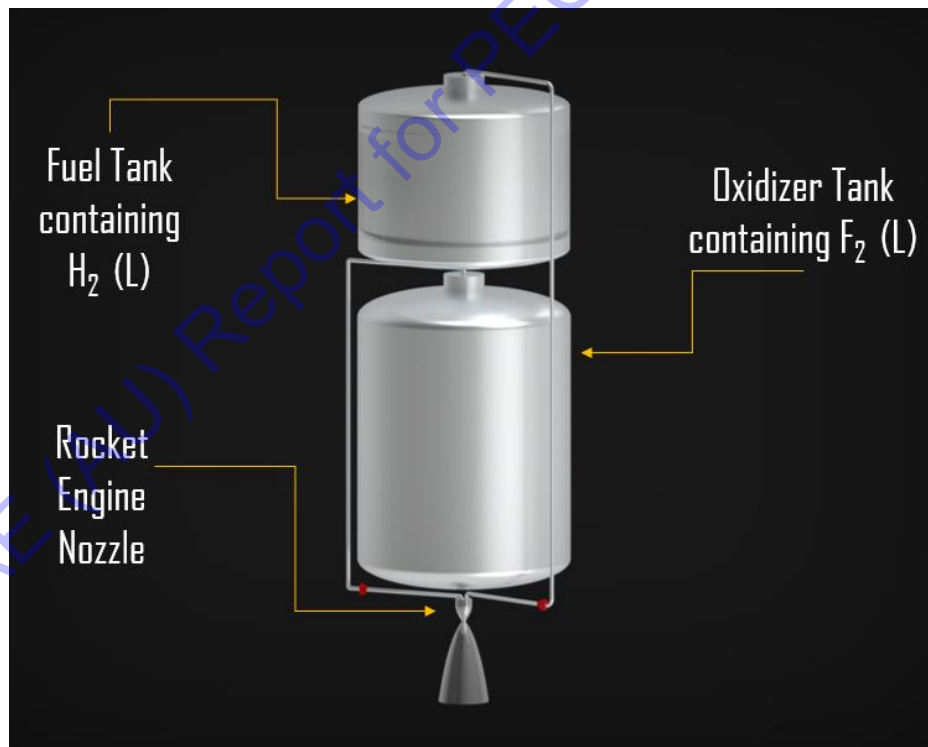


Figure 4.11 Propulsion Module

Image below shows the CAD model of main rocket engine nozzle, the details of which are mentioned in section 4.6 and section 6.3.3

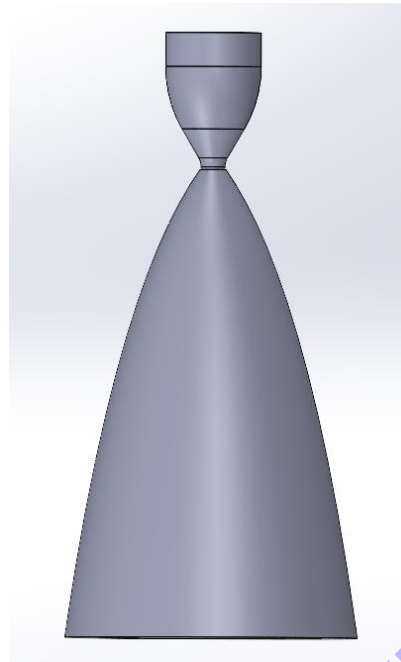


Figure 4.12 Rocket engine nozzle

#### 4.4 Payload Subsystem

Payloads refer to the scientific instruments, devices and equipment that interact with the subject to achieve the objectives of the mission. Payloads for space debris remediation missions may include tether net, harpoon systems and robotic arms, collecting, or removing debris from the Earth's orbit to ensure safe space exploration and operation. Selecting the appropriate payload for a space mission is crucial in achieving the intended objectives and ensuring mission success. Considering the mission sequence of H2Z, multiple payloads options were considered and extensively evaluated to determine the most suitable for the mission's requirements. The selected payloads for H2Z are as follows.

##### 4.4.1 Robotic Arm

H2Z uses a 4DoF Robotic arm as its primary payload. The design used in H2Z is influenced by the robotic arm that was developed at SERP Lab, NUST. This robotic arm will be used for capturing the debris in low earth orbit. This robotic arm uses actuators, motors and Arduino for its automation purposes. The specifications of the components attached in this robotic arm are attached in the form of tables of this section

#### I. Components:

##### Motors

- i. For Joint 1,2 and 3:



Table 4.3 Motor Specifications for Joint 1, 2 and 3

Power HD-9150MG	
Modulation	Digital
Torque	4.8V: 180.500z-in(13kg-cm)
Speed	4.8V: 0.20sec/60°
Weight	61grams
Dimensions	40.6min
Motor type	Coreless
Gear type	Metal
Rotation/ Support	Metal

- ii. For Joint 4 and for opening and closing of End effector:

Table 4.4 Motor Specifications for Joint 4 and End effector

HS-485HB	
Modulation	Analog
Torque	4.8V: 67.00 oz/in (4.82 kg-cm)
Speed	4.8V: 0.22sec/60°
Weight	45.1g
Dimensions	399mm (Length)
Motor Type	3-pole
Gear type	Plastic
Rotation/ Support	Single bearing

- iii. Motor used for Lidar-scan:

Table 4.5 Motor Specifications for LIDAR-Scan

Tower Pro SG90	
Modulation	Analog
Torque	4.8V: 25.00 oz-in (1.80kg-cm)
Speed	4.8V: 0.12sec/60°
Weight	9grams
Dimensions	Length: 23mm

Motor Type	3-Pole
Gear type	Plastic
Rotation/ Support	Bushing

**ARDUINO Mega 2560:**

Table 4.6 ARDUINO Mega 2560 Specifications

Microcontroller	AT mega 2560
Operating voltage	5V
Input Voltage (Recommended)	7-12V
Input Voltage (Limit)	6-20V
Digital I/O pins	54(off which 15 provide PWM output)
DC current per I/O pin	20mA
DC current for 3.3V pin	50ma
Flash memory	256Kb
SRAM	8Kb
EEPROM	4Kb
Clock speed	16Mhz
Length	101.52mm
Width	53.3mm
Weight	37g

**ARDUINO UNO:**

Table 4.7 ARDUINO UNO Specifications

Microcontroller	AT mega 2560
Operating voltage	5V
Input Voltage (Recommended)	7-12V
Input Voltage (Limit)	6-20V
Digital I/O pins	14(off which 6 provide PWAM output)
DC current per I/O pin	20mA
DC current for 3.3V pin	50ma
Flash memory	32Kb

SRAM	2Kb
EEPROM	1Kb
Clock speed	16Mhz
Length	68.6mm
Width	53.4mm
Weight	25g
Analog I/O Pins	6

### RF-Module

Table 4.8 RF Module Specifications

HC-12 RF Module	
Operating Voltage	5V
Transmission range	1000m
Working frequency range	433.4 – 473MHz
Maximum Transmitting power	100mV
Wireless receiving sensitivity	-117dBm
Idle current	16mA

### JOYSTICK

Table 4.9 Joystick Specifications

3KY – 023	
Operational Voltage	5V
Supply current	4.8mA to 11mA
Operating Temperature	-25° to 80°
Dimensions	4cm x 2.6cm x 3.2cm

#### 4.4.2 Imaging Payload

As a secondary payload for H2Z, SIMERA SENSE TriScape 200 is selected, which is consistent with the mission definition. This RGB color snapshot imager is primarily designed for earth observation applications on small satellites. A 65-megapixel CMOS (complementary metal oxide semiconductor) imaging sensor with RGB Bayer filter is used. At 10-bit pixel depth, it provides snapshot imaging at 30 frames per second at full resolution. It has a GSD of 1.5m and a ground

footprint of 14 km x 10.5 km at 500km altitude. Some other features of this imaging camera drafted from [18] are listed below:

- 65-megapixels (9344 x 7000)
- 10-bit pixel depth
- Up to 30 full resolution frames per second
- 1.5 m GSD (at 500 km orbit height)
- Ground footprint equal to 14 km x 10.5 km (at 500 km orbit height)
- Integrated RGB Bayer filter in the visible spectral range
- 128 Gigabyte non-volatile storage capacity for over 1000 full resolution image frames
- Control options include I<sup>2</sup>C, SPI, SpaceWire, RS422, CAN 2.0B
- Image data output options include LVDS, SpaceWire, USART
- Expected lifetime of more than five years

Major specifications of this imaging payload are listed below in Table 4.10

Table 4.10 Specifications of Imaging payload

<b>Optics</b>	
Focal length	1067 mm $\pm$ 1 mm
Aperture	190 mm
Full Field of View	1.6° (across-track); 1.2° (along-track)
<b>Imaging</b>	
Configuration	Snapshot, global shutter
Sensor technology	CMOS
Resolution	9344 x 7000 pixels
Pixel size	3.2 $\mu$ m
Pixel Depth	10-bit
Spectral filter	RGB Bayer with NIR blocking Filter (filter cut-off at 670nm)
Maximum Frame Rate	30fps
Power Supply	5 V DC $\pm$ 150mV
Power Consumption	2.5 W when idle or during readout. 5.8 W during imaging
<b>Mechanical</b>	
Mass	12.1 kg $\pm$ 2%
Dimensions	216 x 216 x 304 mm

Environmental	
Operating Temperature Range	-10 to 50 °C
Survivable Temperature Range	-20 to 60 °C
Sun-facing duration	Sun can be within FFOV for up to 3 minutes
Radiation (TID)	Tested beyond 25 kRad, without shielding, using a <sup>60</sup> Co source

#### 4.5 Structure Subsystem

The structure of things is what holds them together. It supports all load environments from pre-launch to launch, including on-orbit loads. H2Z is a cuboid shaped satellite made of solid Aluminum with T6 surface treatment. Following table shows the structural design specifications of H2Z.

Table 4.11 Specifications of structure subsystem

Specifications	
Shape	Cuboid
Dimensions	1m x 1m x 1.5m
Number of Panels	4 side panels (Rectangular) 2 panels for top & bottom (Square)
Panels material	Aluminum 6061
<b>Longerons</b>	
Material	Aluminum 6061
Number of Longerons	4
LV interface	Adapter ring
Scheme	Passive with few heaters Thermal Control Hardware

##### 4.5.1 Material Selection and Evaluation

Material selection is one of the important steps in structural design. This selection has very significant effects on structure such as mass, strength, reliability and manufacturing cost. Some important properties for material selection to be considered in structural design are listed in the Table 4.12. Aluminum alloy is the most used metal for spacecraft structures due to its strength, low density, and

availability. It is also easy to machine and relatively inexpensive. The stiffness-to-weight ratio of aluminum is like that of steel, but the strength-to-weight ratio is often higher. If harder or denser materials are required, steel or titanium may be chosen instead.

Table 4.12 Properties for material selection

Material Properties	Cost, Schedule and Risk
<ul style="list-style-type: none"> <li>• Stiffness (Young’s modulus &amp; Poisson’s ratio)</li> <li>• Ultimate &amp; Yield strength (Allowable stresses)</li> <li>• Ductility (Elongation)</li> <li>• Fatigue resistance &amp; fracture toughness</li> <li>• Mass density</li> <li>• Corrosion resistance</li> <li>• Creep resistance</li> <li>• Wear or galling resistance</li> <li>• Outgassing</li> <li>• Thermal conductivity, absorptivity &amp; emissivity</li> <li>• Thermal expansion</li> </ul>	<ul style="list-style-type: none"> <li>• Availability</li> <li>• Raw material cost</li> <li>• Machining and tooling cost</li> <li>• Ease of control in test processes</li> <li>• Changeability in critical properties</li> </ul>

Table below gives a comparison of most frequently used metal alloys in structural design

DMAE (AU) Report for PEC FYDP 2022-23

Table 4.13 Comparison of frequently used metal alloys

Material	Advantages	Disadvantages	Typical Applications
<b>Titanium</b>	<ul style="list-style-type: none"> <li>• High strength / weight ratio</li> <li>• Low thermal expansion coefficient</li> <li>• High and good thermal properties</li> </ul>	<ul style="list-style-type: none"> <li>• Hard to machine and form</li> <li>• Expensive</li> </ul>	<ul style="list-style-type: none"> <li>• Mechanical interface for advanced composite structures</li> <li>• Fastener (Especially used with graphite/matrix composites)</li> </ul>
<b>Aluminum</b>	<ul style="list-style-type: none"> <li>• High strength / weight ratio</li> <li>• Easily available</li> <li>• Low cost</li> <li>• Ductile</li> <li>• Easy to machine and form</li> <li>• High buckling resistance / weight ratio</li> <li>• Weldable</li> </ul>	<ul style="list-style-type: none"> <li>• Low strength / volume ratio</li> <li>• Low galling and abrasion resistance</li> <li>• High thermal expansion coefficient</li> <li>• High heat during welding decreases its strength</li> </ul>	<ul style="list-style-type: none"> <li>• Panel, beam, skin, frame, appendage structures and brackets</li> <li>• Face sheet for sandwich composites</li> </ul>
<b>Steel</b>	<ul style="list-style-type: none"> <li>• High stiffness and strength/volume ratio</li> <li>• Variations in different strength, hardness and ductility</li> <li>• Easy to machine</li> <li>• Weldable</li> <li>• Low cost</li> </ul>	<ul style="list-style-type: none"> <li>• High mass density; causes low buckling strength/weight ratio</li> <li>• Magnetic</li> </ul>	<ul style="list-style-type: none"> <li>• Fasteners (bolt, nut, washer, pin, insert, etc.)</li> <li>• Threaded parts</li> <li>• Gears</li> <li>• Bearings</li> </ul>

Design properties for some commonly used Metals are shown below,

Material Alloy and Form	$\rho$ 10 <sup>3</sup> kg/m <sup>3</sup> (lb/in <sup>3</sup> )	$F_{tu}$ 10 <sup>6</sup> N/m <sup>2</sup> (10 <sup>3</sup> lb/in <sup>2</sup> )	$F_{cy}$ 10 <sup>6</sup> N/m <sup>2</sup> (10 <sup>3</sup> lb/in <sup>2</sup> )	$E$ 10 <sup>9</sup> N/m <sup>2</sup> (10 <sup>8</sup> lb/in <sup>2</sup> )	$e$ %	$\alpha$ 10 <sup>-6</sup> /°C (10 <sup>-6</sup> /°F)
<b>Aluminum</b>						
2219-T851 1" Plate	2.85 (0.103)	420 (61)	320 (47)	72 (10.5)	7	22.1 (12.3)
6061-T6 Bar	2.71 (0.098)	290 (42)	240 (35)	68 (9.9)	10	22.9 (12.7)
7075-T73 Sheet	2.80 (0.101)	460 (67)	380 (55)	71 (10.3)	8	22.1 (12.3)
<b>Steel</b>						
17-4PH H1150z Bar	7.86 (0.284)	860 (125)	620 (90)	196 (28.5)	16	11.2 (6.2)
<b>Heat-Res. Alloy</b>						
A-286 2" Bar	7.94 (0.287)	970 (140)	660 (95)	201 (29.1)	12	18.2 (9.0)
Inconel 718 4" Bar	8.22 (0.297)	1280 (185)	1,080 (156)	203 (29.4)	12	12.2 (6.8)
<b>Magnesium</b>						
AZ31B H24 Sheet	1.77 (0.064)	270 (39)	165 (24)	45 (6.5)	6	25.4 (14.1)
<b>Titanium</b>						
Ti-6Al-4V Annealed Plate	4.43 (0.160)	900 (130)	855 (124)	110 (16.0)	10	8.8 (4.9)
<b>Beryllium</b>						
AMS 7906 Bar	1.85 (0.067)	320 (47)	—	290 (42)	2	11.5 (6.4)

Figure 4.13 Design properties for some commonly used Metals SMAD

In the above fig,

$\rho$  = Density

$F_{tu}$  = The Allowable Ultimate Tensile Stress.

$F_{cy}$  = Allowable Compressive Yield Stress.

$E$  = Young's Modulus.

$e$  = Elongation, a measure of ductility.

$\alpha$  = Coefficient of thermal expansion. The values given for  $\alpha$  in the figure are at room temperature.

Al-6061 meets the required criteria for material selection therefore, Aluminum 6061 was chosen as the structural material for the structure of space tug.

#### 4.5.2 Launch Vehicle Interface

Selection of a suitable LV interface which is compatible with the H2Z was also a critical step in the design process. Long March 3B is chosen as launch vehicle to be used for this mission.

The design team carefully evaluated the available options and ultimately chose the Long March 3B as the launch vehicle for the H2Z mission. The interface between the LV and the SC comprises both mechanical and electrical interfaces. The



mechanical interface ensures that the payload is mechanically mated with the LV, while the electrical interface is responsible for the electrical connection between the LV and SC [19]. The design team carefully evaluated the available options and ultimately chose the Long March 3B as the launch vehicle for the H2Z mission. The interface between the LV and the SC comprises both mechanical and electrical interfaces. The mechanical interface ensures that the payload is mechanically mated with the LV, while the electrical interface is responsible for the electrical connection between the LV and SC. 1194 Payload Adapter (Encapsulation-on-pad) is chosen as the mechanical interface for H2Z. The adapter is 650mm high with the largest diameter of 1748mm and the smallest diameter of 1215mm. Details of this mechanical interface are listed in [19]

### 4.5.3 Mass Budget

Mass Budget of H2Z is attached in the table below:

Table 4.14 Mass Budget

Sr. NO	Subsystem name	Mass (Kg)
1	ADCS	79.3
2	Thermal	22.08
3	Power	128
4	Structure	72.28
5	TTC	23.441
6	CDH	28.110
7	GNC	23.441
8	Payload	125.49
9	Propellant Mass	398.03
	Total Mass	900

### 4.6 Propulsion Subsystem

Propulsion systems in H2Z perform two major tasks.

- Perform orbital maneuvers.
- Provide thrust for attitude control and orbit corrections.

H2Z will use a chemical rocket engine as its main engine to perform orbital maneuvers and micro thrusters will be used for attitude corrections.

A chemical rocket engine involves the burning of fuel and oxidizer, which is used to raise the temperature and pressure of gas. This gas is then expanded in a Converging-Diverging nozzle to produce thrust. The main engine of H2Z shall use a liquid propellant. This decision of choosing an LPRE (Liquid Propellant Rocket Engine) is backed up by a strong comparative analysis provided in [20]. Table 4.15 lists the advantages and disadvantages of different types of chemical engines.

Table 4.15 Comparison between chemical engines

Type of Engine	Advantages	Disadvantages
Solid Propellant Rocket Engines (SPRE)	<ul style="list-style-type: none"> <li>• Simplicity in design and development, and easy handling and storage</li> <li>• High reliability, low detonation hazards, and easier multistaging</li> <li>• Lower development and production costs, particularly in the high-thrust range</li> </ul>	<ul style="list-style-type: none"> <li>• Lower specific impulse and difficulties in turning off operation compared to LPREs and HPREs</li> <li>• Cumbersome transport and handling of solid propellants, and challenges with thrust vector control and modulation</li> <li>• No active cooling possible, careful nozzle design needed to avoid erosion of throat area by high-temperature solid particles which can adversely affect performance.</li> </ul>
Liquid Propellant Rocket Engines (LPRE)	<ul style="list-style-type: none"> <li>• Achieve greater thrust for a given amount of propellant.</li> <li>• LPREs offer more precise thrust control and can be turned off and on as needed.</li> <li>• LPREs are less prone to nozzle erosion compared to SPREs, as they do not generate solid particles during operation.</li> </ul>	<ul style="list-style-type: none"> <li>• Typically, more complex to design, develop, and operate, which can lead to higher development and production costs.</li> <li>• Require complex and expensive feed systems to deliver propellants to the engine, which can also increase overall launch costs.</li> <li>• Require careful handling and storage of their volatile propellants, which can be hazardous and requires specialized facilities and personnel</li> </ul>
Hybrid Propellant Rocket Engines (SPRE)	<ul style="list-style-type: none"> <li>• HPREs are generally safer and less prone to catastrophic failure than LPREs due to their inherent design and lack of high-pressure liquid propellants.</li> <li>• HPREs can offer simpler and more cost-effective engine</li> </ul>	<ul style="list-style-type: none"> <li>• HPREs typically have lower specific impulse compared to LPREs, meaning they may require more propellant to achieve the same level of thrust.</li> <li>• HPREs can be more difficult to throttle or modulate compared to</li> </ul>

	designs compared to LPREs, as they do not require complex liquid propellant feed systems. <ul style="list-style-type: none"> <li>• HPREs are often more environmentally friendly than LPREs, as they can use non-toxic or low-toxicity propellants.</li> </ul>	LPREs due to the complexity of their combustion process. <ul style="list-style-type: none"> <li>• HPREs can be more difficult to design and develop compared to SPREs due to the need for specialized hybrid rocket technology expertise</li> </ul>
--	--	---

A hypergolic fuel with LF2/LH2 bipropellant is used for the main engine of H2Z. Reason for using this kind of high impulse fuel is driven by the requirement of producing high thrust with minimum propellant consumption. Some of the specifications of propellant after mixing contribute to the mathematical model as described in section 5.3.3 are listed in Table 4.16 below:

Table 4.16 Propellant Specifications

Propellant Specifications	
Propellant type	Liquid; Bipropellant
Hypergolic	Yes
Oxidizer	F <sub>2</sub> (L)
Fuel	H <sub>2</sub> (L)
O/F ratio	2.5
Specific Impulse (vacuum)	445.68s
Specific Impulse (optimum)	439.37
Molecular weight of products, $\mathfrak{M}$	6.2301 g/mole
Ratio of specific heats, k	1.234
Gas constant, R	1334.53717 J/kg-K

Selection of the nozzle contour offers several choices. Common nozzle geometries include conical, bell, de Laval and Rao. [21] give us the pros and cons of selecting each nozzle contour and allows us to select the suitable nozzle contour after doing a comparative analysis by listing all the key features of each type in table below.

Table 4.17 Comparison between different types of nozzle

Type of Nozzle	Key features
Conical nozzles	<ul style="list-style-type: none"> <li>• Simple in concept</li> <li>• Easy to manufacture</li> <li>• Thrust losses due to oblique shock formation when flow expands</li> <li>• Thrust loss due to radial velocity component at the exit plane</li> </ul>
deLaval nozzles	<ul style="list-style-type: none"> <li>• Minimized thrust losses</li> <li>• It is designed to expand the flow to minimize thrust losses from oblique shocks</li> <li>• Axial velocity profile at nozzle exit plane</li> <li>• But to maximize thrust, nozzle is relatively long, resulting in a larger mass and geometric envelope</li> </ul>
Rao nozzles	<ul style="list-style-type: none"> <li>• Expands the flow</li> <li>• Axial velocity profile at nozzle exit plane</li> <li>• Minimum length and thrust losses</li> <li>• Fabricating its contour is difficult compared to other designs</li> </ul>
Bell nozzle	<ul style="list-style-type: none"> <li>• Good performance</li> <li>• Simpler to design</li> <li>• Shorter and lighter</li> <li>• It turns and expands the flow with only small losses and produces a nearly axial flow at the nozzle exit plane</li> <li>• This combination of features makes it very popular</li> </ul>

The above listed comparative analysis of the nozzles compelled us to choose bell nozzle for our propulsion subsystem of H2Z.

#### 4.7 Attitude Determination and Control Subsystem

H2Z is a satellite that is stabilized along three axes and has a pointing accuracy of 0.5 to 1 degree. It has pointing stability that is better than 0.1 degree per second, and its pointing knowledge is better than 0.3 degrees. Figure 4.14 depicts the major components of a standard ADCS system.

In the H2Z system, the links between components play a critical role in identifying the major interactions that occur within the system. These links are depicted graphically using arrows, which indicate a cause-and-effect relationship. In other words, the arrows represent the channels through which information flows between different components of the system.

For instance, the satellite's structure is subject to time-varying torques from torquers, which are devices that generate or control torque. As a result of these torques, the structure shall respond with the attitude motion that will be detected by sensors. The outputs from these sensors are then sent to both on-board and ground control station computers, where they are analyzed to determine the torques that should be applied to the structure. This information is then sent back to the torquers via the same channels of communication [6]

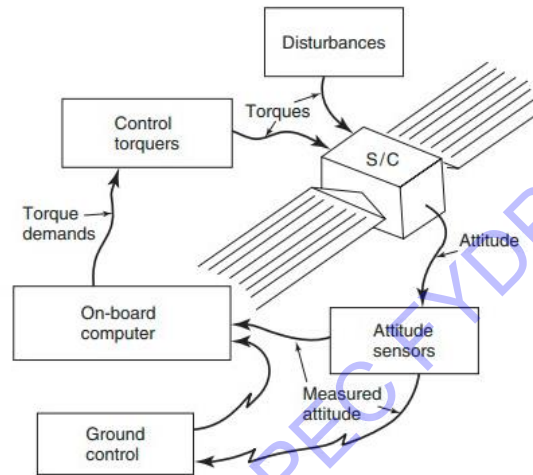


Figure 4.14 Major components of a general ACS system

The links between the components are crucial for ensuring that the system operates as intended. They enable the efficient flow of information between different components of the system, allowing for timely and effective decision-making. In addition, the arrows representing the links can be used to identify potential areas of concern or improvement within the system.

To ensure that the links between components are optimized, the EE team carefully evaluated the system requirements and identified the critical interactions between components. This thorough analysis has allowed the team to develop a system that is robust, reliable, and able to perform its intended functions with a high degree of precision.

The use of arrows to represent these links facilitates the identification of cause-and-effect relationships and potential areas for improvement. The careful analysis of system requirements and critical interactions has allowed the design team to develop a system that is optimized for performance and reliability.

Specifications of ADCS which will be used in H2Z listed by EE team in [22] are compiled in the Table 4.18 below

Table 4.18 Specifications in ADCS

Specifications	
Stabilization	3-Axis Stabilized Pointing knowledge $\geq 0.5^\circ$ (3-Axis)
Pointing Accuracy	$\geq 1^\circ$ (3-Axis, Imaging Mode) $\geq 5^\circ$ (3-Axis, Non-Imaging Mode)
Pointing Stability	$\geq 0.01^\circ$ (3-Axis, Imaging Mode) $\geq 0.1^\circ$ (3-Axis, Non-Imaging Mode)
Sensors	Earth sensors, Sun Sensor, Magnetometer
Actuators	Reaction wheels, Magnetorquers
Orbit Determination	Through GPS

Sizing of the momentum and reaction wheels along with the estimation of worst case disturbance torques are discussed in the section of results and analysis. A thorough market survey was conducted afterwards, on the result of which the commercially available components were selected as displayed in table below

Table 4.19 Selected market ADCS components

Component	No.	Model
Magneto Meters	3	Space Quest MAG-3
Sun Sensor	1	Red Wire Space (Fine Pointing Sun Sensor)
Earth/Horizon Sensor	2	Solar Mems HSNS
Star Tracker	1	Arsec saggita

Magnetic Torquer	3	ZARM-MT1-1
Reaction Wheels	3	RWA RW4-12.0
Micro thrusters	8	NASA C-POD MicroCubeSat propulsion unit

#### 4.8 Guidance Navigation and Control Subsystem

These systems are essential for spacecraft to achieve their intended mission objectives. GNC systems provide the ability to steer, maneuver, and maintain the spacecraft's position and orientation in space. We use navigation to refer to orbit determination, guiding to indicate orbit control, and the control system to denote attitude control system for satellite.

The guidance system is responsible for determining the spacecraft's trajectory and ensuring that it reaches the desired destination. Navigation systems use sensors and data from external sources to determine the spacecraft's location and velocity accurately. Control systems use this information to adjust the spacecraft's attitude, position, and velocity, enabling it to execute mission objectives.

The importance of GNC systems in spacecraft cannot be overstated, as they enable the spacecraft to operate autonomously in space, overcome obstacles, and achieve mission objectives. Without GNC systems, spacecraft would be unable to perform critical tasks such as docking, rendezvous, and landing.

Since ADCS is used as a separate subsystem, H2Z shall use GNC to only perform Orbit Determination and Control. Orbit control is required for satellite only when:

- Targeting to achieve an end orbit or position-as in satellite rendezvous altitude maintenance in low-Earth orbit or geosynchronous station-keeping.
- Constellation maintenance.

Observations for orbit determination can come from tracking on the ground, tracking from space, or from autonomous or semi-autonomous systems on the spacecraft.

Advantages and disadvantages of alternative navigation systems are show in the fig below

System	Advantages	Disadvantages
<i>Ground Tracking</i>	Traditional approach Methods and tools well established	Accuracy depends on ground-station coverage Can be operations intensive
<i>TDRS Tracking</i>	Standard method for NASA spacecraft High accuracy Same hardware for tracking and data links	Not autonomous Available mostly for NASA missions Requires TDRS tracking antenna
<i>Global Positioning System (GPS); GLONASS</i>	High accuracy Provides time signal as well as position	Semi-autonomous Depends on long-term maintenance and structure of GPS Orbit only (see text for discussion) Must initialize some units
<i>Microcosm Autonomous Navigation System (MANS)</i>	Fully autonomous Uses attitude-sensing hardware Provides orbit, attitude, ground look-point, and direction to Sun	First flight test in 1993 Initialization and convergence speeds depend on geometry
<i>Space Sextant</i>	Could be fully autonomous	Flight-tested prototype only— not a current production product Relatively heavy and high power
<i>Stellar Refraction</i>	Could be fully autonomous Uses attitude-sensing hardware	Still in concept and test stage
<i>Landmark Tracking</i>	Can use data from observation payload sensor	Still in concept stage Landmark identification may be difficult May have geometrical singularities
<i>Satellite Crosslinks</i>	Can use crosslink hardware already on the spacecraft for other purposes	Unique to each constellation No absolute position reference Potential problems with system deployment and spacecraft failures
<i>Earth and Star Sensing</i>	Earth and stars available nearly continuously in vicinity of Earth	Cost and complexity of star sensors Potential difficulty identifying stars

Figure 4.15 Alternative navigation systems [5]

We select Global Positioning System (GPS) for Orbit Determination and Control

Table 4.20 Specifications of GPS

Specifications of GPS	
Basis	Network of navigation satellites
Determines	Orbit
Typical accuracy ( $3\sigma$ )	15m-100m in LEO
Operating Range	LEO only
Comments	Semi-autonomous

PODRIX GNSS Receiver is selected as GPS system to be used for H2Z.

The multi-constellation and multi-frequency GNSS Precise Orbit Determination Receiver, called PODRIX, by RUAG Space, is suitable for LEO applications. It offers



an on-board real-time navigation solution with an accuracy of less than one meter. Key specifications along with the physical and environmental properties are listed in [23].

#### 4.9 Electrical Power Subsystem

The Electrical Power Subsystem (EPS) is one of the most critical subsystems in satellites. Its primary function is to provide reliable and uninterrupted electrical power to all other subsystems and payloads on the satellite. The EPS typically includes solar arrays for power generation, batteries for energy storage, power conditioning and distribution electronics, and thermal control systems to maintain safe operating temperatures. Without a properly functioning EPS, a satellite cannot function, and its mission could fail.

H2Z's electrical power subsystem will employ an unregulated MPPT scheme as well as a centralized power distribution model. H2Z will have a battery-regulated bus voltage of 28 V and a Li-ion battery as a backup power source. Triple Junction GaAs cells will be used in body-mounted solar panels to provide more than 600W of average output. Table 4.21 below represents the main specifications of the EPS.

Table 4.21 Specifications of EPS

Specifications	
Solar cells	AZUR Triple Junction (GaAS) Solar Cell 3G30C-Advanced
Solar array approach	Body mounted
Battery	Li Ion
Number of batteries	2 Batteries
Bus voltage	28 V
Bus type	Unregulated
Scheme	MPPT
Power distribution	Centralized
Power	>600 W

The H2Z system will utilize two Li-Ion batteries due to their significant advantages over other space batteries, providing redundancy and supporting the use of multiple batteries. Furthermore, H2Z uses body mounted solar cell approach because of the prior knowledge and experience in hands of our team from the previous projects of UmDan-1, AASMAN-2 and PNSS-1. Specifications of the battery are listed in the table below.

Table 4.22 Specifications of typical Li-ion battery

Battery Specifications	
Battery model	Li-ion Rechargeable Battery ABSL 8s3p 29.6V 8.4Ah
Voltage	29.6V
Capacity	8.4Ah
Energy	248.6Wh
Dimensions	176mm x 96mm x 98mm
Weight	1.66 kg

#### 4.9.1 Power Budget

Power budget table is constructed for eclipse and sunlight modes. Eclipse mode involves non-transmission and transmission modes, while sunlight mode involves the nominal and peak power mode which is also referred to as payload operation mode. Although payload shouldn't be operated during eclipse mode as it is the lowest power mode but it is necessary in case the space tug passes over our site of interest during eclipse. The Peak Power mode or payload operation mode consume the highest power requirements, so power requirements of this mode are considered for the solar array sizing. Moreover, during the sunlight solar arrays first meet the operational requirements of satellite and then charge the battery. Table 4.23 shows the power budget of H2Z.

- $T_{eclipse} = 36.26min$
- $Orbit\ Period = 98min$
- $T_{sunlight} = 61.74min$

From Table 4.23 we find that the average power required for sunlight phases ( $P_{sun}$ ) and average power required for eclipse phases ( $P_{eclipse}$ ) is 637.4W and 194.5W respectively

$$\text{Average Power Required for Sunlight Phases: } \frac{(642.8 \times 50 \times 60) + (610 \times 10 \times 60)}{60 \times 60}$$

$$P_{sun} = 637.47.1W$$

$$\text{Average Power Required for Eclipse phases: } \frac{(328.067 \times 25 \times 60) + (347.173 \times 10 \times 60)}{35 \times 60}$$

$$P_e = 194.5W$$

Table 4.23 Power Budget

<b>Power Budget</b>				
<b>H2Z</b>	<b>Sunlight (60min)</b>		<b>Eclipse (35min)</b>	
	<b>Peak Power (50 min)</b>	<b>Nominal Mode (10min)</b>	<b>Non-Transmission Mode (25min)</b>	<b>Transmission Mode (10min)</b>
ADCS	70	61	63	63
TCS	0	0	20	20
TTCS	80	80	80	80
EPS	172	150	65	75
CDHS	20	20	20	20
Propulsion	80	40	40	40
GNC	25	20.5	20.5	20.5
<b>Platform Total</b>	<b>447</b>	<b>371.5</b>	<b>308.5</b>	<b>318.5</b>
Robotic Arm	30	—	—	—
Camera	40	16.66666667	16.66666667	28.33333333
Battery Charging Requirement	120	217	—	—
Harness Losses	5.8	5.7	2.9	0.34
<b>Total Power Required</b>	<b>642.8</b>	<b>610.8666667</b>	<b>328.0666667</b>	<b>347.1733333</b>
Average Power Output From Solar Array	703.9151104	668.9456706	—	—
Margin (%)	8.682170543	8.682170543	—	—
Power Required From Battery	—	—	328.0666667	347.1733333
Battery DOD (%)	—	0	70	70
Average Margin (%)	8.682170543		N/A	

Two methods, ‘component efficiency method’ and ‘damage fluence method’ are thoroughly discussed in the section of mathematical modelling and then their results are compared in section of results and analysis. Some of the input parameters to be used in the method of component efficiency are attached in Table 4.24 below. While input parameters associated with damage fluence method are listed in Table 4.25

Table 4.24 Input parameters to component efficiency method

Input Parameter	Comments
$P_{array} = 925.159 \text{ W}$	Maximum size of solar array panels with oversizing effect
$S = 1400 \text{ W/m}^2$	Solar Flux
$\eta_{cell} = 30\%$	Solar cell efficiency for Tipple Junction GaAs cells
$\eta_{packing} = 90\%$	Cell packing efficiency
$D = 3\%$	Array degradation factor (9% ~ 3%)
$\delta\theta = 1\%$	Array pointing error
$\eta_{misc} = 2\%$	Miscellaneous degradation of the solar cell.

Table 4.25 Input parameters to damage fluence method

<b>Orbit type</b>	Sun-synchronous
<b>Altitude</b>	500km
<b>Inclination</b>	97.4065°
<b>Cell thickness</b>	0.30mm
<b>Cover slip (Shielding thickness)</b>	0.15mm
<b>Power at end of life</b>	925.159 W
<b>Life</b>	2 years

#### 4.10 Telemetry, Tracking and Command Subsystem

The TT&C subsystem between a satellite and its ground control station is responsible for telemetry, command, data handling, and processing functions. It facilitates the two-way transfer of information, with transmission (downlink) and reception (uplink) functions, and supports ranging and payload services. The system design depends on the mission, orbit, payload, and selected ground control station. [6].

Figure 4.16 depicts the context of the telemetry, command, and data-handling subsystem in relation to the other primary subsystems..

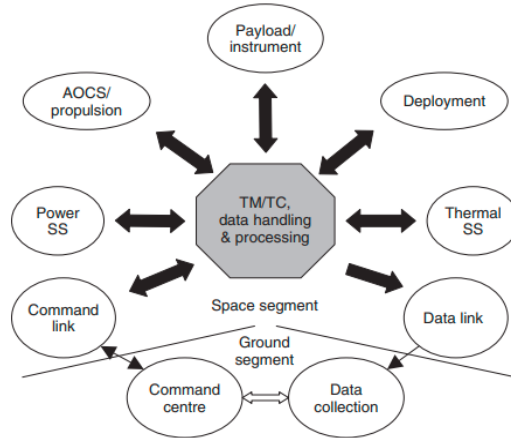


Figure 4.16 System context of TTC

H2Z will use UHF for downlink and VHF for uplink communication. The UHF/VHF antennas will have omnidirectional (4pi radians) coverage and a 0.5W transmitter power. The main specifications of this TT&C subsystem described by EE team is show in table below

Table 4.26 Specifications of TTCS

TM Downlink	
Frequency	UHF Band 434.9MHz
Data Rate	1.19kbps
Protocol	A.25
Modulation	AFSK
Satellite EIRP	4.5dBW
Ground Station G/T	-9.6dB/k
TC Uplink	
Frequency	VHF Band 145.9MHz
Data Rate	1.19kbps
Protocol	A.25
Modulation	AFSK

Mathematical model of the critical parameters of this system have been discussed in detail in Chapters of Mathematical modelling and Results. However the list of selected components are for TT&C subsystem is displayed in table below

Table 4.27 Selected Components of TT&C

Name	Type	Manufacturer
AstroSDR	SDR	Rincon Research Corporation
CubeCat	Optical Com	Hyperion Technologies
GPSRM 1 Kit	GNSS Reciever	Pumpkin
VHF Uplink + UHF Downlink Transceiver	Transceiver	Innovative Solutions In Space

#### 4.10.1 TT&C Link Budget

Link Budget of TT&C subsystem has been established for H2Z and is presented below.

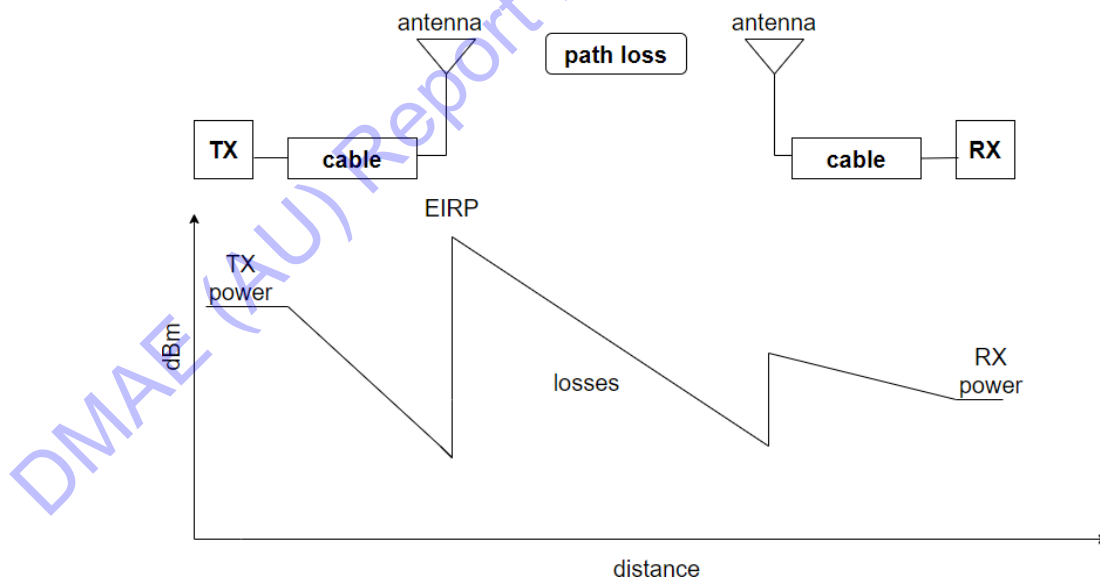


Figure 4.17 Link Budget

Table 4.28 TM Downlink Link Budget

<b>TM Downlink Link Budget</b>	
Carrier to noise density ratio C/No	64.21 dB
Energy per bit to noise density ratio Eb/No	33.21 dB
Received Isotropic Power	-155 dB
Receive Antenna Diameter Dr	2.34 m
Transmit Antenna Diameter	0.33 m
Half Power beamwidth	0.02
Noise Power N	0.14a w/Hz
Downlink Frequency	434.9
Orbit Height	500
Minimum Angle	10
Telemetry Transmit Output Power	0.5 W
Telemetry Transmit Antenna Gain	2 dB
Satellite Output Section / On Board Losses	8 dB
Satellite EIRP	4.5 dBW
Range of Satellite	1696.69 Km
Free Space Path Loss	149.80 dB
Atmospheric Losses	0.5 dB
Receive Antenna Gain	19 dB
Ground Station Antenna Mis Pointing	0.5 dB
Ground Station Coupling Losses	0.5 dB
G/T	-3.1 dBk
Received Power	-111.81dBm
Ground Station Sensitivity	-122
TC Carrier Recovery Margin	10.19 dB
Implementation and Demodulation	8 dB
Bandwidth of Input signal	0.05 MHz
TC Data Recovery Margin	12.75 dB

Table 4.29 TC Uplink Link Budget

<b>TC Uplink Link Budget</b>	
Carrier to noise density ratio C/No	78.54 dB
Energy per bit to noise density ratio Eb/No	47.78 dB
Received Isotropic Power	-114 dB
Receive Antenna Diameter Dr	0.3115 m
Transmit Antenna Diameter	4.937 m
Half Power beamwidth	0.46
Noise Power N	15.2a w/Hz
Orbit Height	500
Transmit Frequency	145.9
Minimum Angle	10
Transmit Antenna Gain	16 dB
Transmit BUC Power	75 watts
Transmit BUC Power	18.75 dBW
Transmit Chain Path Loss	6 dB
BUC Output Back OFF	3 dB
Transmit Antenna Mis pointing	0.5 dB
Transmit EIRP	26.75 dBW
Polarization Mismatch	0.5 dB
Satellite Receive Antenna Gain	-8 dB
Satellite Receive Chain Losses	8 dB
Satellite G/T	-42.58 dBK
Range of Satellite	1696.69 Km
Free Space Path Loss	140.31 dB
Atmospheric Losses	0.5 dB
Received Power	-102.06
Receiver Sensitivity	-108 dBm
TC Carrier Recovery Margin	5.94 dB
Implementation and Demodulation	8 dB
Bandwidth of Input signal	0.05 MHz
TC Data Recovery Margin	27.28 dB



### 4.11 Command and Data Handling Subsystem

The Command and Data Handling (C&DH) subsystem is used for managing and processing commands sent to a spacecraft or satellite and for collecting, processing, and storing data acquired by the spacecraft's various instruments and sensors.

The C&DH subsystem plays a critical role in the success of a spacecraft. It allows ground controllers to communicate with the spacecraft and send commands for performing various operations such as changing the spacecraft's orientation, adjusting its trajectory, or turning on or off its instruments. The C&DH subsystem also receives telemetry data from the spacecraft, which is used to monitor the spacecraft's health and status.

The C&DH subsystem's importance is highlighted in scenarios where a spacecraft may encounter unexpected events or anomalies, requiring it to switch to a safe mode or execute contingency plans. In such cases, the C&DH subsystem allows ground controllers to remotely reconfigure the spacecraft's operations, mitigate the issue, and resume the mission.

H2Z shall have a Centralized Data Bus scheme with RS 422 interface as well as CAN/I2C/RS 485/RS 232 interface. CDH Subsystem will perform the following functions:

- Bus Management
- Autonomous Operations

Key specifications of the CDH subsystem taken out from are listed in the table below

Table 4.30 Specifications of CDH

Specifications	
Data Bus	RS-422
Mass 0.99 Processing memory	9 kg
Power Consumption	< 38 W
Reliability	0.99
In-Orbit Life Time	Up to 20 years

The H2Z's Command and Data Handling Subsystem of choice is The OBC NG is the newest in a long line of on-board computers that have powered numerous LEO, MEO, GEO, and interplanetary missions.

Some processing functions and block diagram of the selected subsystem is shown in fig below. However a detailed list of specification can be seen in [24]

### Processing function

- SPARC V8 LEON FT
- 93 DMIPS @ 75 MHz
- 32 Kbytes instruction cache
- 16 Kbytes data cache
- 512 MiB processing memory
- 32 KiB Boot PROM
- 8 MiB SW Image Storage
- Gigabit Ethernet Debug Link
- Real-Time Processor Trace Dump
- Hardware Driver Software

### Block Diagram

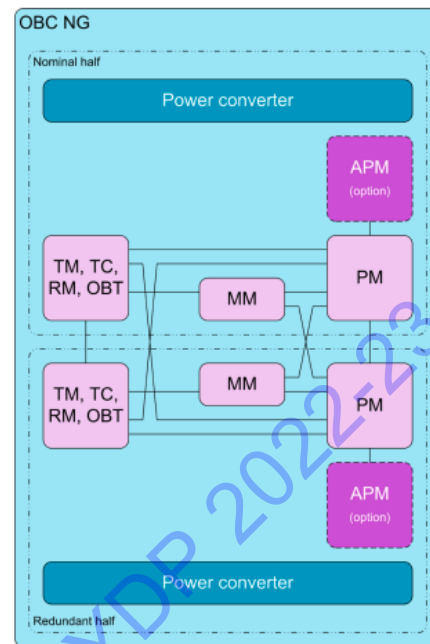


Figure 4.18 Interfaces and capabilities of CDH subsystem

### 4.12 Thermal Control Subsystem

The Thermal Control Subsystem is in charge of regulating the temperature of various spacecraft components within acceptable limits, despite the extreme thermal environments encountered during orbit. Effective thermal control is crucial for ensuring the reliability and performance of satellites. Temperature fluctuations can cause significant damage to onboard electronics, leading to malfunctions or even complete failure. Furthermore, excessive temperature variations can impact the accuracy of onboard sensors and instruments, affecting the quality of data collected.

The thermal control subsystem employs a combination of passive and active thermal control techniques to regulate the temperature of the satellite. Heaters, and heat pipes are examples for the active thermal hardware, and coatings, paints, multilayer insulation blankets (MLI), radiators, and thermal interface materials are example of passive thermal hardware. In addition, coatings, paints, multilayer insulation blankets, and radiators work with the radiation heat transfer principle, and heaters, heat pipes and thermal interface materials work with the conduction heat transfer principle [25]. Environmental heat loads are solar flux (1326-1417 W/m<sup>2</sup> for aphelion and perihelion, respectively but constant solar flux value is accepted by the space community as 1366.1

$W/m^2$ ), albedo (30% of the solar flux), Earth infrared emission ( $255\text{ K} = 240\text{ W/m}^2$ ) [26]

Figure 4.19 gives a representation of how a typical spacecraft thermal environment looks like

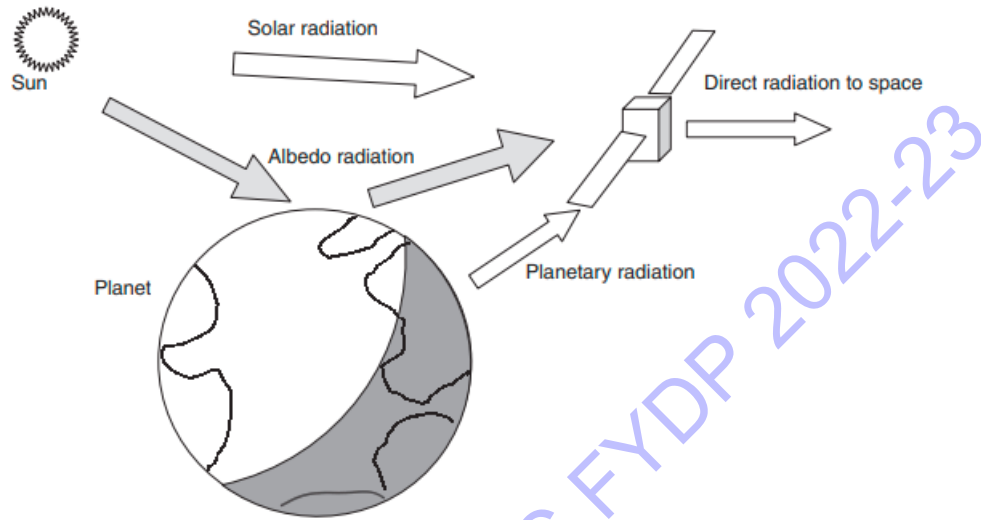


Figure 4.19 Thermal environment of a spacecraft

H2Z shall have a passive thermal design which will include the usage of MLIs, paints, coatings and conducting pastes.

Unit operating temperature ranges in Celsius are given below:

Table 4.31 H2Z Unit Temperature Ranges

Sr No	UNIT	T min	T max
1	TM/TC Transceiver	0	45
2	Imaging Payload (camera)	-10	50
3	Motor for Lidar-scan	0	55
4	Motor for Joint 1,2 and 3	-10	50
5	Motor for Joint 4 and closing of end effector	-20	60
6	Arduino Mega 2560	-40	85
7	Arduino Uno	-40	85
8	RF- Module	-40	85
9	Joystick	0	70
10	Filter, switches, isolators, etc	0	50
11	PCU	0	50
12	PDU	0	45

13	Battery	10	30
14	DHU	0	45
15	ACS-OBC	0	45
16	Sun Sensor	-40	85
17	Earth Sensor	-40	80
18	Reaction Wheel	-40	70
19	Magneto Torquer	-40	60
20	Magnetometer	-50	85
21	GPS Receiver	-30	60
22	Solar Array	-40	85
23	Antennae	-40	85

Paints are aimed to manage the Sun radiation and equipment heat conditions. Common paints are black and white; black paint is used to heat rejection inside of the satellite because absorptivity of the black is 0.95, and white paint is used for cooling because emissivity of the white paint is 0.87. Paints are applied to complex surface which are not appropriate to coating.

Multilayer insulation (MLI) and single-layer radiation shields are widely used in spacecraft for thermal control. MLI blankets are utilized to prevent both excessive heat loss and heating from environmental fluxes or rocket plumes. MLI blankets cover most spacecraft, with radiator areas cut out to reject internally generated waste heat. MLI blankets are applied to exterior components, antenna, batteries, propellant tanks etc [5]. Table below provides basic specifications of thermal control subsystem and also provides input to the mathematical model discussed in section 5.3.7 to find the average operating temperature of H2Z.

Table 4.32 Specification of TCS

<b>Scheme</b>	Passive with Paints, Coatings, Conductive Pastes
<b>Paints</b>	SG 21 FD White Paint Multi-Layer Insulation (MLI) Black Paint
<b>Absorptivity of material</b>	0.87

<b>Emissivity of material</b>	0.98
<b>Solar Flux</b>	1400 W/m <sup>2</sup>

#### 4.12.1 Dissipation Budget

To be done as a part of later project.

DMAE (AU) Report for PEC FYDP 2022-23

## Chapter 5: Mathematical Formulation

During its entire mission, the satellite will perform various maneuvers which will be supported by specific sub-systems. A complete mathematical formulation of both mission and systems is described below.

### 5.1 Debris Selection Math Model

The number of DOE cases was reduced, and the most sensitive variables were found by performing sensitivity analysis. For sensitivity analysis, a reference delta V value for each element was calculated by increasing the value of that specific orbital by 5%. Next, the orbital element was increased to 50% by an interval of 10% and each value was then non-dimensionalized.

$$\Delta V_x = \frac{\Delta V_{x_{ins}}}{\Delta V_{x_{ref}}} \quad 5.1$$

Where,

$x_{ins}$  is the percent increase in variable

$x_{ref}$  is the reference value (5% increase in the variable)

$\Delta V_{x_{ins}}$  is the delta-V at  $x_{ins}$

$\Delta V_{x_{ref}}$  is the delta-V at  $x_{ref}$

$x$  is the 5 orbital elements  $a, e, i, \Omega, \omega$

The  $\Delta V_x$  for each orbital element are shown below:

Table 5.1 Sensitivity Analysis Data

X	SMA	ECC	INC	RAAN	AOP
	$\Delta V_x$	$\Delta V_x$	$\Delta V_x$	$\Delta V_x$	$\Delta V_x$
5%	1	1	1	1	1
10%	1.084	1.069	1.263	1.496	1.001
20%	1.238	1.287	1.867	2.433	1.004
30%	1.373	1.478	2.487	3.251	1.006
40%	1.492	1.672	3.098	3.906	1.008
50%	1.598	1.877	3.694	4.361	1.008

Based on this sensitivity analysis a Figure of Merit Approach was adopted to establish selection criteria for the debris. The three sensitive variables were non-dimensionalized to the parking orbital elements of H2Z.

$$e^* = \frac{e_{debris}}{e_{PO}} \quad 5.2$$

$$i^* = \frac{i_{debris}}{i_{PO}} \quad 5.3$$

$$\Omega^* = \frac{\Omega_{debris}}{\Omega_{PO}} \quad 5.4$$

The figure of merit variable (overall mission efficiency) was then calculated: 5.5

$$\eta_o = [1 - (e^* i^* \Omega^*)] \Delta V$$

By using the overall mission efficiency 5 debris was selected for the mission.

## 5.2 Mission Math Model

Two mission sequences were analyzed in detail and their math model is as follows:

### 5.2.1 Home Capture

Home capture means grabbing the debris from its orbit by changing the chaser's orbit. This means the chaser goes into the debris orbit, grabs it, and then de-orbits it. The mission sequence is defined below:

- (1) H2Z performs Hohmann Transfer initially. This maneuver helps in changing the semi-major axis and eccentricity of the chaser's orbit. If the initial apogee altitude is higher then, the satellite performs maneuver at the apogee else at perigee.

Velocity at any point in an orbit can be determined by:

$$V_i = \sqrt{\mu \left( \frac{2}{r_i} - \frac{1}{a_i} \right)} \quad 5.6$$

The radial position of a satellite at any point in orbit can be determined by:

$$r_i = \frac{a(1 - e^2)}{1 + e \cos(\theta_i)} \quad 5.7$$

Velocity change at perigee:

$$\Delta V_p = V_{pt} - V_{pi} \quad 5.8$$

Velocity change at apogee:

$$\Delta V_a = V_{fa} - V_{at} \quad 5.9$$

Total Velocity change:

$$\Delta V_T = \Delta V_p + \Delta V_a \quad 5.10$$

The time of flight for the maneuver is:

$$T_f = \frac{\pi a^{\frac{3}{2}}}{\sqrt{\mu}} \quad 5.11$$

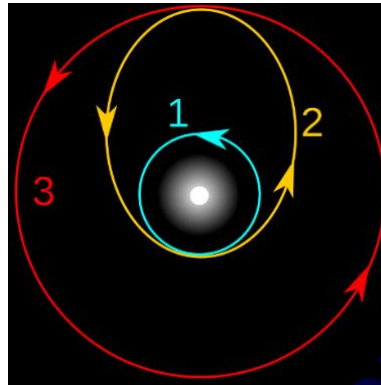


Figure 5.1 Hohmann Transfer

- (2) A general plane change maneuver is performed next to alter the right ascension of ascending node and the inclination of the H2Z orbit. For this purpose, the argument of latitude is determined first which tells the point of application of maneuver in the orbit.

The change of right ascension of ascending node is determined by:

$$\Delta\Omega = \Omega_d - \Omega_c \quad 5.12$$

The angle between two orbital planes is determined by:

$$\cos(\alpha) = \cos(i_d) \cos(i_c) + \sin(i_d) \sin(i_c) \cos(\Delta\Omega) \quad 5.13$$

The argument of latitude is determined by:

$$\cos u_c = \frac{\cos i_c \cos \alpha - \cos i_d}{\sin i_c \sin \alpha} \quad 5.14$$

The true anomaly of the point of application of maneuver is:

$$u_c = \theta_c + \omega_c \quad 5.15$$

Velocity change is determined by:

$$\Delta V = 2V_c \sin\left(\frac{\alpha}{2}\right) \quad 5.16$$



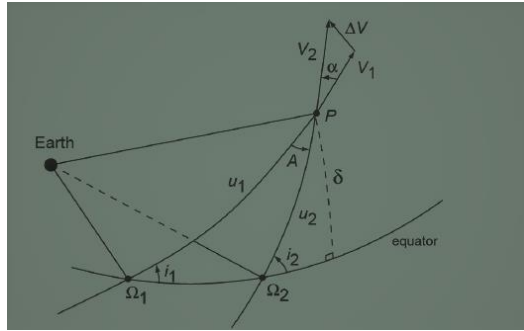


Figure 5.2 General Plane Change Maneuver

- (3) Apse Line Rotation Maneuver is now performed so that the apses line of the two orbits becomes collinear

The difference between the argument of perigee is:

$$\eta = \omega_c - \omega_d \quad 5.17$$

The angular momentum of an orbit is determined by:

$$h_i = \sqrt{r_p \mu (1 + e)} \quad 5.18$$

The coefficients are:

$$a = e_c h_d^2 - e_d h_c^2 \cos \eta \quad 5.19$$

$$b = -e_d h_c^2 \sin \eta \quad 5.20$$

$$c = h_c^2 - h_d^2 \quad 5.21$$

The angle from the local horizon to the delta-V vector is:

$$\Phi = \tan^{-1} \frac{b}{a} \quad 5.22$$

The true anomaly of the point of application of maneuver is:

$$\theta_{1,2} = \Phi \pm \cos^{-1} \left( \frac{c}{a} \cos \Phi \right) \quad 5.23$$

The tangential velocity of any orbit is:

$$v_{it} = \frac{h_i}{r_i} \quad 5.24$$

The radial velocity of the chaser's orbit is:

$$v_{cr} = \frac{\mu}{h_c} e_c \sin \theta_1 \quad 5.25$$

The radial velocity of debris orbit is:

$$v_{dr} = \frac{\mu}{h_d} e_d \sin(\theta_1 - \eta) \quad 5.26$$

The flight path angle is:

$$\gamma_i = \tan^{-1} \left( \frac{V_{ri}}{V_{ti}} \right) \quad 5.27$$

The velocity of the orbit is:

$$V_i = \sqrt{V_{ti}^2 + V_{ri}^2} \quad 5.28$$

The velocity change is:

$$\Delta V = \sqrt{V_1^2 + V_2^2 - 2V_1V_2 \cos(\gamma_1 - \gamma_2)} \quad 5.29$$

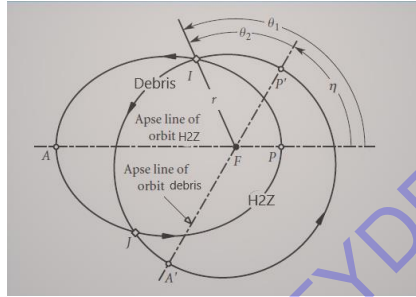


Figure 5.3 Apse Line Rotation Maneuver

- (4) Correction in semi-major axis and eccentricity. After performing the above maneuver there is a small change in the semi-major axis and eccentricity of the orbit. A Hohmann transfer is performed to compensate for this change. Since only a small change is desirable therefore it is less expensive in terms of cost.
- (5) Phasing Maneuver is now performed for space rendezvous. This rendezvous maneuver is used when two objects are in the same orbit. Depending upon the position of the chaser from debris there could be two types of orbits; phase in or phase out. This maneuver is always performed on perigee to get a low delta-V value. The mathematical model is described below:

The semi-major axis of the phasing orbit is determined by:

$$a = \left( \frac{T\sqrt{\mu}}{2\pi} \right)^{\frac{2}{3}} \quad 5.30$$

The change in velocity is determined by:

$$\Delta V_p = V_{pt} - V_i \quad 5.31$$

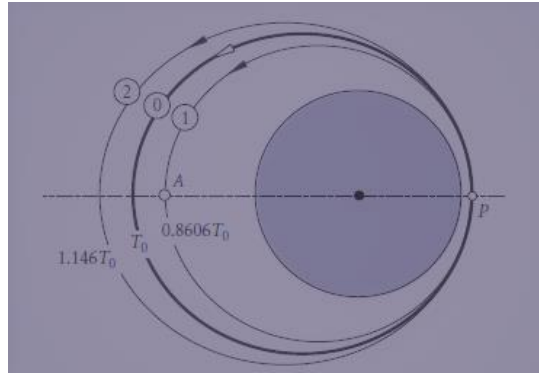


Figure 5.4 Phasing Maneuver

- (6) The next step is to perform terminal rendezvous but since it was beyond the scope of this project, this maneuver is not discussed here. Hohmann Transfer to re-entry altitude (150 km) is performed next for the disposal of the space junk. The eccentricity is also changed and the orbit is circularized to get the maximum effect of atmospheric drag on the debris.
- (7) Drop the debris at re-entry altitude. At this altitude, the second most important force after the gravitational pull is the atmospheric drag that will pull down the debris and cause it to burn in the atmosphere.
- (8) Hohmann transfer is performed next to get back to the parking orbit.
- (9) A general plane change maneuver is performed at last to change the right ascension of ascending node and the inclination of the H2Z orbit.

### 5.2.2 Node Capture

The home capture strategy is much more expensive as the value of the delta-V budget is very large. To reduce the cost of the mission another strategy was evolved which was 'Node Capture'. It means the chaser captures the debris while not changing its orbital plane. The mission sequence is defined below:

- (1) H2Z waits in its parking orbit for a certain amount of time so that when it performs the Hohmann transfer in the next step the relative angular difference of both objects is small (at least less than  $10^\circ$ , this ensures that the phasing orbit in step 3 would have a very small change in its semi-major axis, consequently leading to a small delta-V budget)
- (2) H2Z performs Hohmann Transfer initially. This maneuver helps in changing the semi-major axis and eccentricity of the chaser's orbit. If the initial apogee altitude is higher then, the satellite performs maneuver at the apogee else at perigee. This maneuver also ensures that the two orbits (H2Z and debris) intersect at two points in space. After this maneuver, the angular position difference between the objects is determined by plotting the argument of perigee and true anomalies of both objects on a circle just after the Hohmann transfer is done.

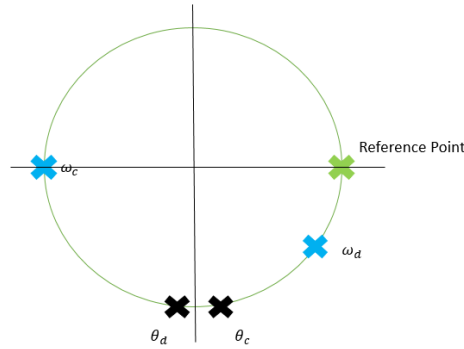


Figure 5.5 Angular difference between both objects

- (3) The next step is determining the intersection point of the two orbits. This point shall be the rendezvous point.

The change of right ascension of ascending node is determined by:

$$\Delta\Omega = \Omega_d - \Omega_c \quad 5.32$$

The angle between two orbital planes is determined by:

$$\cos(\alpha) = \cos(i_d)\cos(i_c) + \sin(i_d)\sin(i_c)\cos(\Delta\Omega) \quad 5.33$$

The argument of latitude is determined by:

$$\cos u_c = \frac{\cos i_c \cos \alpha - \cos i_d}{\sin i_c \sin \alpha} \quad 5.34$$

The true anomaly of the rendezvous point is:

$$u_c = \theta_c + \omega_c \quad 5.35$$

- (4) Phasing maneuver is now performed for space rendezvous. This rendezvous maneuver is used when two objects are in the same orbit. Depending upon the position of the chaser from debris there could be two types of orbits; phase in or phase out. The point of application of this maneuver is at the intersection point. The mathematical model is described below:

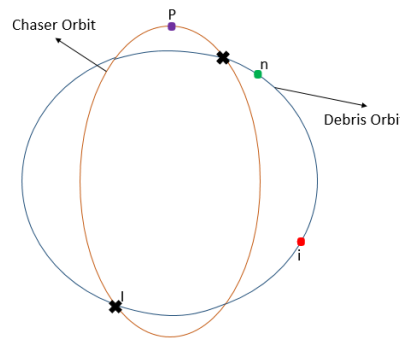


Figure 5.6 Orbits after Hohmann Transfer

The period of any orbit 'm' is determined by:

$$T_m = \frac{2\pi}{\mu^3} \left( \frac{h_m}{\sqrt{1 - e_m^2}} \right)^3 \quad 5.36$$

Determine the time since perigee to any point 'x' in debris orbit

$$t_{D,x} = \frac{T_D}{2\pi} (E_{D,x} - e_D \sin E_{D,x}) \quad 5.37$$

The period of phasing orbit is:

$$T_{C,phasing} = |t_{D,i} - t_{D,n}| + T_D \quad 5.38$$

The semi-major axis of the phasing orbit is determined by:

$$a = \left( \frac{T_{C,phasing} \sqrt{\mu}}{2\pi} \right)^{\frac{2}{3}} \quad 5.39$$

The change in velocity is determined by:

$$\Delta V = V_{pt} - V_i \quad 5.40$$

- (5) The next step is to perform terminal rendezvous but since it was beyond the scope of this project, this maneuver is not discussed here. Hohmann Transfer to re-entry altitude (150 km) is performed next for the disposal of the space junk. The eccentricity is also changed and the orbit is circularized to get the maximum effect of atmospheric drag on the debris.
- (6) Drop the debris at re-entry altitude. At this altitude, the second most important force after the gravitational pull is the atmospheric drag that will pull down the debris and cause it to burn in the atmosphere.
- (7) Hohmann transfer is performed at last to get back to the parking orbit.

### 5.3 System Math Model

A detailed discussion of the equations governing each subsystem of H2Z can be found in this section. The mathematical modeling of these subsystems provides a comprehensive picture of how H2Z functions. The incorporation of these equations into the design process facilitates a thorough and systematic approach to spacecraft development, ensuring that all critical parameters are taken into account and that the resulting design is robust and effective. There are many uncertainties and values associated with the commercially available subsystems addressed in Chapter 3 that have been considered to ensure the accuracy of the math behind these subsystems.

### 5.3.1 Payload Subsystem

#### 1. Imaging Payload:

This section presents the mathematical foundations underlying the imaging payload, with a focus on the equations that are essential for understanding key parameters such as Ground Sampling Distance, Swath width, and Angular field of view. These parameters are critical for designing an effective imaging system for space-based applications.

Ground Sampling Distance (GSD) refers to the distance between adjacent pixels in the image, and it determines the spatial resolution of the imaging system.

The smaller the GSD, the higher the resolution of the image, and the more detail that can be seen in the image. Table 5.2 clearly explains the concept of GSD.

Table 5.2 GSD Representation



<p>GSD of 5 cm means that one pixel in the image represents linearly 5 cm on the ground (<math>5 \times 5 = 25</math> square centimeters).</p>  <p>Figure 5.7 GSD 5 cm</p>	<p>A GSD of 30 cm means that one pixel in the image represents linearly 30 cm on the ground (<math>30 \times 30 = 900</math> square centimeters)[27]</p>  <p>Figure 5.8 GSD 30 cm</p>
---	---

Figure 5.9 shows Ground sampling Distance with respect to the Swath width (angular) and focal length of the lens

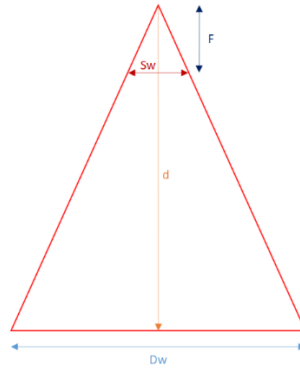


Figure 5.9 Ground Sampling Distance [27]

GSD of the Imaging Payload is given by Triangle Law which is:

$$GSD = \frac{h * \text{pixel size}}{\text{focal length}} \quad 5.41$$

Swath width is the width of the land strip viewed by a sensor in a single scan. It is determined by the sensor's field of view and altitude above the ground. Wider swath width can cover more area in one pass and benefits applications like mapping and environmental monitoring. However, it may lead to a decrease in spatial resolution due to a larger coverage area [28].

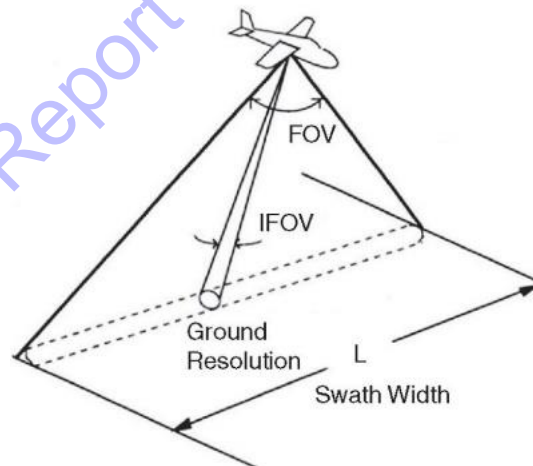


Figure 5.10 Swath width Representation

Swath width is given by the following set of equations:

$$\sin \rho = \frac{R_E}{R_E + h} \quad 5.42$$

$$\sin n = \cos \epsilon \sin \rho \quad 5.43$$

$$\lambda = 90 - n - \epsilon \quad 5.44$$

$$SW = 2\lambda \quad 5.45$$

A satellite's Angular Field of View (AFOV) is the total solid angle its sensor can view. Wider AFOV lets the sensor capture a larger ground area but decreases spatial resolution, making AFOV a trade-off between coverage area and image resolution. Selection of the AFOV depends on the specific requirements of the application. Angular field of view is given by:

$$\theta_{FOV} = 2 \tan^{-1} \frac{d}{2f} \quad 5.46$$

## 2. Robotic Arm:

The fundamental equations of relative motion analysis using both translating and rotating axes are given below:

The position of point B with reference to A is given by: 5.47

$$\mathbf{r}_B = \mathbf{r}_A + \mathbf{r}_{B/A}$$

Where,

$\mathbf{r}_B$  is the position vector of point B

$\mathbf{r}_A$  is the position vector of point A (Origin)

$\mathbf{r}_{B/A}$  is the relative position vector of point B with respect to A

The velocity of point B is given as:

$$\mathbf{v}_B = \mathbf{v}_A + (\boldsymbol{\Omega} \times \mathbf{r}_{B/A}) + (\mathbf{v}_{B/A})_{xyz} \quad 5.48$$

Where,

$\mathbf{v}_B$  is the velocity vector of point B

$\mathbf{v}_A$  is the velocity vector of point A (Origin of xyz frame of reference)

$\mathbf{v}_{B/A}$  is the relative velocity vector of point B with respect to A as measured by an observer attached to the rotating frame of reference

$\boldsymbol{\Omega}$  is the angular velocity of the frame of reference



$\mathbf{r}_{B/A}$  is the relative position vector of point B with respect to A

The acceleration point B is determined by:

$$\mathbf{a}_B = \mathbf{a}_A + (\dot{\Omega} \times \mathbf{r}_{B/A}) + \Omega \times (\Omega \times \mathbf{r}_{B/A}) + 2\Omega \times (\mathbf{v}_{B/A})_{xyz} + (\mathbf{a}_{B/A})_{xyz} \quad 5.49$$

Where,

$\mathbf{a}_B$  is the acceleration vector of point B

$\mathbf{a}_A$  is the acceleration vector of point A (Origin of xyz frame of reference)

$\mathbf{v}_{B/A}$ ,  $\mathbf{a}_{B/A}$  are relative velocity and acceleration vectors of point B with respect to A as measured by an observer attached to the rotating frame of reference

$\Omega$ ,  $\dot{\Omega}$  is angular velocity and angular acceleration of the frame of reference

$\mathbf{r}_{B/A}$  is the relative position vector of point B with respect to A

### 5.3.2 Structure Subsystem

The mathematical model of this subsystem encapsulates the essential equations used to perform an initial spacecraft sizing. Equations 3.49 to 3.52 provide the fundamental math behind the initial sizing of any cuboid-shaped satellite. Through the use of this model, engineers and researchers can effectively evaluate the feasibility of a given design concept and make informed decisions regarding the spacecraft's structural characteristics and performance. Volume of the spacecraft is given by:

$$V = 0.01M \quad 5.50$$

Linear Dimension is given by:

$$s = 0.25M^{\frac{1}{3}} \quad 5.51$$

Cross-Sectional Area and Moment of Inertia are given by:

$$A_b = s^2 \quad 5.52$$

$$I = 0.01M^{\frac{5}{3}} \quad 5.53$$

### 5.3.3 Propulsion Subsystem

This section outlines the fundamental equations that underpin the design of the main rocket engine for the H2Z.

The mass of the Propellant which is consumed in the entire mission is calculated through equation 3.53 while the total time in which the entire propellant was consumed also known as burn time is given by equation 3.54.

$$m_p = m_o \left[ 1 - e^{-\left(\frac{\Delta V}{I_{sp}g_o}\right)} \right] \quad 5.54$$

$$t_b = \frac{m_i}{\dot{m}} \left[ 1 - e^{-\left(\frac{\Delta V}{I_{sp}g_o}\right)} \right] \quad 5.55$$

The mass of the propellant is a key factor in the derivation of individual fuel and oxidizer masses [21], as outlined in equations 3.55 and 3.56 . These individual masses play a crucial role in the sizing of the propellant tanks required for the spacecraft.

$$m_{fuel} = \frac{m_p}{1 + O/F} \quad 5.56$$

$$m_{ox} = \frac{m_p(O/F)}{1 + O/F} \quad 5.57$$

Exhaust Velocity refers to the speed at which the propellant is expelled from the engine nozzle. It is a crucial parameter in determining the amount of thrust that the engine can generate. The exhaust velocity of a Liquid propellant engine is given by equation 3.57 while equation 3.58 gives the main equation for the thrust that the engine will generate [7]

$$v_2 = \sqrt{\frac{2k}{k-1} RT_1 \left[ 1 - \left(\frac{p_2}{p_1}\right)^{\frac{(k-1)}{k}} \right]} \quad 5.58$$

$$F = \dot{m}I_{sp}g_o \quad 5.59$$

While designing a rocket engine, sizing the throat is very critical as it ensures the maximum flow of propellant through the engine resulting in maximum thrust. Similarly, if the temperature in the throat is too high, it can lead to thermal degradation of nozzle materials which can compromise the structural integrity of the engine. Conversely, if the temperature is too low, it can reduce the engine's efficiency and thrust. Throat Area and temperature are given by.

$$A_t = \frac{\dot{m}}{p_1} \sqrt{\frac{RT_1}{k[2/(k+1)]^{(k+1)/(k-1)}}} \quad 5.60$$

$$T_t = \frac{2T_1}{k+1} \quad 5.61$$

Equation 5.62 can be used to account for  $C_f$  and offers a relationship for calculating the thrust coefficient experimentally using the data of chamber pressure, throat diameter, and thrust. The thrust coefficient is a dimensionless yet critical analysis parameter. The thrust coefficient can be thought of as the amplification of thrust caused by the gas expanding in the supersonic nozzle as compared to the thrust that would be exerted if the chamber pressure just operated on the throat region. The thrust coefficient ranges from roughly 0.8 to 1.9 [7].

$$C_F = \frac{F}{A_t p_1} \quad 5.62$$

The combustion chamber must be large enough to allow the propellants to completely mix, atomize and burn. Detailed analysis of these coupled processes is complex and is still based on empirical data. [21] gives all the fundamental equations required for chamber design and sizing. The combustion chamber's characteristic length ( $L^*$ ) can be defined as:

$$L^* = \frac{V_c}{A_t} \quad 5.63$$

Next, we need to determine the Length and Diameter of the combustion chamber which can be calculated using:

$$\frac{A_c}{A_t} = \frac{1}{M} \left[ \left( \frac{2}{\gamma + 1} \right) \left( 1 + \frac{k-1}{2} M^2 \right) \right]^{\frac{k+1}{2(k-1)}} \quad 5.64$$

$$L_c = L^* \frac{A_t}{A_c} \quad 5.65$$

We must understand that  $L_c$  is the length of the combustion chamber up to the converging part of the nozzle and  $L_{con}$  is the length from the converging cone entrance to the nozzle throat, this can be approximated as:

$$L_{con} = \frac{D_c - D_t}{2 \tan \beta} \quad 5.66$$

Now we can find the volume of the combustion chamber if we simplify things by assuming a simple circular cylinder.

$$V_c = A_c L_c = \frac{\pi D_c^2}{4} L_c \quad 5.67$$

For conical nozzles, the length of the nozzle depends on the divergence half-angle ( $\theta_{cn}$ ). The greater the divergence angle, the shorter the nozzle for a given expansion ratio. However, an increased divergence angle means a greater thrust loss because the radial-velocity component increases. This effect is captured in the nozzle efficiency, which for an inviscid conical nozzle is.

$$\lambda = \frac{1}{2} (1 + \cos \theta_{cn}) \quad 5.68$$

For a conical nozzle with a circular cross-section, the length of the diverging section is given by:

$$L_n = \frac{D_e - D_t}{2 \tan \theta_{cn}} \quad 5.69$$

We use parabolic – geometry approximation to find out the bell nozzle dimensions. A routinely used term for designing bell nozzles is the “percent bell”: 80% bell and 70% bel, and so on. The phrase refers to the length of the bell nozzle compared to the 15° conical nozzle.

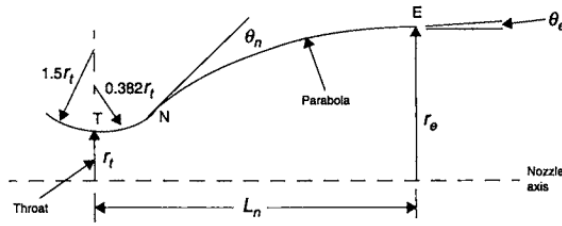


Figure 5.11 Nozzle Contour [21]

The upstream throat contour is circular, with a radius of 1.5 times the throat radius. Similarly, the downstream throat contour is also circular, with a radius 0.382 times the throat radius.

$$r_{upstream} = 1.5r_t \quad 5.70$$

$$r_{downstream} = 0.382r_t \quad 5.71$$

However, to find the length of the bell nozzle we know that:

$$L_n = 80\% \text{ of (length of } 15^\circ \text{ conical nozzle)}$$

### 5.3.4 Attitude Determination and Control Subsystem

This section presents the fundamental equations that underpin the design of the ADC (Attitude Determination and Control) subsystem in compliance with the mission objectives of the H2Z spacecraft. The equations presented below have been carefully selected from [22] to provide a comprehensive overview of the key considerations involved in the design of the ADC subsystem. With these equations, we can accurately model the behavior of the spacecraft and ensure that it maintains the desired attitude and orientation throughout the mission. By incorporating these critical equations into the overall design process, the ADC subsystem can be optimized for maximum performance, reliability, and operational efficiency.

Firstly, the size of external torques which the ADCS must tolerate is determined. Only three or four sources of torque matter for the typical Earth-orbiting spacecraft. They are gravity-gradient effects, magnetic-field torques on the vehicle, impingement by solar-radiation, and, for low-altitude orbits, aerodynamic torques. Equations 3.71 to 3.74 account help us in estimating the worst-case disturbance torques.

Gravity gradient is given by:

$$T_g = \frac{3\mu}{2R^3} |I_z - I_y| \sin(2\theta) \quad 5.72$$

Solar Radiation is given by:

$$T_{sp} = F(c_{ps} - c_g) \quad 5.73$$

Magnetic Field is given by:

$$T_m = DB \quad 5.74$$

Aerodynamic torque is given by:

$$T_a = F(c_{pa} - c_g) = FL \quad 5.75$$

The following equations show the fundamental mathematics involved in sizing reaction wheels, momentum wheels, and magnetic torquers.

Slew Torque for Reaction Wheels is given by:

$$\frac{\theta}{2} = \frac{1}{2} \frac{T}{I} \left(\frac{t}{2}\right)^2 \quad 5.76$$

$$T = 4\theta \frac{I}{t^2} \quad 5.77$$

Momentum Storage in Reaction wheels is given by:

$$h = (T_D) \frac{(\text{Orbital Period})}{4} \quad (0.707) \quad 5.78$$

Momentum Storage in Momentum Wheels is given by:

$$T \times \frac{P}{4} = h \theta a \quad 5.79$$

Momentum Storage in Spinner is given by:

$$w_s = \frac{h}{I} \quad 5.80$$

Torque from Magnetic Torquers is given by:

$$D = T/B \quad 5.81$$

### 5.3.5 Telemetry, Tracking, and Command Subsystem

In this section, we present the fundamental equations that form the basis of the design of the TT&C (Telemetry, Tracking, and Command) Subsystem in compliance with the

mission objectives of the H2Z spacecraft. These equations have been carefully selected from [22] to provide a comprehensive overview of the key considerations involved in the design of the TT&C subsystem. This section provides the fundamental equations of both TM Downlink and TM Uplink.

The term carrier-to-noise density ratio refers to the strength of the signal received by a ground station from the spacecraft, relative to the level of noise present in the receiving system and is given by the following equations:

$$\frac{C}{N_o} = EIRP + L_S + L_a + \frac{G_T}{T_S} + 228.6 \quad 5.82$$

$$EIRP = P + L_e + G \quad 5.83$$

$$L_S = 20 \log c - 20 \log 4\pi - 20 \log S - 20 \log f \quad 5.84$$

$E_b/N_o$  is a measure of the energy per bit of transmitted data relative to the noise density in the communication channel. A higher  $E_b/N_o$  value indicates a stronger signal relative to the noise level, which can result in a higher data transfer rate and/or a more reliable data transfer. RIP, on the other hand, is a measure of the power of the signal received by the ground station from the spacecraft. It takes into account the distance between the satellite and the ground station, as well as the orientation of the satellite's antenna and the ground station's antenna.

Energy per bit to noise density is:

$$\frac{C}{N_o} = \frac{E_b}{N_o} + 10 \log R \quad 5.85$$

Received Isotropic Power is determined by:

$$RIP = \frac{E_b}{N_o} - \frac{G_T}{T_S} - 228.6 + 10 \log R \quad 5.86$$

The diameter of the receiver antenna refers to the physical size of the antenna used by the ground station to receive signals from the spacecraft. The diameter of the transmitter

antenna, on the other hand, refers to the physical size of the antenna used by the spacecraft to transmit signals to the ground station.

The diameter of the receiver is:

$$G_T = 20 \log \pi + 20 \log D + 20 \log f - 20 \log c + 10 \log \eta \quad 5.87$$

The diameter of the antenna is determined by:

$$G_T - 20 \log \pi - 20 \log f + 20 \log c - 10 \log \eta = 20 \log D \quad 5.88$$

Diameters of the receiver antenna are given by:

$$G_T = 20 \log \pi + 20 \log D_T - 20 \log c + 10 \log \eta + 20 \log f \quad 5.89$$

Noise power is a type of interference that can degrade the quality of the received signal and make it more difficult to extract the information being transmitted. The presence of noise power in the received signal can be quantified by measuring the noise power density, which is the noise power per unit of bandwidth. It is given by:

$$N = KT_s B \quad 5.90$$

### 5.3.6 Electric Power Subsystem

In this section, we present the fundamental equations that form the basis of the design of the Electric Power subsystem in compliance with the mission objectives of the H2Z spacecraft. The subsystem is analyzed using two distinct approaches, namely the "Component Efficiency" method and the "Damage Fluence" method, to provide a comprehensive understanding of its performance characteristics. The "Component Efficiency" method is used to evaluate the efficiency of each component of the subsystem and identify areas for improvement. In contrast, the "Damage Fluence" method is used to assess the cumulative damage experienced by the subsystem over time and evaluate its long-term performance. By combining these two approaches, engineers and researchers can gain a deep understanding of the Electric Power subsystem's behavior and optimize its design for maximum efficiency, reliability, and durability.

The solar array power necessary to fulfil the eclipse load is given by:



$$\eta = \eta_{BDR}\eta_{BCR}\eta_{SAR} \quad 5.91$$

$$P_{charge}\tau_{sun} = \frac{1}{\eta}P_{eclipse}\tau_{eclipse} \quad 5.92$$

Power required to be available from the array is given by:

$$P_{array} = P_{sun} + P_{charge} \quad 5.93$$

Power output with the sun normal to the surface of the cells is given by:

$$P_o = \eta_{cell} \times S \quad 5.94$$

The following equations gives the Beginning-of-life (BOL) power production capability and End-of-life (EOL) power production capability respectively.

$$P_{BOL} = P_o I_d \cos\theta \quad 5.95$$

$$L_d = (1 - \text{degradation/yr})^{life} \quad 5.96$$

$$P_{EOL} = P_{BOL}L_d \quad 5.97$$

The results of  $P_{array}$  must now be verified against the oversizing requirement (Thumb Rule) for Low Earth Orbit (LEO)

In LEO, where a spacecraft spends about 30 minutes out of every 90 minutes in shadow, solar arrays need to be larger than necessary to account for the reduced sunlight. In this case, the array should be approximately 1.5 times larger than what is needed for full sunlight coverage, resulting in a 50% power excess above the spacecraft's needs.

$$P_{array} = P_{sun} \left( \frac{\tau}{\tau_{sun}} \right) \quad 5.98$$

$$P_{array} = P_{sun} \times 1.5 \quad 5.99$$

In comparison, in the GEO example, the greatest eclipse duration is 70 minutes. The 'oversizing' of the array in this case is merely 5%. This factor has a significant impact on the solar array design. For GEO:

$$P_{array} = P_{sun} \times 1.05 \quad 5.100$$

The following equations account for the Battery stored energy and estimated battery mass respectively.

$$E_B = P_{eclipse}(\tau - \tau_{sun})/(\eta_{charge} \times DOD) \quad 5.101$$

$$M_B = \frac{E_B}{\text{Energy density}} \quad 5.102$$

**a) Component Efficiency Method:**

This method determines the total surface area required for a solar array by combining the efficiency of each component and then associating them with power generation. This method depends on the following variables:

- Solar flux (S) i.e., solar power available per unit area. It is calculated to be 1000 W/m<sup>2</sup> at the surface of the earth and increases to 1360 W/m<sup>2</sup> at an altitude of 450km and keeps on increasing as we move away from Earth's surface.
- Conversion efficiency ( $\eta_{cell}$ ) of the cells used. For Tripple Junction GaAs cells, it is about 30%.
- Packing efficiency ( $\eta_{packing}$ ) of the solar array. It depends on how efficiently the solar cells are assembled on the solar array. A solar array does not comprise solely solar cells. Some of the space on the solar array is taken by solar sensors and temperature sensors while some is consumed in providing intercellular spacing. The solar array allocates approximately 90% of its total area for the installation of solar cells.
- Degradation factor (D) for the cells represents degradation in performance of the cells with time.
- Miscellaneous degradation ( $\eta_{misc}$ ) of the solar cell. This includes degradation due to temperature fluctuations and other factors. Usually, it is taken to be between 2 to 5%.

- Array pointing error ( $\delta\theta$ ) which is usually taken to be 1%

To calculate the area of the solar array to produce the needed power, we have:

$$A_{array} = \frac{P_{array}}{S \times \cos \delta\theta \times \eta_{cell} \times \eta_{packing} \times (1 - \eta_{misc}) \times (1 - D)} \quad 5.103$$

To calculate an estimated mass of solar array we used:

$$M_{SA} = \frac{P_{SA}}{\text{Specific Performance (W/kg)}} \quad 5.104$$

### b) Damage Fluence Method

To calculate the total radiation fluence absorbed by the solar cell, fluences must be determined. The inputs required for solar array sizing are given in the table below.

Using this method, required area of active solar cells for a specific mission at the end-of-life (EOL) performance can be determined. It is a six-step method.

- **Step 1**

The first step is to determine the equivalent fluence damage due to protons and electron from Figure 5.12

- **Step 2**

In the second step, the total damage incurred by the spacecraft over its life span is calculated by multiplying fluence damage with the lifespan of the spacecraft i.e., 2 yr.

- **Step 3**

Then from Figure 5.13, we determine the power density for total damage.

- **Step 4**

Now we see from Figure 5.14, if a shielding or coverslip of thickness 0.15mm is used then  $F=0.8$ . Expected radiation at the end of life is calculated by power density for total damage and  $F$ .

- **Step 5**

Power per unit area after catering for shielding is converted to  $W/m^2$ .

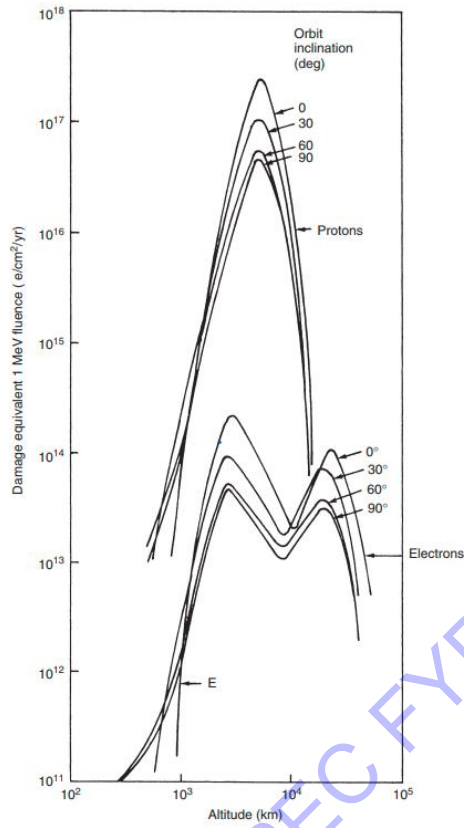


Figure 5.12 Altitude versus Damage Fluence Graph

DMAE (AU) Report for PEC FYDP 2022-23

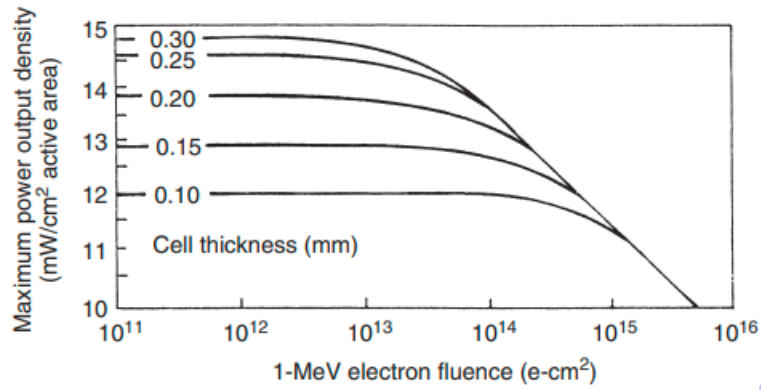


Figure 5.13 Power density versus Electron Fluence Graph

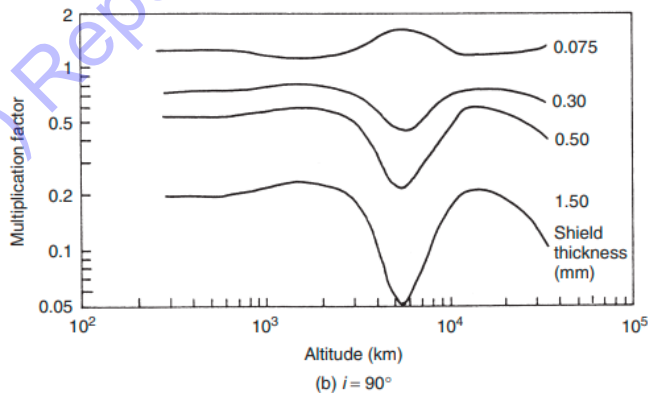
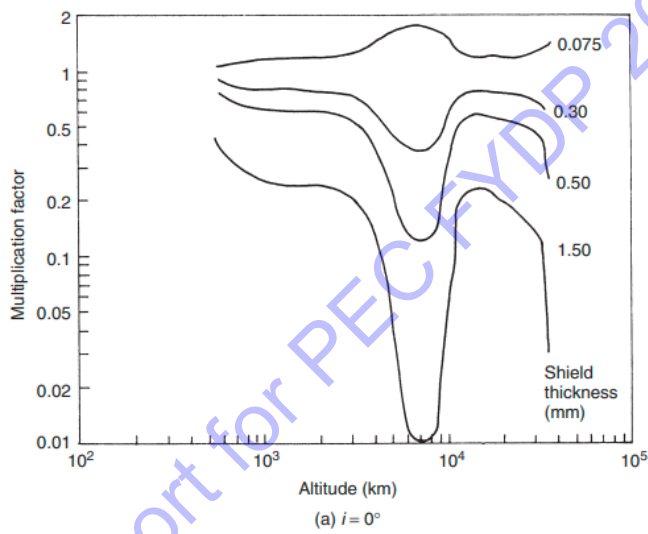


Figure 5.14 Multiplication factor versus Altitude Graph

• **Step 6**

From this power density, we calculate the area required to generate 956W (see equation by:

$$A_{array} = \frac{\text{size of solar array in LEO}}{\text{Power per unit area after catering for shielding}} \quad 5.105$$

### 5.3.7 Thermal Control System

This subsystem does not require any significant math since mainly H2Z uses a passive thermal control scheme as discussed in section 4.12. However, the average temperature that is to be maintained in the satellite, is calculated by using Kirchoff's law. The expression for Kirchoff's Law is as shown:

$$T_{avg} = \left( \frac{\alpha \times G_s}{6 \times \sigma \times \epsilon} \right)^{1/4}$$

5.106

DMAE (AU) Report for PEC FYDP 2022-23

## Chapter 6: Results and Discussion

This chapter describes the results and simulations of this project.

### 6.1 Debris Selection

The sensitivity plot is as follows

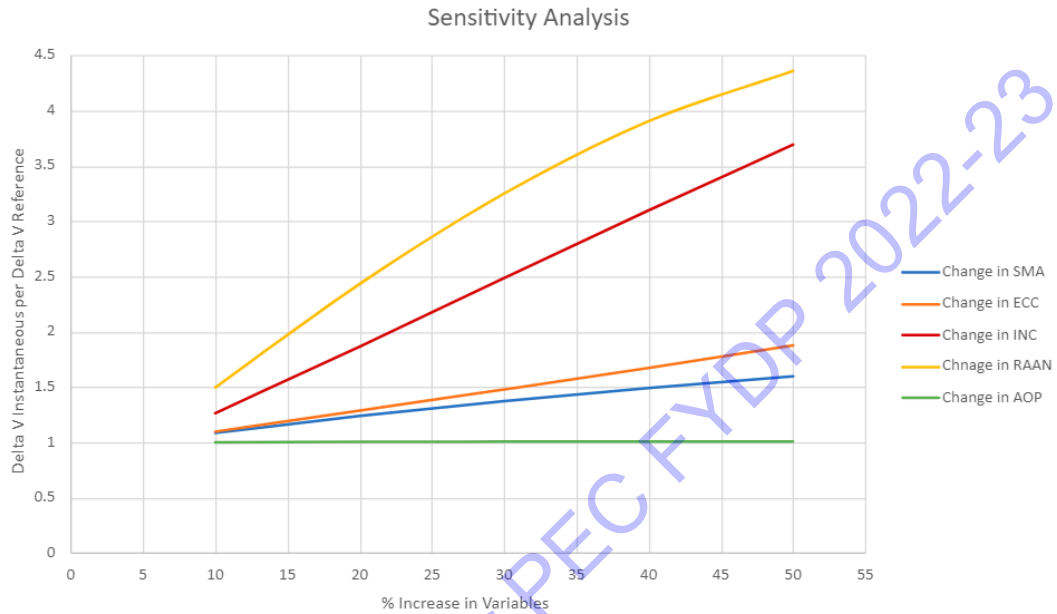


Figure 6.1 Sensitivity Plots

The graph was plotted in Microsoft Excel. It is quite evident from the graph that the variables that have a greater effect on the delta-V are the Right Ascension of Ascending Node, Inclination, and Eccentricity respectively. The list of debris that was selected for the mission is as follows:

Table 6.1 NORAD ID of Selected Debris for Mission

Sr. No	NORAD ID
1	43104
2	43095
3	43096
4	40263
5	39628

## 6.2 Mission Design Results

### 6.2.1 Mission Objectives

Mission objectives are a set of goals that a satellite must achieve during its operational life.

- The primary mission objective of the H2Z satellite is to perform active debris removal by disposing of at least 5 pieces of debris from Low earth Orbit in 1 year.
- The secondary mission objective is to serve as an Earth Observation Satellite when in parking orbit.

### 6.2.2 Mission Requirements

The mission requirements needed to achieve the mission objectives are as follows:

1. The mission duration should be 1 year.
2. The end-of-life duration should be less than 25 years.
3. The mass of the satellite should not exceed 900 kg.
4. The delta-V budget for the entire mission should not exceed 3 km/s.
5. The satellite shall operate within a range of 150 km – 1000 km altitude.

### 6.2.3 Mission Operation Phases and Modes

H2Z mission will consist of the same phases and modes as were used by PNSS-1:

#### 1. Phase of pre-launch

During the Pre-Launch Phase, various integration and testing activities will take place, and this stage will end when the launch sequence begins.

#### 2. LEOP Phase

The launch mode is intact from the integration of the satellite with the launch vehicle until the satellite separates from the launch vehicle. This mode begins from the Power-OFF mode.

- Initial Startup Mode: In this mode, the subsystem that are essential for a transformation to survival mode are switched on for the first time.
- Survival Mode: In this mode, the satellite enters in its safe configuration. This is the most significant mode of the satellite.



### 3. Performance Check-Up Phase

- Performance Check-Up Mode: In this mode on-orbit checkup of all the spacecraft subsystems is performed.

### 4. Nominal Phase

The satellite shall remain in orbit for most of their lifetime in this phase. Satellite shall be required to change its attitude according to the mission needs in this phase. The spacecraft shall generate power through solar panels during this phase which will qualify the satellite for on-orbit operations.

- Standby Mode: The satellite's default mode during the nominal phase is standby mode, with a coarse sun-pointing attitude and powered-off payload units
- Payload Operations Mode: Payload operations mode is used for required operations, with a fine nadir-pointing attitude and activated payload units. Secondly it will be used for debris capturing with the help of robotic arm.
  - Payload operations mode involves imaging payload operations, which include imaging, storage, and data transmission and debris capturing and releasing at very low altitude.
  - Additionally, communication payload operations include data receiving, processing, and transmission.

### 5. Mission Event Sequence

Table 6.2 Mission event sequence

Sr. No	Event Name	Time
1	Launch Vehicle/Spacecraft Separation Time	T0
2	Battery and Solar Array Isolation Switch Closed	T0
3	Units Power ON (PCU, PDU, DHU, OBC, ACS Sensors and Actuators, TM Tx and TC Rx)	T0 Duration (30 sec)
4	Attitude Rate Damping	T0 + 40-sec Duration (5 min)
5	Sun Acquisition	T0 + 6 min
6	Antennae Deployment	T0 + 6 min Duration (1 min)
7	GPS Power ON and Time Synchronization	T0 + 8 min Duration (3 min)
8	Earth Acquisition	T0 + 10 min Duration (15 min)
9	Nadir Pointing	T0 + 25 min Duration (10 min)
10	Prepare for Performance Check up	Ground Access – 5 min

### 6.2.4 Satellite Parking Orbit

The parking orbit for H2Z is selected as the same as of PNSS-1 which is a sun-synchronous orbit. H2Z shall operate within the Low Earth Orbit throughout its mission. The altitude range shall be 150-710 km. The parking orbit elements (POE) are listed in the table:

Table 6.3 Parking Orbit Elements of H2Z

Parking Orbit Elements (POE)	Value
Semi-Major Axis (SMA)	6878.1363 km
Eccentricity (ECC)	0.0001
Inclination (INC)	97.4065°
Right Ascension of Ascending Node (RAAN)	270.92°
Argument of Perigee (AOP)	0°

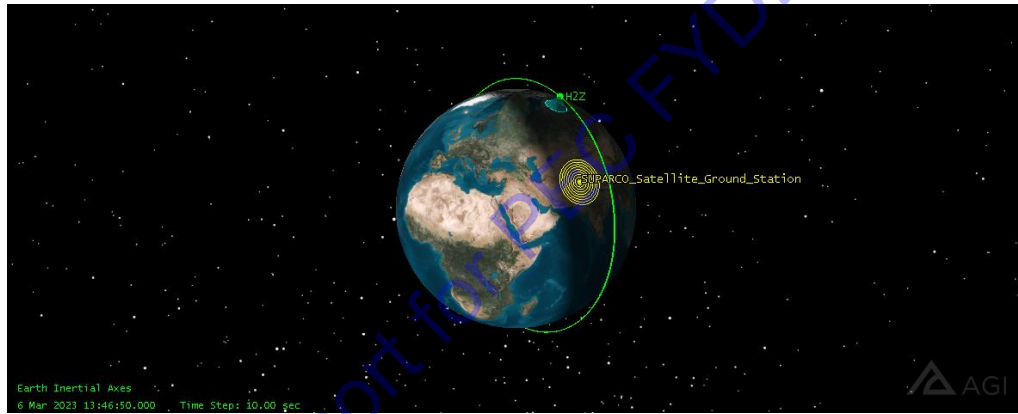


Figure 6.2 Parking Orbit of H2Z

### 6.2.5 Orbit Environment

The impact flux of debris and meteoroid in the environment where the satellite operates is shown below:

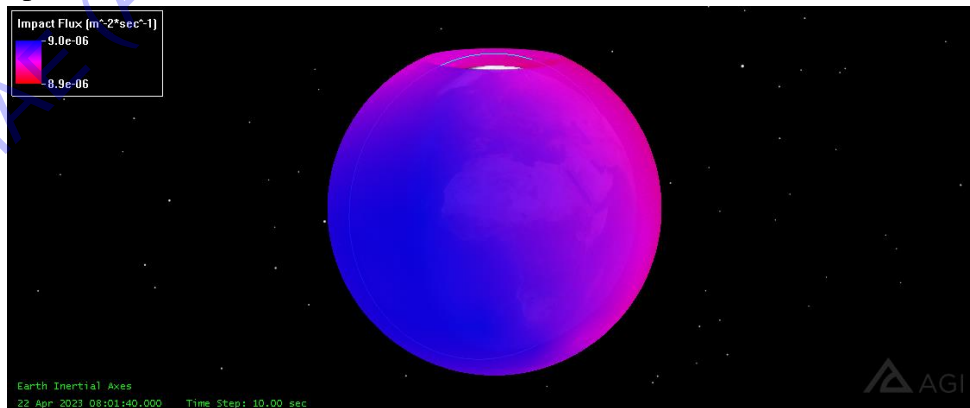


Figure 6.3 Impact Flux of Debris and Meteoroid

Electron and Proton radiation contours in the specific altitude range are shown below:

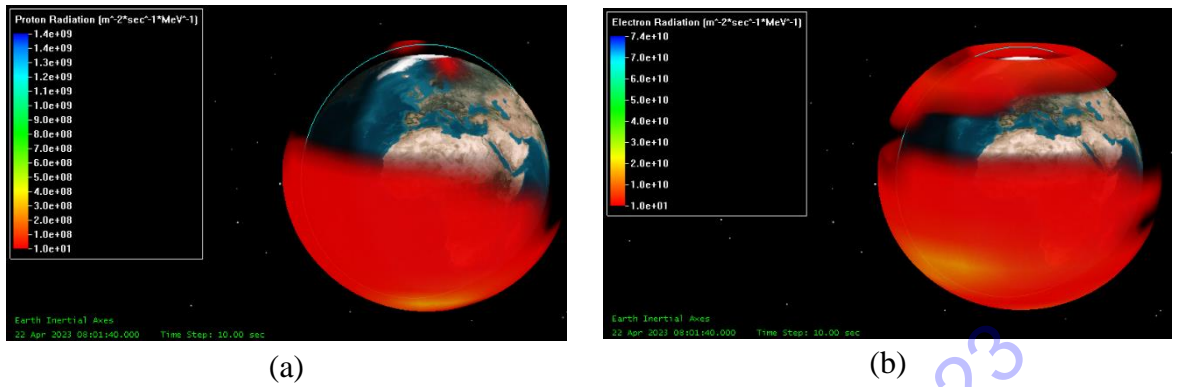


Figure 6.4 Radiation Environment within altitude (150 km - 1000km)

### 6.2.6 Illumination Condition Analysis

For the parking orbit of H2Z, the illumination characteristics are as follows:

- Beta Angle varies between  $-83.573^\circ$  to  $83.573^\circ$  for 1 year
- The illumination duration is 75.4% during 1 year

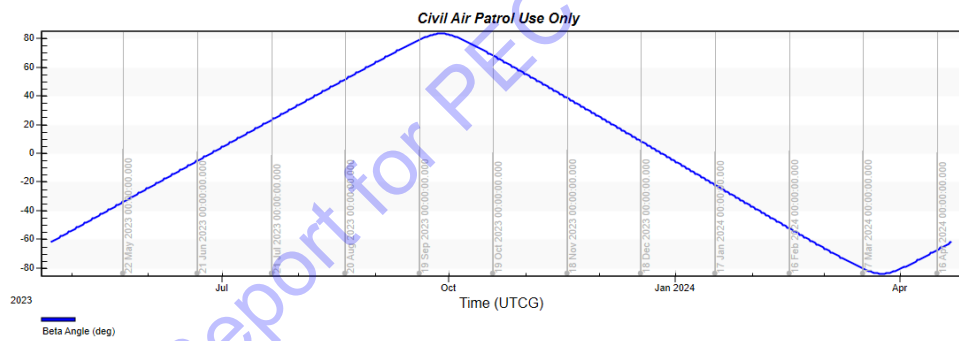


Figure 6.5 Beta Angle Graph for 1 year

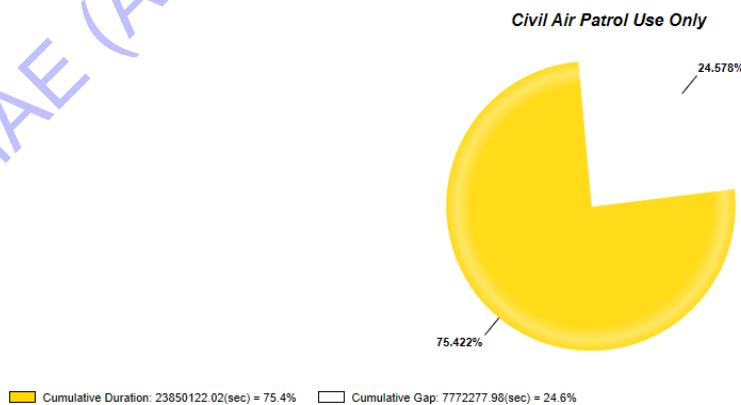


Figure 6.6 Illumination duration for 1 year

### 6.2.7 Ground Station

The best ground station in Pakistan for this mission shall be the Rawat Ground Station. This can be seen from the graph below:

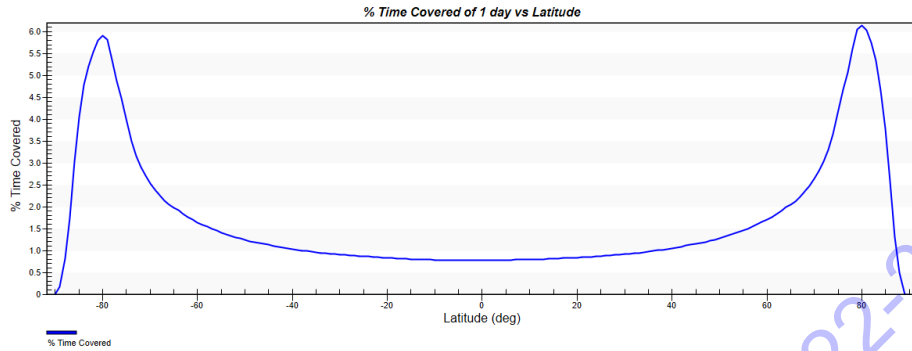


Figure 6.7 Percent Time coverage of 1 day vs. Latitude

As Pakistan is situated between a latitude of 23°N - 37°N, the greater the value of latitude, the greater shall be the coverage time of an area. Since of the already established ground stations in Pakistan, Rawat is located at a latitude of 33.4951°N and no other ground stations exist at higher latitudes therefore it will be the best choice for this mission. The coverage time contour for the satellite when in parking orbit is shown below

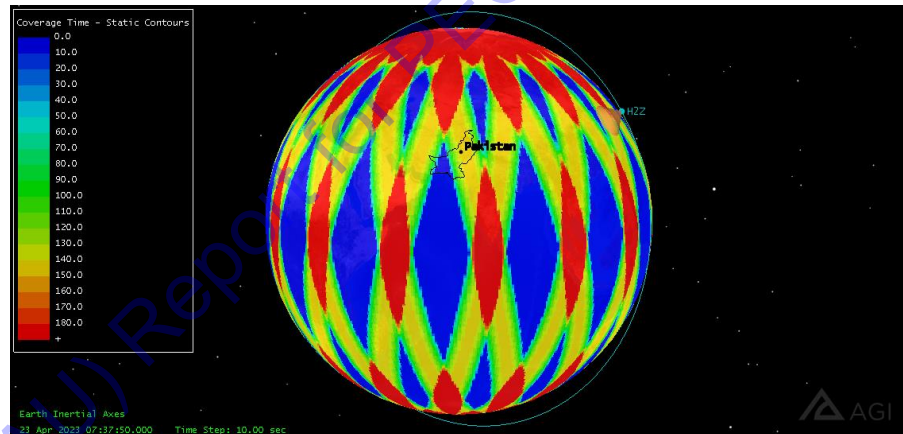


Figure 6.8 Coverage time contour

### 6.2.8 Analysis of Orbit Ground Coverage

H2Z access to the ground station in Rawat is calculated for 1 day (23 April 2023 to 24 April 2023) and the results are given below:

Ground_Station_Rawat-To-H2Z				
Access	Start Time (UTCG)	Stop Time (UTCG)	Duration (sec)	
1	23 Apr 2023 10:42:35.212	23 Apr 2023 10:53:22.350	647.139	
2	23 Apr 2023 12:16:26.512	23 Apr 2023 12:26:25.434	598.922	
3	23 Apr 2023 21:18:08.815	23 Apr 2023 21:25:37.936	449.121	
4	23 Apr 2023 22:49:14.154	23 Apr 2023 23:00:42.380	688.226	
5	24 Apr 2023 00:27:59.253	24 Apr 2023 00:30:22.106	142.853	
Global Statistics				
Min Duration	5	24 Apr 2023 00:27:59.253	24 Apr 2023 00:30:22.106	142.853
Max Duration	4	23 Apr 2023 22:49:14.154	23 Apr 2023 23:00:42.380	688.226
Mean Duration				505.252
Total Duration				2526.260

Figure 6.9 Summary of Access to Ground Station

The ground track plot is shown below:

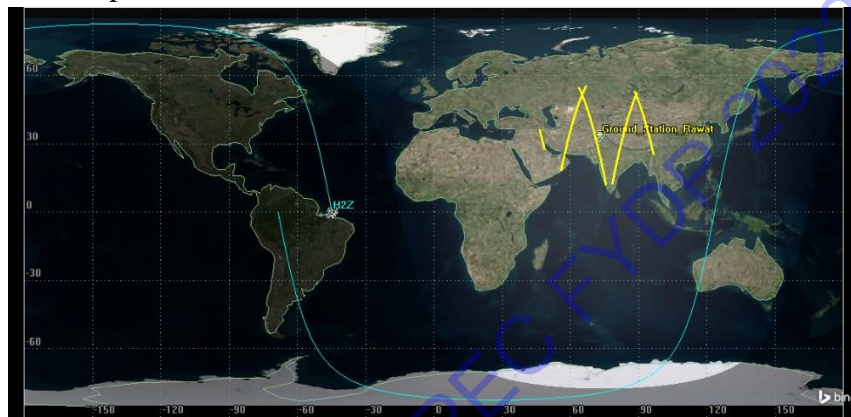


Figure 6.10 Ground Track Plot for Rawat

### 6.2.9 Mission Life

The mission life of H2Z is intended to be 1 year from launch till the end of life. All payloads and systems used in the satellite shall have a life of 2 years.

### 6.2.10 End-of-Life Analysis

The End-of-Life analysis was done for H2Z using STK 11.2. It indicates the duration a satellite shall remain in orbit (after completing its mission) before re-entering Earth. After performing its mission H2Z shall return to its parking orbit where it will spend the rest of its life. The key parameters used for the analysis are listed below:

Table 6.4 Key parameters for EOL

Key Parameter	Value
Drag Area	3 m <sup>2</sup>
Drag Area to Mass Ratio	0.00061074 m <sup>2</sup> /kg
Area Exposed to Sun	6.66 m <sup>2</sup>
Solar Area to Mass Ratio	0.01355 m <sup>2</sup> /kg
Drag Coefficient	2.2
Mass	491.2 kg

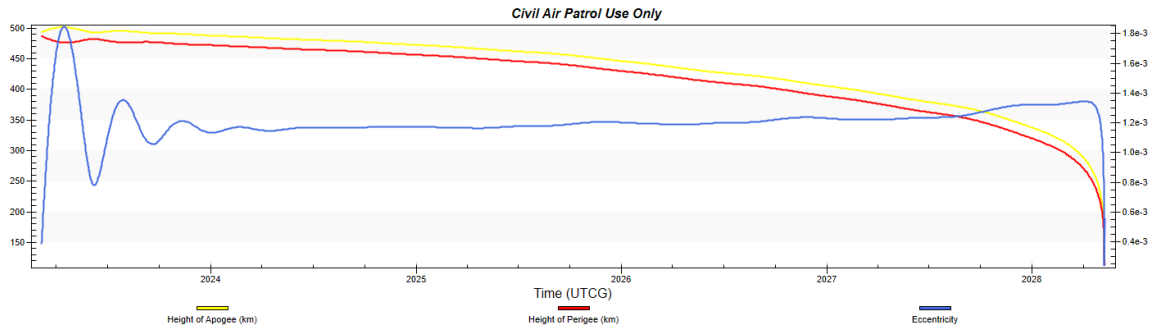


Figure 6.11 Height of apogee, perigee, and inclination graph for EOL

Results show that the lifetime is 5.2 years (at 500 km altitude). This also shows that the satellite shall follow the IADC guidelines by decaying within the prescribed limit of 25 years.

### 6.2.11 Mission Strategies

A total of 14 different mission sequences (strategies) were defined for the debris removal mission, out of which only two were selected and analyzed in detail and the delta-V budget was determined for both of these strategies. These are Home capture and Node capture. The list of strategies and their combination that contains different maneuvers are shown below:

Table 6.5 Description of Maneuvers

Maneuver	Description
Hohmann	Changes the SMA and ECC.
GPC	General Plane Change – changes RAAN and INC
SPC	Single Plane Change – changes the INC
CPCA	Combined Plane Change (at apogee) – changes SMA, ECC, INC and RAAN
CPCN	Combined Plane Change (at node near apogee) – changes SMA, ECC, and INC – no change in RAAN
ALRM	Apses Line Rotation Maneuver – changes AOP (requires correction in SMA and ECC)
STM	Semi-tangential Maneuver – tangent to initial orbit only
WTM	Waiting Time Maneuver (Co-planar Rendezvous)
PM	Phasing Maneuver (Co-orbital Rendezvous)

Table 6.6 Strategies List

Sr. No	Hohmann	GPC	SPC	CPCA	CPCN	ALRM	STM	WTM	PM
1	✓	✓				✓			✓
2	✓	✓		✓		✓			✓
3	✓				✓	✓			✓
4	✓	✓		✓				✓	
5	✓	✓		✓				✓	
6	✓	✓			✓			✓	
7	✓	✓					✓		
8	✓	✓		✓			✓		
9	✓	✓			✓		✓		
10	✓		✓			✓			✓
11	✓					✓			✓
12	✓						✓		
13	✓							✓	
14	✓								✓

### 6.2.12 Home Capture

The Home Capture strategy (catching the debris in the debris's orbit) was simulated using the General Mission Analysis Tool (GMAT). The results of delta V were evaluated for each of the 5 debris and are shown below:

Table 6.7 Home Capture Delta-V Budget

Home Capture	
NORAD ID	Delta-V (km/s)
43104	2.52614
43095	2.4548
43096	5.14507
40263	2.4136
39628	1.70063
<b>Total Delta-V</b>	<b>14.24024</b>

The simulations of the Home capture mission sequence were made in General Mission Analysis Tool (GMAT) 2020 and are shown below:

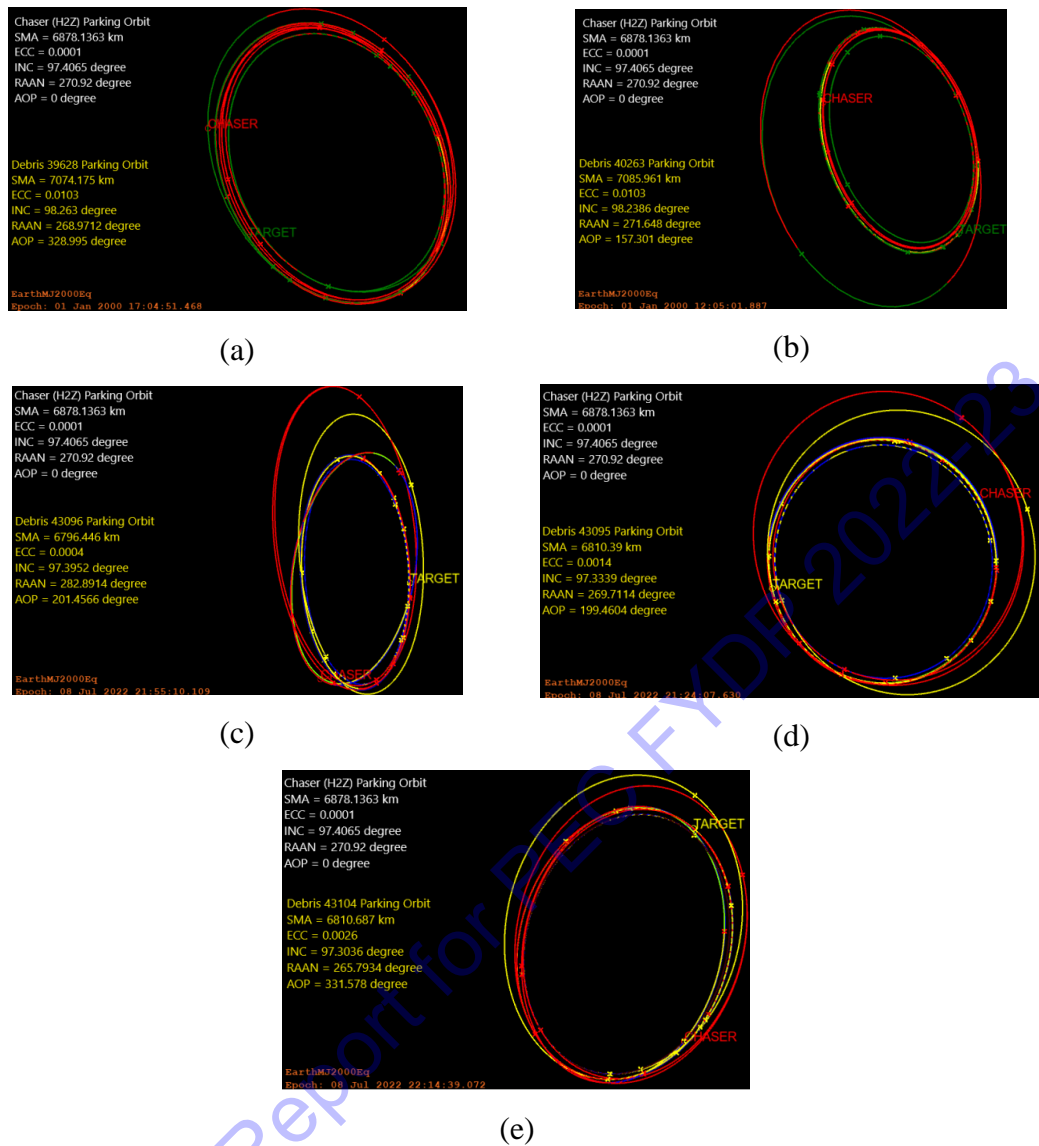


Figure 6.12 Home Capture Simulations

### 6.2.13 Node Capture

The Home Capture strategy is much more expensive and also involves the risk of colliding with debris itself. So another strategy was evolved which is called the Node Capture. The results for node capture were evaluated and are shown below:

Table 6.8 Node Capture Delta-V Budget

Node Capture	
NORAD ID	Delta-V (km/s)
43104	0.43918
43095	0.42848
43096	0.438495



40263	0.61999
39628	0.6266
<b>Total Delta-V</b>	<b>2.552745</b>

The simulations of the Node capture mission sequence were made in General Mission Analysis Tool (GMAT) 2020 and are shown below:

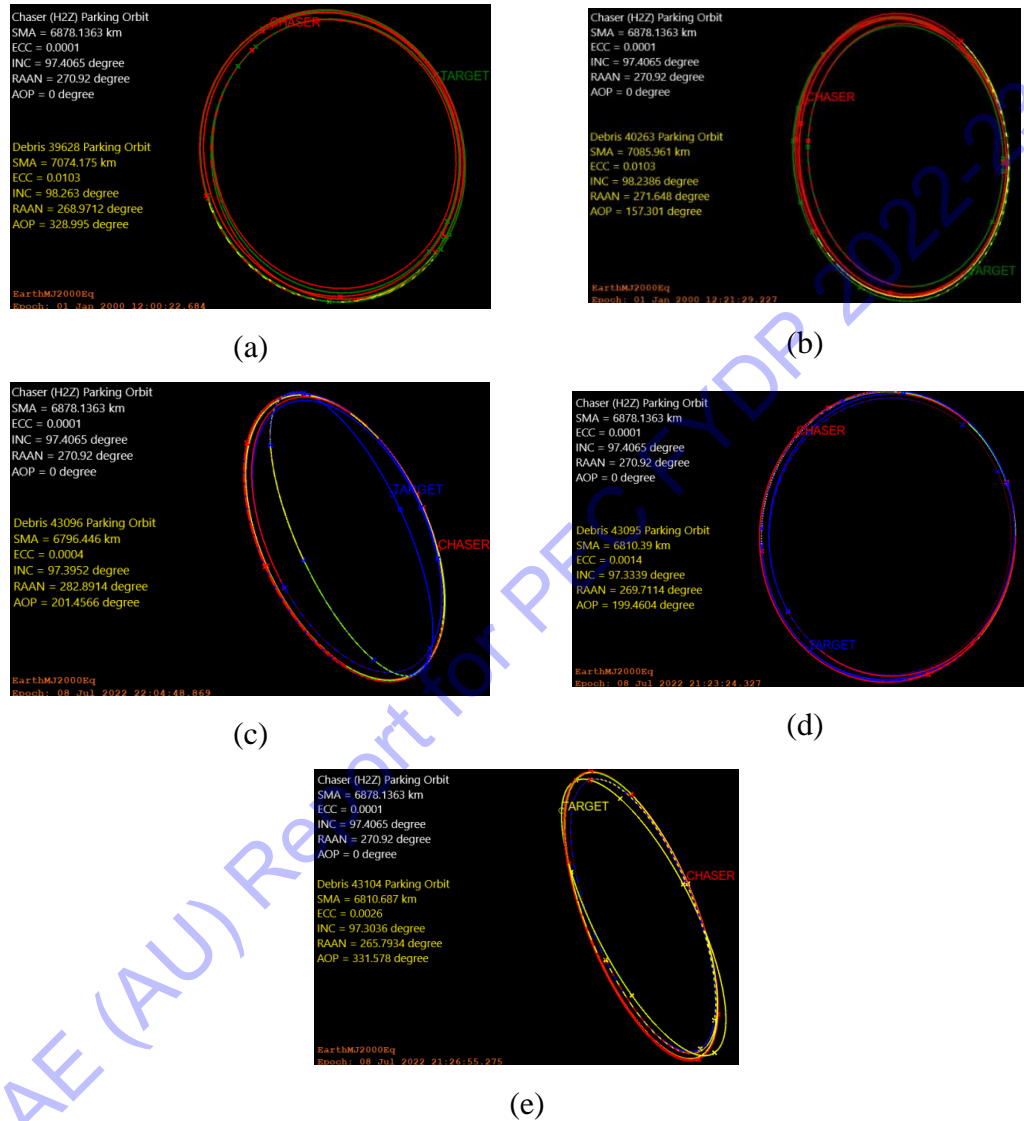


Figure 6.13 Node Capture Simulations

### 6.3 System Design

This section presents the outcomes obtained after taking into account each subsystem of H2Z. These findings offer a comprehensive understanding of how each of the subsystems of H2Z will perform to accomplish its mission objectives, as described in Section 6.2.1. The results of each subsystem are presented in the same sequence as that of the mathematical model, which was presented in the previous section. Furthermore,

this chapter concludes with a static, modal, and thermal analysis, which aims to ensure that H2Z remains secure in the environmental conditions to which it is exposed. To supplement these results, critical parameters associated with each subsystem have also been included. The incorporation of these vital parameters into the design process has enabled us to create a highly effective conceptual design that complies with the rigorous performance requirements of the H2Z mission.

To arrive at these outcomes, a rigorous methodology was employed, which entailed the utilization of cutting-edge tools and techniques. Each subsystem was subjected to a thorough analysis that took into account a wide range of factors, including but not limited to, cost, performance, efficiency, and reliability. The analysis revealed critical insights into the strengths and limitations of each subsystem, which played a vital role in the development of an effective conceptual design.

The results of the analysis have significant implications for the future of H2Z, as they provide valuable information on how the subsystems will perform in the field. Armed with this knowledge, we can take proactive steps to optimize the design, making it more resilient and adaptable to the challenges that may arise in the field. Ultimately, the results presented in this chapter represent a major milestone in the development of H2Z, bringing us one step closer to realizing our mission objectives.

### **6.3.1 Payload**

#### **1. Robotic Arm:**

A 4-DOF Robotic arm, used as a primary payload is developed and used as the debris capturing mechanism. Major specifications of this robotic arm has already been listed in section 4.4.1. The robot manipulator was found to have 3 position axes of freedom and 1 orientation axis of freedom. Joints 1, 2 and 3 rotate at 0.18sec/60° while joint 4 and end-effector rotate at 0.21sec/60° to stay within the power budget of satellite

#### **2. Imaging Payload**

H2Z will be equipped with an imaging payload that has a ground sample distance (GSD) of approximately 1.5 meters, a swath width of 18.77 degrees, and an angular field of view of 11.55 degrees. In addition to these parameters, the table also includes the diameter of the lens, which was determined using the F# of SIMERA SENSE TriScape 200.

By leveraging the insights provided by the mathematical model and the critical parameters listed in Table 6.9, we selected an imaging payload that meets the stringent requirements of the H2Z mission. This payload will play a pivotal role in enabling H2Z to gather high-quality imagery and achieve its mission objectives with utmost precision and accuracy.

Table 6.9 Key Parameters of Imaging Payload

Parameter	Result
GSD	1.499m
SW in degrees	18.77deg
D (Aperture)	190.53mm
AFOV ( $\theta_{FOV}$ )	11.559deg
SW in Km	101.214km

### 6.3.2 Structure Subsystem

In section 4.5, we presented the key specifications of the structure subsystem, and in this section, we will focus on the major sizing results. The volume of the spacecraft bus was calculated to be  $1.367\text{m}^3$ ; however, due to the unavailability of a commercially standard mechanical bus, a bus of  $1.5\text{m}^3$  was chosen. In light of this, a mechanical bus of 1500U (where 1U is equivalent to  $1000\text{cm}^3$ ) was selected after the first design iteration.

Table 6.10 represents all of the sizing parameters that emerged as a result of implementing the mathematical model, which is explained in detailed in section 5.3.2. These parameters play a crucial role in the overall structural integrity and performance of the spacecraft. They include the volume, linear dimension, cross-section area, and moment of inertia of the bus.

Table 6.10 Sizing Parameters of H2Z Bus

Parameter	Result
Volume of the Spacecraft bus	$1.367\text{m}^3$
Linear Dimension	1.29m
Cross section area	$1.6641\text{m}^2$
Moment of Inertia, I	$37.706\text{m}^2$

During the second design iteration, the reduction of the delta-V budget to 2.55 km/s made it necessary to reconsider the size of the spacecraft. This is because the volume

of the spacecraft is directly dependent on the loaded mass of the spacecraft, which in turn is influenced by the mass distribution and propellant mass. Upon performing the second design iteration, the volume of the spacecraft was calculated to be  $4.29\text{m}^3$ .

Upon reconsidering the size of the spacecraft, it was found that the initial design iteration was more suitable as it offered good compactness, which is a key factor in sizing the bus of the spacecraft. This is because compactness allows for more efficient use of available space and enables the spacecraft to carry a larger payload while minimizing the overall mass and size.

The sizing of the spacecraft is a critical aspect of the design process, as it directly impacts the overall performance and capability of the spacecraft. By carefully considering factors such as delta V budget, mass distribution, and propellant mass, we can arrive at an optimal size for the spacecraft that ensures efficient use of available resources while meeting mission objectives. In this case, the initial design iteration was found to be the most suitable, based on the sizing results obtained through rigorous analysis and optimization.

### **6.3.3 Propulsion Subsystem**

The success of the mission hinged on the design of the main engine, which required a high thrust and minimum propellant consumption. To fulfill these criteria, an  $\text{LF}_2/\text{LH}_2$  bipropellant liquid rocket engine with a bell-shaped nozzle contour was designed. This engine was intended to generate approximately 415N of thrust and consume around 398kg of propellant during a burn time of about 4189s. During the first design iteration, the length and diameter of the chamber were found to be 232.218mm and 18.5233mm, respectively. However, excessively long and thin chambers are known to result in a greater pressure loss, so a chamber length and diameter must be chosen that enables complete combustion and minimum pressure loss. Therefore, using a commercially recognized tool, Rocket Propulsion Analysis (RPA), the length-to-diameter ratio of the chamber was carefully adjusted, resulting in a chamber length and diameter of 59.58mm and 42.41mm, respectively. All the results derived from implementing the mathematical model discussed in section 5.3.3 are listed in Table 6.11. These results pertain to the propellant specifications, which are listed in section 4.6 and were used as input for the model. The propellant specifications include the chemical makeup, mass, and other characteristics of the propellant used in the engine

Table 6.11 Main Engine design for H2Z

Parameter	Result
Mass of propellant consumed	398.032kg
Mass of fuel	113.732kg
Mass of Oxidizer	284.308kg
Volume of the fuel tank	0.09958m <sup>3</sup>
Volume of the oxidizer tank	0.18841m <sup>3</sup>
Exhaust Velocity	4583.61757m/s
Throat Area	9.0094 x 10 <sup>-5</sup> m <sup>2</sup>
Throat diameter	0.01071307m
Exit Area	0.01351416m <sup>2</sup>
Exit diameter	0.13120783m
Throat temperature	1766.48274K
Chamber Thrust (optimum)	409.470872N
Chamber Thrust (vacuum)	415.351476N
Thrust coefficient(optimum)	1.75
Thrust coefficient(vacuum)	1.77
Characteristic velocity	2470m/s
Characteristic Length	0.64m
Chamber contraction ratio	2.9895746
Combustion chamber length	59.518mm
Area of chamber	2.693 x 10 <sup>-4</sup> m <sup>2</sup>
Diameter of chamber	42.41mm
Volume of chamber	5.776 x 10 <sup>-5</sup> m <sup>2</sup>
Length from the converging cone entrance to the nozzle throat	0.0145741m
Length of conical nozzle length	0.2248643
Radius of upstream throat	8.0348 x 10 <sup>-3</sup> m
Radius of downstream throat	2.0462 x 10 <sup>-3</sup> m
Length of bell nozzle	0.179877m

### 6.3.4 Attitude Determination and Control Subsystem

Parameters listed in Table 6.12 were drafted out as a result of implementing the mathematical model explained in Section 5.3.4 and in [22]. Table 6.12 shows the worst-case disturbances torques.

Table 6.12 Disturbance torques

Parameter	Result
Gravity gradient	$1.65 \times 10^{-5} \text{Nm}$ at $\theta=1^\circ$ & $4.1 \times 10^{-4} \text{Nm}$ at $\theta=30^\circ$
Solar radiation	$5.73 \times 10^{-4} \text{Nm}$
Magnetic field	$4.8 \times 10^{-5} \text{Nm}$
Aerodynamics	$1.65 \times 10^{-5} \text{Nm}$

Table 6.13 holds all the results for the sizing of reaction wheels and momentum wheels.

Table 6.13 Sizing of reaction wheels and momentum wheels

Parameter	Result
Slew Torque for Reaction Wheels	$5.08 \times 10^{-3} \text{Nm}$
Momentum Storage in Reaction Wheels	0.0479Nms
Momentum Storage in Momentum Wheels	$40.4 \text{Nm.s}$ at $\theta=0.1^\circ$ Accuracy $4.04 \text{N.m.s}$ at $\theta=1^\circ$ Accuracy
Momentum Storage in Spinner	0.046 rad/s
Torque from Magnetic Torquers	$1 \text{A.m}^2$

Additionally, ADCS used 8 micro thrusters for adjusting its attitude, the details of which are mentioned in section 4.7

### 6.3.5 Electric Power Subsystem

It was found out that H2Z shall have an EPS which will be able to produce a power of approximately 956.216W. Two very common approaches were analyzed, the component efficiency method and the damage fluence method. As a result, It was found the component efficiency method requires 40.9% less area to generate the same amount of power as compared to the damage fluence method. However, this difference can be associated with the fact that the damage fluence method accounts for both the efficiencies of components of the solar array as well as radiation damages experienced

during the mission while the component efficiency method does not consider the radiation damage that may occur during the mission. For producing such power, it has been found that H2Z will require a solar array having an area of approximately  $6.5\text{m}^2$ . Other key factors associated with this subsystem which serves as input are discussed in section 4.9

Table 6.14 EPS Result

Parameter	Results
Power required from solar array in eclipse phase	156.759W
Power required from the array	794.237W
Power output with the sun normal to the surface of the cells	420W
Beginning-of-life (BOL) power production capability per unit area of the array	$296.577\text{W}/\text{m}^2$
End-of-life (EOL) power production capability per unit area of the array	$280\text{W}/\text{m}^2$
The approximate size of the solar array in LEO is	956.2167W
The approximate size of the solar array in GEO is	669.35W
Battery-stored Energy	180.609W-hrs
Estimated Battery mass	1.602kg

Using the component efficiency method, it was found that H2Z requires a solar array having an area of approximately  $2.66\text{m}^2$  and the mass of the solar blanket to be 19.124kg. However, when the damage fluence method was used, it was found that H2Z requires a solar array having an area of approximately  $6.50\text{m}^2$  and the mass of the solar blanket to be 46.74kg. The damage fluence method being a more conservative approach compelled us to go with its results. Other parameters found from the damage fluence method are listed in Table 6.15

Table 6.15 EPS parameters from damage Fluence Method

Parameter	Results
Damage equivalent 1 MeV fluence due to Electrons	$1.8 \times 10^{11} \text{ e}/\text{cm}^2/\text{yr}$
Total Damage equivalent 1 MeV fluence due to Electrons	$3.6 \times 10^{11} \text{ e}/\text{cm}^2/\text{yr}$
Maximum Power Output Density for total damage	$14.7\text{mW}/\text{cm}^2$
Multiplication factor for 0.15mm Shield thickness	0.8

Expected radiation at the end of life	$2.8 \times 10^{11}$
Power per unit area after catering for shielding	147W/m <sup>2</sup>

### 6.3.6 Telemetry, Tracking, and Command Subsystems

The parameters presented in Table 6.16 were obtained by implementing the mathematical model described in section 4.10 and in the [22]. The TM Uplink and Downlink conditions were both analyzed and interpreted to arrive at these results. It is important to note that there are other specifications associated with this subsystem, which can be found in section 4.10. The mathematical model used in this analysis considered various factors that could impact the performance of the system. These factors include the power budget, data rate, modulation scheme, and carrier frequency. By analyzing these factors, it was possible to identify the optimal parameters for TM Uplink and Downlink. The results presented in Table 6.16 and Table 6.17 provide a comprehensive overview of these parameters, including carrier frequency, data rate, and power requirements.

Table 6.16 TM Uplink results

Parameter	Results
Carrier-to-noise density ratio	78.54dB
Equivalent Isotropic Radiated Power	26.75dBw
Space loss	140.31dB
Energy per bit to noise density ratio	47.78dB
Received Isotropic Power	-114dB
Receive Antenna Diameter	0.3115m
Transmit Antenna Diameter	4.937mm
Half Power beam width	0.46°
Noise Power	15.2aw/Hz

Table 6.17 TM Downlink

Parameter	Results
Carrier-to-noise density ratio	64.21dB
Equivalent Isotropic Radiated Power	4.5dBw



Space loss	149.79dB
Energy per bit to noise density ratio	33.21dB
Received Isotropic Power	-155dB
Receive Antenna Diameter	2.34m
Transmit Antenna Diameter	0.33m
Half Power beam width	0.02°
Noise Power	0.14aw/Hz

### 6.3.7 Thermal Control System

The average temperature that is to be maintained in the satellite is found to be 244.85K which is found to be approximately the same as the average temperature which was obtained in UmDan-1. This came out to be a suitable value for H2Z to operate in as all the components had sufficient margin in their surviving and operating temperatures. Other key specifications of TCS are discussed in detail in section 4.12

### 6.4 Analysis

Linear static and modal for H2Z is done using the MSc Nastran Patran software while thermal analysis was done on COMSOL Multiphysics 6.1. Deformations, stresses, normal mode frequencies, and Maximum/Minimum temperatures were extracted as a result of performing these analyses. Detail stepwise procedure for the analysis is attached below

#### a) Step 1: Importing the Geometry/ Geometry Creation

By using the geometry creation tools available in Patran, the tri-modular bus structure was modelled.

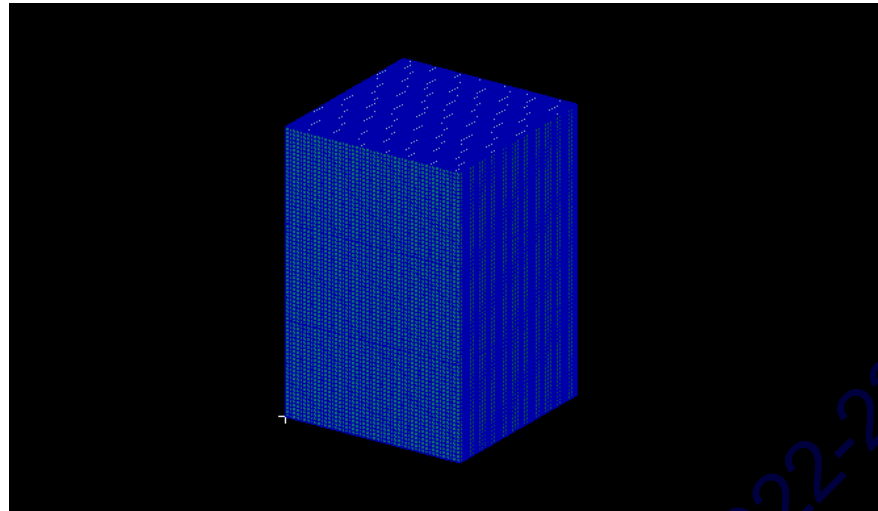


Figure 6.14 Geometry

**b) Step 2: Material Definition**

Aluminum 6061 is the material that is applied to the entire Satellite body. Table 6.18 gives the mechanical and thermal properties of the material

Table 6.18 Aluminum 6061 Mechanical and Thermal properties

Property	Metric	Imperial
<b>Mechanical Properties</b>		
Density	2.7 g/cm <sup>3</sup> or 2700 kg/m <sup>3</sup>	0.0975 lb/in <sup>3</sup>
Poisson's Ration	0.33	0.33
Tensile Yield Strength	276 MPa	40000 psi
Tensile Ultimate Strength	310 MPa	45000 psi
Young's Modulus	68.9 MPa	10000 ksi
Bulk Modulus	76.0 GPa	11000 ksi
Shear Modulus	26 GPa	3770 ksi
<b>Thermal Properties</b>		
Coefficient of Thermal Expansion	23.2 (10 <sup>-6</sup> /°C)	
Thermal Conductivity	167W/mK	970 BTU-in/hr-ft <sup>2</sup> -°F

**c) Step 3: Creating Mesh:**

Table 6.19 shows the Mesh properties of the Satellite. Hybrid mesh was used to mesh the satellite as it had surfaces with curvatures so it was a better option.

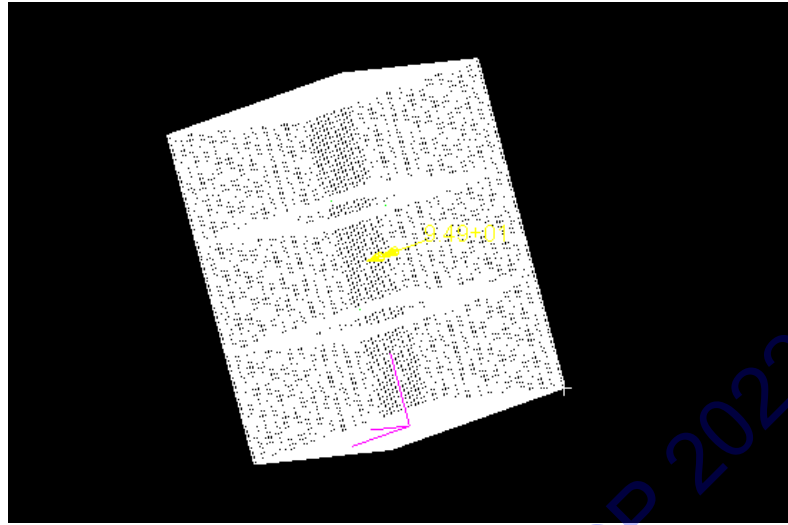


Figure 6.15 Mesh

Table 6.19 Mesh Properties

<b>Total Nodes</b>	49479
<b>Total Elements</b>	49547
<b>Global Edge Length</b>	0.02
<b>Type of Mesh</b>	Hybrid

**d) Step 4: Applying Loads/Boundary Conditions**

Following inertial loads were applied to simulate the stresses generated during launch.

Table 6.20 Loads/BC's

<b>Inertial loads</b>	<b>Values</b>
X	2g (lateral)
Y	2g (lateral)
Z	-10g (longitudinal)

**e) Step 5: Analyze**

1. Set solution type to 'Linear static' to run the solution for static analysis and set the solution type to 'Normal modes' to run the solution for modal analysis.

2. Select the results output format to 'XDB'
3. Select the relevant subcases 'Apply'

#### 6.4.1 H2Z Linear Static Analysis:

There were two cases simulated as a part of this analysis. Table 6.21 shows the maximum stress and deformation results obtained for both types of static analysis.

##### 1. Launch Static Analysis:

The three modular structure is considered clamped in 3 translational degrees of freedom. The maximum deformation for the launch static analysis is seen in Figure 6.16 to be 46.2MPa at node 20163. After comparing the maximum stress obtained from the static analysis with the allowable stress or yield strength of aluminum 6061 (276MPa), it was found that H2Z is safe with a considerable factor of safety 5.9

##### 2. Component Level Analysis:

In this case the forces applied by each component were modeled. The maximum deformation for the component level analysis is seen in Figure 6.17 to be 98.8MPa at node 1177. After comparing the maximum stress obtained from the static analysis with the allowable stress or yield strength of aluminum 6061 (276MPa), it was found that H2Z is safe with a considerable factor of safety 2.79

Table 6.21 Results of Linear Static Analysis

Case	Stress( MPa)		FOS	Maximum Deformation
	Maximum	Minimum		Unit (mm)
<b>Launch Static</b>	46.2MPa	2.09KPa	5.9	19.5 @ Nd 27423
<b>Component Level</b>	98.8 MPa	0 MPa	2.79	3.15 @ Nd 1201

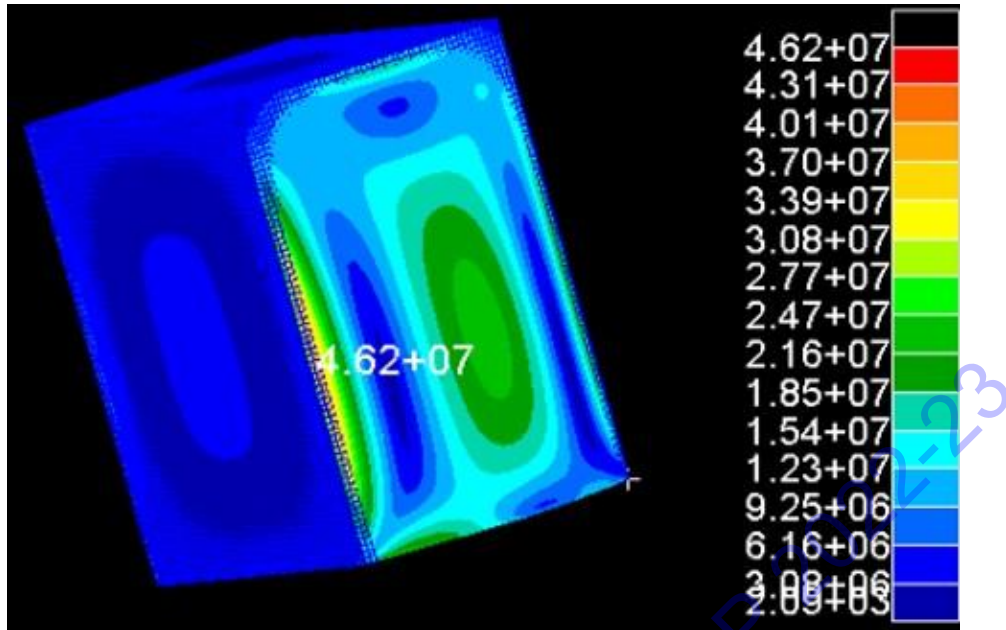


Figure 6.16 Launch Static Simulation

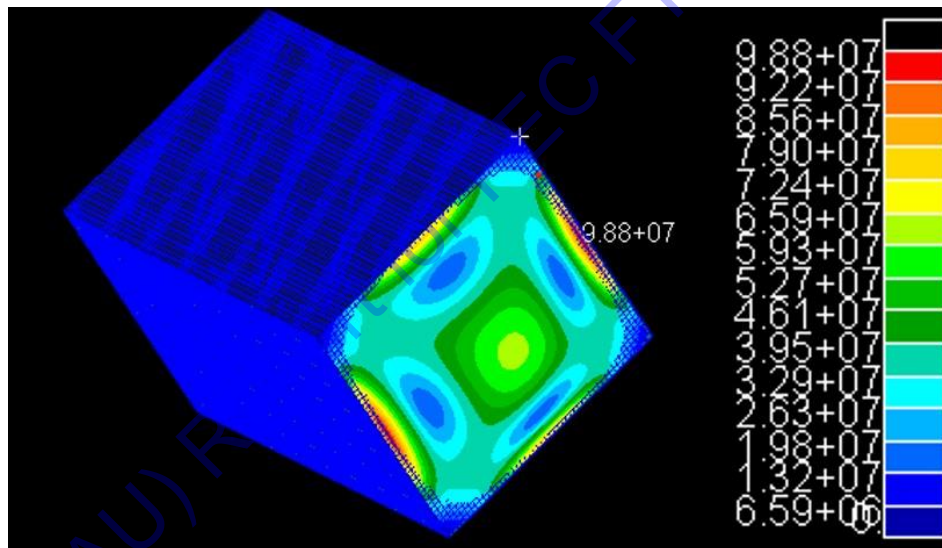


Figure 6.17 Component level Simulation

#### 6.4.2 H2Z Modal Analysis

As per the requirements of Long March 3B launch vehicle, the proposed structure is required to have a first mode frequency above 10Hz. The maximum and minimum frequencies were observed to be greater than natural frequency of the launch vehicle adapter, therefore occurrence of resonance was not possible and H2Z is considered to be safe. The natural frequencies associated with respective mode of vibration are shown in Table 6.22

Table 6.22 Modal Frequencies for modes 1-10

Mode	Frequency
1	13.533
2	14.776
3	16.404
4	17.049
5	18.553
6	18.553
7	18.553
8	18.553
9	18.695
10	20.291

Figure 6.18 shows the mode with highest frequency.

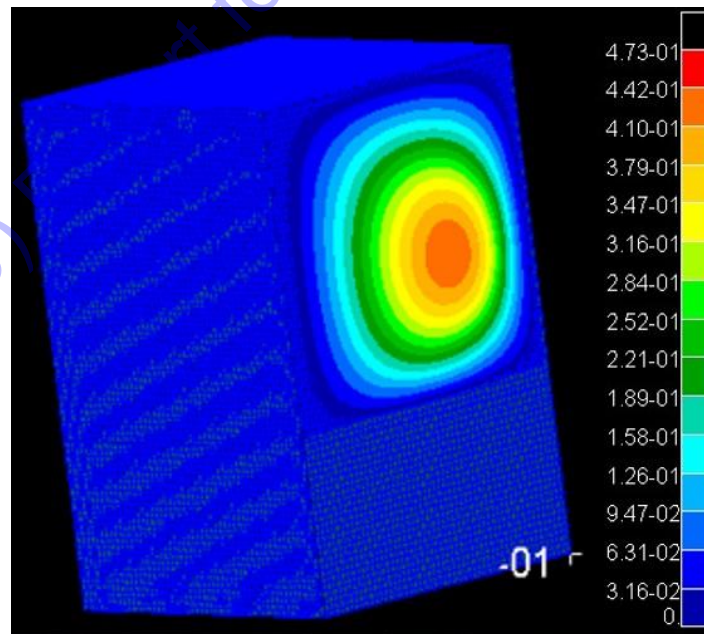


Figure 6.18 Maximum normal mode frequency

Figure 6.19 shows the first mode frequency.

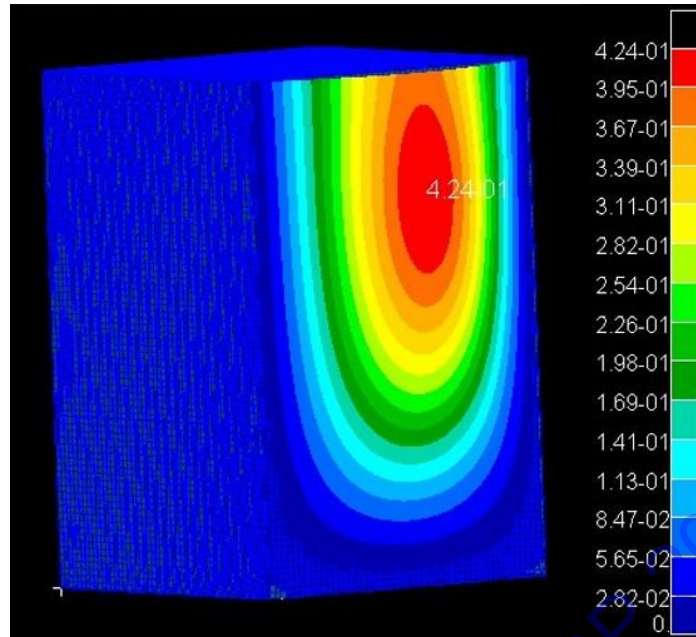


Figure 6.19 First normal mode frequency

### 6.4.3 H2Z Thermal Analysis

Thermal analysis of the H2Z conducted on COMSOL Multiphysics 6.1 revealed that after being exposed to intensive solar environment, H2Z will experience a maximum temperature of about 91.2 °C or 364.35K and a minimum temperature of -51.2 Celsius or 221.95K. The temperature range in LEO goes from -65 °C to +125 °C with thermal cycling dependent on the orbit height [29]. Obtained results showed that our spacecraft is safe and falls well within the safe range.

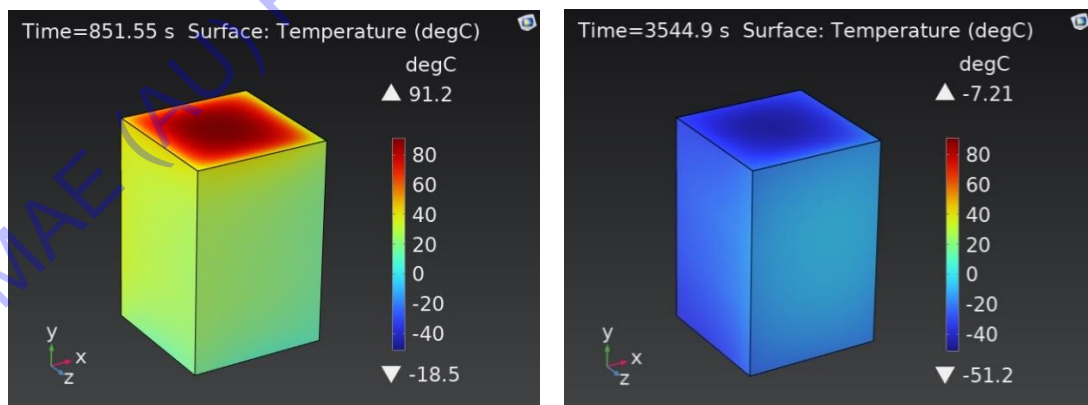


Figure 6.20 Thermal Analysis of H2Z (maximum and minimum temperatures)

## **Chapter 7: Conclusions and Recommendations**

The project is a continuation of the work that has been carried out SERP Lab NUST where a 4 DoF robotic arm was developed for debris remediation and the PNSS-1 satellite

### **7.1 Mission Conclusions**

This project aimed at developing minimal energy mission for removing space debris from Low Earth Orbit. Several mission strategies were explored for removing debris. The whole process began by the selection of debris for which a unique mathematical model was developed. Based on the selection criteria 5 debris were selected that would (cause a satellite located in a specific parking orbit), least amount of propellant to dispose of the debris. By using the standard satellite maneuvers in the literature, 14 different mission strategies were developed, out of which only two were analysed in detail and their results and math model are presented in detail in previous chapters. The Home capture strategy was quite expensive in terms of the mass of propellant (delta-V budget). Furthermore this strategy also had the risk of collision with the debris since the satellite would have to enter the debris cloud. However this strategy could be useful if there are no requirements of plane change during the mission. To reduce the cost, another mission strategy was evolved which is the Node Capture. The results indicate that this strategy is much less expensive in terms of delta-V budget. It was also identified that it is relatively safer mission yet a precise one as the terminal rendezvous occurs precisely at the node of the orbits. This eliminates the need of plane change maneuver while still grabbing the debris that orbiting the Earth in different planes. Despite its several benefits this mission strategy is only applicable to certain range of orbits, since the orbits of both satellite and debris must intersect in space. All simulations were designed in both General Mission Analysis Tool (GMAT) and STK. For the sake of simplicity, all perturbations were neglected at this stage while designing the mission simulations and the simple two-body problem was solved.

### **7.2 System Conclusions**

A concept design of functional a space tug that could capture the debris was intended at the start of this project. Multiple design iterations were conducted to achieve the desired results with special focus on the Structure, Propulsion and Electrical Power



subsystems to ensure the compact sizing, high structural integrity, generation of huge thrust with minimum propellant consumption and a conserved solar array size to be mounted on H2Z considering its power requirements. A thorough design study on the ADC and TTC subsystems was also conducted by the team of Dr. Muhammad Talal Saeed from Department of Electrical Engineering. Along with a 4-DoF Robotic arm, commercially available products were selected from reliable sources and modelled in SOLIDWORKS to get a better visualization of the final look of H2Z. At the end, a static linear, modal and thermal analysis was conducted to verify that the spacecraft is structurally and thermally capable to withstand the harsh environment conditions. The resulting design ensures the H2Z system's capability to capture debris while meeting the required mission objectives, with the potential to make a significant contribution to space debris mitigation efforts

### **7.3 Recommendations for Further Work**

The node capture strategy is a novel mission developed at Air University and requires exploring different aspects of it. To overcome the short comings of this strategy a constellation of space debris remediation satellites must be designed so that they may operate in different range of orbits. A basic analysis was done at this stage using the two-body problem, however this mission requires a more advanced analysis where the effects of both J2 perturbations and the atmospheric drag must be taken into account.

In this report, comprehensive analysis and design of all subsystem parameters have been undertaken. Despite being in the concept design phase of the project, the obtained results are fairly accurate. However, a detailed design of each subsystem is still pending, and hence further refinement and optimization of the design will be necessary to ensure optimal performance of the subsystems. The mission simulations were carried out on General Mission Analysis Tool (GMAT) using two body problem. However, the third body perturbations and the effect of atmospheric drag must also be accounted for since the debris is in Low Earth Orbit.

## References

- [1] D. J. Kessler, N. L. Johnson, J. C. Liou, and M. Matney, "Kessler Syndrome-AAS Paper.pdf," *Adv. Astronaut. Sci.*, 2010, [Online]. Available: <https://pdfs.semanticscholar.org/2276/55e022441d1379dfdc395173ed2e776d54ee.pdf>
- [2] R. Hall and A. Ocampo, "Center for Space Standards & Innovation," no. September 2010, 2014.
- [3] S. Cresto Aleina, N. Viola, F. Stesina, M. A. Viscio, and S. Ferraris, "Reusable space tug concept and mission," *Acta Astronaut.*, vol. 128, pp. 21–32, 2016, doi: 10.1016/j.actaastro.2016.07.003.
- [4] F. Report, "HybridSail Hybrid Solar Sails for Active Debris," 2011.
- [5] J. . R. . W. W . J . Larson, *Space Mission Analysis and Design (Space Mission Analysis and Design , 3rd edition*, no. 1999. 2020.
- [6] G. S. Aglietti *et al.*, *Spacecraft Systems Engineering*, Fourth.
- [7] G. P. Sutton and O. Biblarz, *Rocket Propulsion Elements*, Eighth.
- [8] K. Wakker, *Fundamentals of Astrodynamics*. 2015.
- [9] B. Noble, Y. Almanee, A. Shakir, and S. Park, "Design and evaluation of an Orbital Debris Remediation system," *2016 IEEE Syst. Inf. Eng. Des. Symp. SIEDS 2016*, pp. 159–164, 2016, doi: 10.1109/SIEDS.2016.7489290.
- [10] S. Raguraman, R. N. S. Sarath, and J. Varghese, "Space Debris Removal: Challenges and Techniques-A Review," *ICRITO 2020 - IEEE 8th Int. Conf. Reliab. Infocom Technol. Optim. (Trends Futur. Dir.*, pp. 1361–1366, 2020, doi: 10.1109/ICRITO48877.2020.9197877.
- [11] G. Zhai and J. R. Zhang, "Space tether net system for debris capture and removal," *Proc. 2012 4th Int. Conf. Intell. Human-Machine Syst. Cybern. IHMSC 2012*, vol. 1, pp. 257–261, 2012, doi: 10.1109/IHMSC.2012.71.
- [12] M. Kanazaki, Y. Yamada, and M. Nakamiya, "Multi-objective path optimization of a satellite for multiple active space debris removal based on a method for the travelling serviceman problem," *Adv. Sci. Technol. Eng. Syst.*, vol. 3, no. 6, pp. 479–488, 2018, doi: 10.25046/aj030656.
- [13] B. Fram, L. Sauter, S. Buckley, B. Summers, and A. Rogers, "SHERPA: A flexible & responsive small satellite transport vehicle," *IEEE Aerosp. Conf. Proc.*, vol. 2005, 2005, doi: 10.1109/AERO.2005.1559583.
- [14] W. Wang, X. Song, and M. Shao, "Operational Research in Multi Space Debris Removal Using Space Maneuver Vehicle," *Proc. 2018 Chinese Autom. Congr. CAC 2018*, pp. 3299–3306, 2019, doi: 10.1109/CAC.2018.8623496.
- [15] W. Yan, N. Qi, J. Ai, and L. Sun, "A redundant manipulator design for active space debris removal," *Chinese Control Conf. CCC*, vol. 2016-Augus, pp. 4585–4590, 2016, doi: 10.1109/ChiCC.2016.7554065.
- [16] B. Dadhich, R. Guha, S. Shekhar, and V. Malhotra, "Autonomous Space Debris

- Capturing System for Recycling,” *IEEE Aerosp. Conf. Proc.*, vol. 2021-March, pp. 1–12, 2021, doi: 10.1109/AERO50100.2021.9438495.
- [17] A. Ruggiero, P. Pergola, and M. Andrenucci, “Small Electric Propulsion Platform for Active Space Debris Removal,” *IEEE Trans. Plasma Sci.*, vol. 43, no. 12, pp. 4200–4209, 2015, doi: 10.1109/TPS.2015.2491649.
- [18] “TriScape200 Satellite Payloads.” <https://simera-sense.com/products/xscape200/triscape200/> (accessed May 06, 2023).
- [19] S. This *et al.*, “LM-3B USER’S MANUAL CHAPTER 6,” pp. 1–24, 1999.
- [20] D. D. P. Mishra, *Fundamentals of Rocket Propulsion*.
- [21] R. W. Humble, G. N. Henry, and W. J. Larson, “space-propulsion-analysis-and-design-1nbsped-0070313202-9780070313200\_compress.pdf.”
- [22] D. . M. T. SAEED, U. FALAK, D. A. SAROSH, M. A. NAVEED, and R. JAVAID, “System and Components Level Design of ADCS and TT & C Subsystem For LEO Based Space Tug FACULTY OF ENGINEERING,” 2023.
- [23] B. Gravity, “PODRIX GNSS Receiver.” [https://satcatalog.s3.amazonaws.com/components/1216/SatCatalog\\_-\\_Beyond\\_Gravity\\_-\\_PODRIX\\_GNSS\\_Receiver\\_-\\_Datasheet.pdf?lastmod=20230222073318](https://satcatalog.s3.amazonaws.com/components/1216/SatCatalog_-_Beyond_Gravity_-_PODRIX_GNSS_Receiver_-_Datasheet.pdf?lastmod=20230222073318)
- [24] ISIS, “On Board Computer (iOBC),” pp. 64–65, 2014, [Online]. Available: <https://www.cubesatshop.com/wp-content/uploads/2016/06/iOBC-Brochure-v1.pdf>
- [25] D. Sar-i, “STUDENT DESGIN PROJECT: SAR BASED EARTH OBSERVATION SATELLITE SAR BASED EARTH OBSERVATION SATELLITE DESIGN aa,” no. August 2020, 2019, doi: 10.13140/RG.2.2.20877.77288.
- [26] A. Okan, “AST 486 : Spacecraft Design,” no. May, 2018.
- [27] “Ground sampling distance (GSD) in photogrammetry,” *Pix4D*, 2011. <https://support.pix4d.com/hc/en-us/articles/202559809-Ground-sampling-distance-GSD-in-photogrammetry>
- [28] A. D. Aubrey, C. Frankenberg, R. O. Green, M. L. Eastwood, D. R. Thompson, and A. K. Thorpe, “Airborne remote-sensing technologies detect, quantify hydrocarbon releases,” *JPT, Journal of Petroleum Technology*, vol. 67, no. 8, pp. 103–105, 2015. doi: 10.2118/0815-0103-jpt.
- [29] “Environmental Conditions for Space Flight Hardware – A Survey.” [Online]. Available: [https://nepp.nasa.gov/docuploads/C5E0869C-0469-4D11-9FAA8012C8F52351/environmental Testing Survey.doc](https://nepp.nasa.gov/docuploads/C5E0869C-0469-4D11-9FAA8012C8F52351/environmental%20Testing%20Survey.doc)

## Appendix-A Mission Design Codes

### Hohmann Transfer:

```
#Hohmann Trnasfer

import math
a_c = float(input('Enter the semi-major axis of H2Z (in km): '))
a_d = float(input('Enter the semi-
major axis of debris (in km): '))
e_c = float(input('Enter the eccentricity of H2Z: '))
e_d = float(input('Enter the eccentricity of debris: '))
#Calculating the radius of apogee of H2Z
r_ac = a_c * (1+e_c)
#Calculating the radius of perigee of H2Z
r_pc = (2*a_c) - r_ac
#Calculating the radius of apogee of debris
r_ad = a_d * (1+e_d)
#Calculating the radius of perigee of debris
r_pd = (2*a_d) - r_ad
# Calculaing the semi-major axis of transfer orbit
a_tx = (r_ad + r_pc)/2
# Determining velocity of H2Z at perigee of initial orbit
v_ip = math.sqrt(398600 * ((2/r_pc)-(1/a_c)))
# Determining velocity of H2Z at perigee of transfer orbit
v_txp = math.sqrt(398600 * ((2/r_pc)-(1/a_tx)))
# Determining velocity of H2Z at apogee of target orbit
v_txa = math.sqrt(398600 * ((2/r_ad)-(1/a_tx)))
# Determining velocity of H2Z at apogee of initial orbit
v_fa = math.sqrt(398600 * ((2/r_ad)-(1/a_d)))

#Change in velocity at perigee
v_p = v_txp - v_ip
if v_p > 0:
    print("The velocity change at perigee is: {} km/s".format(v_p))
else:
    print("The velocity change at perigee is: {} km/s ".format(-
(v_p)))

#Change in velocity at apogee
v_a = v_fa - v_txa
if v_a > 0:
    print("The velocity change at perigee is: {} km/s".format(v_a))
else:
    print("The velocity change at perigee is: {} km/s".format(-
(v_a)))

#Dela-V for the maneuver
```

```
print('Delta-
V for Hohmann Transfer is {} km/s'.format(v_p + v_a))
```

### General Plane Change Maneuver

```
#General Plane Change Maneuver

import math
a_c = float(input('Enter the semi-major axis of H2Z (in km): '))
e_c = float(input('Enter the eccentricity of H2Z: '))
i_c = float(input('Enter the inclination of H2Z (in degrees): '))
i_d = float(input('Enter the inclination of debris (in degrees): '))
raan_c = float(input('Enter the right ascension of ascending node
of H2Z (in degrees): '))
raan_d = float(input('Enter the right ascension of ascending node
of debris (in degrees): '))
w_c = float(input('Enter the argument of perigee of H2Z (in degrees): '))

#Conversion of elements to radians

i_c_rad = math.radians(i_c)
i_d_rad = math.radians(i_d)
raan_c_rad = math.radians(raan_c)
raan_d_rad = math.radians(raan_d)

#Calculate change in right ascension of ascending node

delta_raan_rad = raan_d_rad - raan_c_rad
delta_raan = math.degrees(delta_raan_rad)
alpha_rad = math.acos(((math.cos(i_c_rad)*(math.cos(i_d_rad))) +
(math.sin(i_c_rad)*(math.sin(i_d_rad))*(math.cos(delta_raan_rad))
)))
alpha = math.degrees(alpha_rad)

#Calculate the argument of latitude of the point of application of
maneuver (in H2Z orbit)

u_rad = math.acos(((math.cos(i_c_rad))*(math.cos(alpha_rad)) -
(math.cos(i_d_rad)))/(math.sin(i_c_rad)*(math.sin(alpha_rad))))
u = math.degrees(u_rad)

#Calculate the true anomaly of the point of application of maneuver
(in H2Z orbit)

theta_c = u - w_c
```

```

print('The true anomaly of point of application of maneuver (in H
2Z orbit) is: {} degrees'.format(theta_c))

#Calculate the radial position of satellite at this point

r_int = (a_c * (1-
(e_c*e_c)))/(1 + (e_c * math.cos(math.radians(theta_c))))

#Calculate the velocity of satellite at this point

v_int = math.sqrt(398600 * ((2/r_int)-(1/a_c)))

#Calculate delta V
V = 2*v_int*(math.sin(alpha_rad/2))
print('Delta-
V for General Plane Change Maneuver is {} km/s'.format(V))

```

#### Phasing Maneuver:

```

#Phasing Maneuver

import math
a_c = float(input('Enter the semi-major axis of H2Z (in km): '))
e_c = float(input('Enter the eccentricity of H2Z: '))
v_d = float(input('Enter true anomaly of debris when H2Z is at th
e perigee (in degrees): '))
v_c = 0 #(in degrees)
#Calculating the radius of apogee of H2Z
r_ac = a_c * (1+e_c)
#Calculating the radius of perigee of H2Z
r_pc = (2*a_c) - r_ac

#Calculate the angular momentum of the initial orbit
h_c = math.sqrt(r_pc * (398600 * (1 + (e_c * math.cos(math.radian
s(0))))))

#Calculate the time period of initial orbit
T_c = (((h_c/math.sqrt(1 - (e_c * e_c)))**3)*(2*math.pi)/(398600*3
98600))

#Calculate the velocity at perigee of initial orbit
v_pc = h_c/r_pc

#Calculate the eccentric anomaly of debris
E_c_rad = 2*math.atan(math.sqrt((1-
e_c)/(1+e_c))*math.tan((v_d*math.pi/360)))
E_c = math.degrees(E_c_rad)

```

```

#Calculate time the debris moves form its initial ponit to the pe
rigger
t = (E_c_rad - (e_c*math.sin(E_c_rad)))*(T_c)/(2*math.pi)

#Calculate time period of phasing orbit
T_phas = T_c - t

#Calculate semi-major axis of phasing orbit
a_phas = ((T_phas * math.sqrt(398600))/(2 * math.pi))**(2/3)

#Calculate the apogee radius of phasing orbit
r_a_phas = (2*a_phas) - r_pc

#Calculate the eccentricity of phasing orbit
e_phas = (r_a_phas - r_pc)/(r_a_phas + r_pc)

#Calculate the angular momentum of the phasing orbit
h_phas = math.sqrt(r_pc * (398600 * (1 + (e_phas * math.cos(math.
radians(0))))))

#Calculate the velocity at perigee of initial orbit
v_p_phas = h_phas/r_pc

#Delta-V for the maneuver
V = v_pc - v_p_phas
if V > 0:
    print("Delta-V for phasing maneuver is: {} km/s".format(V))
else:
    print("Delta-V for phasing maneuver is: {} km/s".format(-(V))

```

DMAE (AU) Report for PEC FYDP 2022-23

## Appendix-B System Design Codes

### Sizing:

```

clc
fprintf(" Inputs : \n") %Defining Inputs
a = 'Loaded Mass in Kg'
fprintf(" H2Z had a loaded mass of 135.428kg \n")
M=input(a)
V=0.001*M %Volume of spacecraft
s=0.25*((M)^0.33)%Linear Dimension
Ab=s^2 %Cross sectional area
I=0.01*((M)^1.667) %Moment of Inertia
    
```

### Propulsion Subsystem:

```

clc
fprintf(" Inputs : \n") %Defining Inputs
a = 'Altitude =';b = 'Thrust = ';c = 'k = ';d = 'p1 = ';e = 'T1 = ';f
= 'M = ';g = 'p2 = ';
h = 'Area ratio =';
m = 'mass flow rate = ';
n = ' Isp = ';
r = 'g_not =';
s = 'R = ';
o = ' Characteristic length ';
p = 'Mach inlet =';
t = 'Divergence half angle';
fprintf('Parameters such as k,R,m_dot,T1 have been calculated from
RPA \n');
fprintf('H2Z uses mass flow rate of about 0.095kg/s \n');
mdot = input(m);
Isp = input(n);
g_not = input(r); %in m/s^2
Alt = input(a); %in km
fprintf('H2Z uses k=1.234 \n');
k = input(c);
fprintf('H2Z uses p1 to be 2.60MPa and p2 to be 64.2Pa \n');
p1 = input(d); %in MPa
p2 = input(g);
fprintf('H2Z uses T1 of 2044.0855 \n');
T1 = input(e); % in Kelvin
fprintf('H2Z uses R = 13334.53717J/kg-k \n');
R = input(s);
fprintf('H2Z uses area expansion ratio of 150 \n');
Area_ratio = input(h);
L_star = input(o)
Mach_inlet=input(p)
%At 55km, the pressure is about
% Then we divide p2 by p1 to get the pressure ratio
Pressure_ratio = (p2)/(p1) %Pressure ratio
v2 = sqrt(((2*k)/(k-1))*R*T1*(1-((Pressure_ratio)^(k-1)/(k))));
%Exhaust velocity
At = ((mdot)/(p1))*(sqrt((R*T1)/((k*((2)/(k+1))^(k+1)/(k-1))))));
%Throat area
A2 = (At)*(Area_ratio) %Exit area
Dt= sqrt((4*At)/(pi)) %throat dia
D2= sqrt((4*A2)/(pi)) %exit dia
Thrust = mdot*Isp*g_not %Throat temperature
Tt = (2*T1)/(k+1);%throat temperature
    
```



```

Cf = (Thrust)/(p1*At)
c_actual = (p1*At)/(mdot)%actul characteristic velocity
c_theo = (sqrt(k*R*T1))/((k)*(sqrt(((2)/(k+1))^(k+1)/(k-1)))));%theoretical characterisitic velocity
c_efficiency = ((c_actual)/(c_theo))*100 % c*efficiency
Vc= At*L_star %chamber volume
Contractrion_ratio=(1/Mach_inlet)*(((2/(k+1))*(1+((k-1)*Mach_inlet^2)/2))))^((k+1)/(2*(k - 1))) %area contraction ratio
Ac=At*Contractrion_ratio %chamber area
Lc=L_star*(1/Contractrion_ratio) %chamber length
Dc=sqrt((4*Vc)/(Lc)) %chamber dia
%theta_cn is the divergence half angle and for conical nozzles it is 15
Theta_cn= input(t)
Ln_conical=(D2-Dt)/2*tan(deg2rad(Theta_cn)) %nozzl length for conical nozzle
%The upstream throat contour is circular, with a radius of 1.5 times the throat radius.
%Similarly the downstream throat contour is also circular, with a radius 0.382
r_upstream=1.5*(Dt/2)
r_downstream=0.382*(Dt/2)
Ln_bell=0.80*(Ln_conical) %nozzl length for bell nozzle

```

### Electrical Power subsystem

```

clc
fprintf(" Inputs : \n") %Defining Inputs
a='Average power req for eclipse phase = ';b='Average power req for sunlight phase = '
c='Eclipse time = ', d='Sunlight time = ';e='total time = '
f='regulator efficiency = ';g='cell efficiency = '
h='inherent degradation = '; i='worst case angle = '
j='Lifetime degradation = '; k='satellite life = ';l='degradation per year = '
m='Depth of discharge = ';n='charge efficiency =';o='Solar flux = '
p='cell efficiency = ';q='packing efficiency = ';r='array degradadation factor =';
s='miscalleneous factor = ';t='specific performance',u='array pointing error'
fprintf('H2Z requires P_sun and P_eclipse to be 637.6471 and 194.5W \n')
P_eclipse= input(a)
fprintf('H2Z uses t_sun and t_eclipse to be 61.74min and 36.26min \n')
t_eclipse=input(c)
fprintf('H2Z uses regulators efficincy to be 0.72 \n')
reg_efficiency=input(f)
t_sun=input(d)
P_sun=input(b)
P_charge= (P_eclipse*t_eclipse)/(reg_efficiency*t_sun) %The power Required from the solar array to meet the eclipse loadThe power Required from the solar array to meet the eclipse load
P_array=P_sun+P_charge %Power Required to be available from array
fprintf('H2Z uses solar flux to be 1400W/m2 \n')
fprintf('H2Z uses a solar cell of 30 percent efficiency \n')
cell_eff=input(p)
S=input(o)
P_not= cell_eff*S %Power output with sun normal to the surface of the cells
fprintf('H2Z uses Inherent degradation of about 0.77\n')

```

```

Id=input(h)
fprintf('H2Z uses solar flux to be 1400W/m2 \n')
fprintf('H2Z uses worst case sun incidence angle to be 23.5 \n')
fprintf('For GaAs cells degradation per yr=2.75 percent \n')
worst_case_angle=input(i)
degradation_per_yr=input(l)
fprintf('Life of H2Z is 2 yrs \n')
satellite_life=input(k)
P_BOL=P_not*Id*cos(deg2rad(worst_case_angle))%Beginning-of-life (BOL)
power production capability
Ld=(1-degradation_per_yr)^satellite_life %Actual lifetime degradation
P_EOL=P_BOL*Ld %End-of-life (EOL) power production capability
P_array_leo=P_sun*1.5 %Size of solar array in LEO
P_array_geo=P_sun*1.05%Size of solar array in GEO
fprintf('H2Z uses charge efficieny of 90 percent \n')
charge_eff=input(n)
fprintf('H2Z uses Depth of discharge to be 70 percent \n')
DOD=input(m)
Eb=(P_eclipse*(t-t_sun))/(charge_eff * DOD)
fprintf('For H2Z, array pointing =0.01 \n')
fprintf('For H2Z, packing efficiency = 0.90 \n')
fprintf('For H2Z, miscellaneous factor = 0.02 \n')
fprintf('For H2Z, array degradation factor = 0.03 \n')
Array_pointing_error=input(u)
packing_eff=input(q)
misc_factor=input(s)
array_degradation_factor=input(r)
Specific_Performance = input(t)
Area_array=
(P_array)/(S*(cos(deg2rad(Array_pointing_error))*cell_eff*packing_eff
*(1-(misc_factor))*(1-array_degradation_factor)))
fprintf('For H2Z, we assume a specific performance of 50W/kg')
Mass_array=P_array_leo/Specific_Performance
    
```

TCS:

```

a='absorptivity=';
b='Stephen boltzmann constant=';
c='Solar irradiance=';
d='Emmisivity=';
alpha=input(a)
Gs=input(c)
sigma=input(b)
e=input(d)
T_avg = ((alpha*Gs)/(6*sigma*e))^0.25
    
```